2013

APPLICATIONS OF ANTIOXIDANT AND ANTI-INFLAMMATORY POLYMERS TO INHIBIT INJURY AND DISEASE

David B. Cochran
University of Kentucky, dave.cochran@uky.edu

STUDENT AGREEMENT:

I represent that my thesis or dissertation and abstract are my original work. Proper attribution has been given to all outside sources. I understand that I am solely responsible for obtaining any needed copyright permissions. I have obtained and attached hereto needed written permission statements(s) from the owner(s) of each third-party copyrighted matter to be included in my work, allowing electronic distribution (if such use is not permitted by the fair use doctrine).

I hereby grant to The University of Kentucky and its agents the non-exclusive license to archive and make accessible my work in whole or in part in all forms of media, now or hereafter known. I agree that the document mentioned above may be made available immediately for worldwide access unless a preapproved embargo applies.

I retain all other ownership rights to the copyright of my work. I also retain the right to use in future works (such as articles or books) all or part of my work. I understand that I am free to register the copyright to my work.

REVIEW, APPROVAL AND ACCEPTANCE

The document mentioned above has been reviewed and accepted by the student's advisor, on behalf of the advisory committee, and by the Director of Graduate Studies (DGS), on behalf of the program; we verify that this is the final, approved version of the student's dissertation including all changes required by the advisory committee. The undersigned agree to abide by the statements above.

David B. Cochran, Student

Dr. Thomas Dziubla, Major Professor

Dr. Thomas Dziubla, Director of Graduate Studies

APPLICATIONS OF ANTIOXIDANT AND ANTI-INFLAMMATORY POLYMERS TO INHIBIT INJURY AND DISEASE

DISSERTATION

A dissertation submitted in partial fulfillment of the
requirements for the degree of Doctor of Philosophy in the
College of Engineering
at the University of Kentucky

By
David B. Cochran

Lexington, Kentucky

Director: Dr. Thomas D. Dziubla, Gill Professor, Associate Professor of Chemical Engineering

Lexington, Kentucky

2013

ABSTRACT OF DISSERTATION

APPLICATIONS OF ANTIOXIDANT AND ANTI-INFLAMMATORY POLYMERS TO INHIBIT INJURY AND DISEASE

There is an undeniable link between oxidative stress, inflammation, and disease. Currently, approaches using antioxidant therapies have been largely unsuccessful due to poor delivery and bioavailability. Responding to these limitations, we have developed classes of polymer and delivery systems that can overcome the challenges of antioxidant and anti-inflammatory therapy.

In our initial studies, nanoparticles of poly(trolox), a polymeric form of trolox, were surface-modified with antibodies. This modification allows for specific targeting to endothelial cells, affording controllable and localized protection against oxidative stress. We have shown these targeted nanoparticles bind, internalize, and provide protection against oxidative stress generation and cytotoxicity from iron oxide nanoparticles.

In a similar fashion, we have tested the ability of poly(trolox) to prevent rheumatoid arthritis *in vivo*. Poly(trolox) nanoparticles were encapsulated in a PEGylated polymer to enhance circulation and biocompatibility. These particles were shown to accumulate in inflamed joint tissue, recover natural antioxidant function, suppress protein oxidation, and inhibit inflammatory markers.

Lastly, we developed a class of polyphenolic compounds utilizing a non-free radical based reaction chemistry of poly(β-amino esters). The polyphenol apigenin was investigated for its anti-inflammatory properties to inhibit inflammation-mediated tumor cell metastasis. PEGylated nanoparticles that incorporated apigenin poly(β-amino ester) were developed and found to retain their anti-inflammatory efficacy while providing a long term release profile. These inhibited the ability of tumor cells to adhere to inflamed vascular cells. We also have shown that these polymers can suppress markers of inflammation responsible in enhancing tumor cell adhesion.

KEYWORDS: Oxidative Stress, Inflammation, Antioxidant Polymers, Nanoparticles, Targeting

David Cochran

9/12/2013

APPLICATIONS OF ANTIOXIDANT AND ANTI-INFLAMMATORY POLYMERS TO INHIBIT INJURY AND DISEASE

By

David B. Cochran

Dr. Thomas D. Dziubla
Director of Dissertation

Dr. Thomas D. Dziubla
Co-Director of Graduate Studies

September 12th, 2013
Date

DEDICATION

I dedicate this body of work and degree to:

Karen and Tom Swenson

Andrea Leydet

Thank you for the continued support and love throughout the ordeals of research.

ACKNOWLEDGEMENTS

While this dissertation is a body of individual work, it could not be possible without the help and direction of multiple people. First I would like to thank Dr. Thomas Dziubla for his continued support and guidance during the past four years. He has not only been a mentor and an advisor, but also a friend.

I'd also like to acknowledge the collaborative efforts and advisement from Dr. Kimberly Anderson and Dr. Richard Eitel. As my IGERT mentors, they have helped me succeed and grow in my scientific endeavors. Other collaborators, such as Dr. Hilt, Dr. Crofford, Dr. Yokel, and Dr. Bradley have also played extremely pivotal roles in my doctoral studies.

I am grateful for my fellow labmates, Paritosh Wattamwar, John Medley, Sundar Prasanth, Andrew Vasilakes, and Prachi Gupta. In addition I'd like to thank my friends, Robert Wydra, Nathaniel Stocke, Jennifer Fischer, and Daniel Schlipf. Without everyone's support, I would not be where I am today.

TABLE OF CONTENTS

LIST OF TABLES

LIST OF FIGURES

Chapter 1. Introduction

Oxidative stress is a key pathological process in a variety of disease states (e.g., ischemia-reperfusion injury [1, 2], hypoxia, and acute lung [3] and renal injury [4]). Oxidative stress is characterized by the formation of a wide range of reactive oxygen species (ROS), which cause an altered cellular redox state leading to severe DNA, protein, and lipid damage; ultimately resulting in dysfunction and death [5, 6].

In addition to the direct lipid and DNA damage caused, oxidative stress can cause cells to produce cytokines and chemokines that play a role in propagation of the inflammatory response [7] such as interleukin-1 (IL-1), interleukin-6 (IL-6), and tumor necrosis factor alpha (TNF-α) [8, 9]. This inflammatory response can in turn induce pathway activations such as the NF-κB [10], ERK [11], and JNK pathway [12], among others. This activation initiates a cascade of gene activation to regulate antioxidant and immune defenses [13]. Endothelial cells, in response to this pathway activation, begin to secrete and express molecules known as Cellular Adhesion Molecules (CAM) on their surfaces to facilitate leukocyte adhesion, vasodilatation, and transmigration [14]. Likewise, immune system cells will respond in kind to secrete nitric oxide as a host defense mechanism against pathogens [15]. Under normal conditions, recruited leukocytes, macrophages, and neutrophils will contain and mitigate further damage. However, in some cases the immune system cannot regulate its defenses due to factors such as persistent infections [16], complications with implanted “biomaterials” [17], or depletion of natural antioxidant

reserves [18]. In these scenarios the immune response can begin to damage viable cells through uncontrolled cytokine production [19].

It is possible to inhibit and reverse these events through supplementation of free radical scavengers, which can intercept ROS; thereby attenuate cellular damage [20-22]. Recently, certain antioxidants have also been shown to suppress some specific inflammation-mediated pathways. For example quercetin, a naturally-derived flavanol, can down regulate Intercellular Adhesion Molecule-1 via inhibiting the ERK-1 pathway [23, 24].

Antioxidants, simply defined, are molecules that can inhibit the oxidation potential of other molecules, such as free radicals. They are broken down into two general categories, small molecule and enzymatic antioxidants. Heavy interest lies in small molecule antioxidants, which unlike antioxidant enzymes can scavenge a large array of free radicals rather than one specific substrate [25-27]. Despite this advantage, there are still many obstacles to overcome for effective treatment using small molecule antioxidants, most notability in the delivery methods [28, 29].

In addition to the antioxidant benefits, researchers have discovered how certain classes of antioxidants can modulate cellular responses and pathway activation or deactivation [30-32]. It has been observed that flavonoids such as quercetin and epicatechin not only inhibit oxidative stress [33, 34], but can suppress the inflammatory pathways NF-κB and AP-1 through inhibition of specific kinase pathways by prevention of transcription factor phosphorylation [31, 35]. Interestingly, quercetin is the only reported flavanol with the ability to suppress both NF-κB activation and the JNK pathway [36, 37]. Flavones on the other hand, have been reported to suppress JNK, ERK, and NF-κB pathways, leading to down regulation of ICAM-1, VCAM-1, and E-selectin [36], making them great candidates

for applications such as cancer metastasis prevention [38, 39]. Apigenin is of special importance as it is shown to be one of the most potent flavones tested for suppression of these multiple inflammatory pathways [36]. As such, apigenin has been selected as the molecule of interest to formulate into an antioxidant polymer for delivery.

While flavonoids have poor water solubility, short biological half-life, and non-specific cellular uptake, these can be overcome utilizing the polymerization strategies described above. Lastly, while trolox, vitamin E, and possibly poly(trolox) show similar recovery effects as the flavanol quercetin in that they can suppress ICAM-1 expression, they do not affect VCAM-1 or E-selectin levels [40], further strengthening the use of apigenin for inflammation-mediated applications.

While the direct mechanism of NF-κB, JNK and ERK pathway suppression is not known, it is theorized that flavonoids can inhibit transcription by preventing complete phosphorylation of the protein portions required for activation [41, 42]. However, as noted by quercetin's ability to only suppress JNK pathways [35, 43], and apigenin's ability to suppress JNK and ERK [37, 44], it becomes clear that antioxidant activity alone cannot explain the anti-inflammatory function.

Because of the limitations of poly(trolox) ester in the inability to control degradation rates outside of molecular weight synthesis [22, 45], and inability of vitamin E to suppress certain inflammatory pathways [40], it is desirable to develop a new antioxidant polymer system that is based on a biologically active flavone PβAE nanoparticle system, that can also be modified through the use of targeting moieties in the future.

In this work, we first evaluate the ability of poly(trolox) to suppress clinically relevant injury and diseases, followed by the development of an anti-inflammatory polymer with desirable long term release properties. We have modified existing poly(trolox) nanoparticles to target specifically to vascular tissue through the use of monoclonal antibodies directed towards PECAM-1. We show that these particles can adhere to the endothelium, internalize, and suppress toxicity and free radical damage caused by iron oxide nanoparticles. Next, we utilized a similar nanoparticle system of poly(trolox) to treat the damaging effects of rheumatoid arthritis *in vivo*. Our results indicate that these particles are small enough to accumulate in disrupted vasculature, recover natural antioxidant capacity, and inhibit certain inflammatory markers such as TNF-α and IL-6. In the last set of work, we have developed an anti-inflammatory system comprised of our unique poly(beta-amino ester) chemistry to deliver the compound apigenin over an extended period of time. It was observed that particles comprised of apigenin PβAE released active apigenin over 72 hours, and were able to inhibit the ability of tumor cells to adhere and metastasize in compromised vascular cells. It was found that this was due to the significant suppression of inflammation markers provided by the apigenin, further reinforcing the link between cancer metastasis and inflammation.

Chapter 2. Background

Based on the book chapter published in:

> David Cochran and T. Dziubla. "Antioxidant Polymers for Tuning Biomaterial Biocompatibility: From Drug Delivery to Tissue Engineering", In G. Cirillo, Antioxidant Polymers Synthesis, Properties, and Applications. Salem, MA: Scrivener

2.1 Introduction

While the original definition of a biocompatible material was one that does not induce deleterious effects (e.g., a host immune response[46]), it has become clear that definition no longer fits with the advanced biomaterials designs. As our fundamental understanding of biological responses to foreign material increased, so did our knowledge that a purely inert material was both unfeasible and in some instances, especially in the area of tissue regeneration, undesired. A classic example is in the case of titanium oxide. While titanium oxide in a bulk phase has traditionally been utilized as an inert coating of implants, it has been found that wear particles in the nanometer size range can elicit a strong oxidative insult [47, 48]. Because of this, a new definition of biocompatibility has been proposed by D.F. Williams that a biomaterial must perform not only its function without undesired consequences, but also generate a beneficial tissue or cellular response [49]. Indeed, this shift in paradigm has not only challenged the "biocompatibility" of classical materials, but also paved the way into development of new and exciting methods to develop a material that can induce a beneficial host response.

2.2 Oxidative stress

Reactive oxygen and nitric species (ROS / RNS) are formed and utilized by all aerobic organisms [50]. As such, ROS/RNS are not inherently undesired as they participate in the key role of cell signaling and activation pathways [51, 52]. This is done

by direct oxidation of residues on proteins [53], degradation of inhibitory proteins [54], regulating immune system function to attack pathogens [55], or even signaling of differentiation or apoptosis [56, 57]. It is when reactive species production overtakes natural antioxidant capacity that oxidative stress is said to occur [18]. This unbalance leads to uncontrolled degradation which can lead to cellular dysfunction and death [58, 59]. Additionally, oxidative stress has been implicated in numerous diseases and conditions, such as tumor pathogenesis [60], systemic inflammation [61], COPD [62], and even aging [11].

2.3 Mechanisms of oxidative stress

Although the term "reactive oxygen species" (ROS) is most commonly used when describing oxidative stress, it is important to note that oxygen-based species are not the only contribution to stress. Nitric species, such as nitric oxide (NO·) and peroxynitrite ($ONOO^-$) play a just as important role in the cascade of signaling and injury [59, 63].

Superoxide ($O2^{\cdot -}$) is the species most often implicated in the initiation of oxidative stress [64, 65]. It can be formed in the presence of the electron-rich environment of the mitochondrial membrane in the respiratory chain [66]. In addition it can be produced endogenously by multiple enzymes. Xanthine-oxidase, which is typically activated and expressed in ischemia-reperfusion injury [67, 68] is one source. Another major source of enzyme-derived superoxide generation is the NADPH-oxidase pathway. NADPH-oxidase is a membrane-bound complex that facilitates superoxide production as a means to inhibit and destroy pathogens [69]. While two molecules of superoxide can dismutate spontaneously, endogenous superoxide dismutase (SOD) significantly speeds up this reaction.

Hydrogen peroxide, while not a free radical in itself, does function as a radical intermediate. It is an important compound because of its ability to penetrate and diffuse across cellular membranes [70]. Hydrogen peroxide can be reduced to hypochlorous acid through myeloperoxidases [71], or into hydroxyl radicals through iron reactions via Fenton chemistry [72].

The hydroxyl radical (·OH) is perhaps the most damaging radical to biological systems [73, 74]. It is produced from multiple sources. Hydrogen peroxide can react with metal irons to form hydroxyl radicals, otherwise known as Fenton chemistry [75]. These radicals can react with unsaturated fatty acids to form lipid radicals, which in turn form lipid hydroperoxides. Lipid hydroperoxide can once again undergo Fenton chemistry, leading to a propagating cycle of lipid oxidation and destruction [76, 77]. In order to combat the potential damage hydroxyl radicals can inflict, cellular defense systems consist of glutathione, a tripeptide which functions as a cellular antioxidant [78].

Table 2-1 outlines the common free radicals, their sources, and the accompanying cellular defense systems.

Table 2-1. Reactive Molecules and Their Sources

Reactive Molecule	Source	Cellular Defense Mechanisms	References
Hydrogen peroxide (H_2O_2)	Glucose oxidase NADPH-oxidase Superoxide dismutase P450 reductase Xanthine oxidase	Catalase Glutathione peroxidase Myeloperoxidase	[79]
Hydroxyl (·OH)	Fenton chemistry H202 degradation	Glutathione	[80]
Nitric Oxide (NO)	Nitric oxide synthase	Glutathione	[81]
Peroxynitrile (ONOO·)	Reaction with nitric oxide		[82]
Superoxide ($O2\cdot^{-}$)	Electron transport chain Cyclooxygenase NADPH-oxidase Xanthine Oxidase	Superoxide Dismutase	[83]

2.4 Oxidative stress in relation to biocompatibility

Oxidative stress occurs when a cell's inherit antioxidant capacity is exceeded by the production of reactive species. Oxidative stress has been identified as a key pathological process in many disease states[1, 84]. This effect has been attributed to the ability of reactive oxygen and reactive nitrogen species (ROS and NOS) to induce oxidation of protein backbones [85, 86], amino acid residues[87], and ultimately to fragmentation of essential proteins in a cell. Accumulation of this oxidized protein has been associated with disease and inflammation [54, 87]. DNA damage associated with fragmented protein base pairs, along with lipid peroxidation can also result in symptoms of cell cycle arrest, depleted antioxidant defense capability, mutations, etc. [88]. The clinical impacts can include carcinogenesis, neurodegeneration, and inflammation/infection. Importantly here, oxidative stress has been shown to play a pivotal role in biomaterial biocompatibility. This connection is best demonstrated through a discussion of the relationship between oxidative stress and inflammation, which will be detailed below.

2.5 Mechanism of immune response

The immune system response is classically separated into two distinct pathways, inflammatory response and adaptive immunity. The inflammatory response confers an immediate and non-specific defense against pathogens, injury, and foreign materials[89]. When a foreign body enters the body (or in our case, a biomaterial is implanted) the natural immune response begins with blood-material protein adsorption, cellular activation and macrophage recruitment, followed finally by fibrous capsule formation [90]. Table 2-2 illustrates the processes involved in the inflammation pathway. Biomaterial failure can occur at any one of these steps. For example, urethane coatings on silicone implants have

been observed to degrade over time, inducing localized oxidative stress. The result of this elicits fibrous encapsulation, which can lead to further complications requiring removal of implants, or permanent scarring[91]. Another non-classical example of biomaterials failure are drug loaded nanoparticles, which can be quickly cleared from the body due to blood-material interactions, known as opsonization.

Table 2-2. Summary of the biomaterial induced inflammatory response

Inflammation Stage	Characterized By	Role of Oxidative Stress	Example of Failure of Biomaterials in this Stage
Opsonization	Foreign material bound by complement molecules (antibodies, etc.). Bound compliments trigger immune defense via WBC recruitment and macrophage activation	Free radicals have shown to initiate compliment pathways (classical, alternative, lectin), leading to cellular activation	Therapeutic nanoparticle systems (PEG, PLGA, etc.) have the potential to be opsonized and quickly cleared [40]
Cellular Activation	Recruitment and activation of macrophages and other monocytes. Tissues increasing expression of chemoattractants such as MIP-1, MCP-1, and CSF-1	Oxidative species play a role in inducing the secretion of other chemokines, as well as possessing the ability to activate circulating immune cells such as leukocytes	Monocyte activation leads to respiratory burst. High concentrations of localized acidic and oxidative environments have been shown to inactivate peptide and proteins[41]
Macrophage Recruitment and Adhesion	Adhesion of macrophages to an implant or injury surface. Chemokine expression recruits circulating macrophages. Adhered macrophages begin to initiate oxidative bursts to destroy foreign material	Generation of superoxide to destroy invaders. Surrounding tissue can be affected and become inflamed in the process	Continual oxidative burst can propagate stress cracks of implants [35] or premature oxidation of metal compounds (such as electrical leads in pacemakers) [36]
Fibrous Encapsulation	Macrophage fusion and full encapsulation of implant. Chronic inflammation and pain	Oxidative species have been shown to trigger macrophage fusion. Chronic inflammation due to elevated levels of reactive species and reduced GSH.	Implant loosening due to fibrous encapsulation [37]. Therapeutic inactivation of controlled release devices due to diffusional barriers

When injected materials, especially free circulating, high surface area particles, are introduced into the blood stream opsonin proteins can adhere to their surfaces, mediating a phagocytic clearance response [92]. This can directly lead to loss of therapeutic efficacy, a failure of the biomaterial intended function.

A central component of the inflammatory response is the induction of oxidative stress. In most scenarios, a material's biocompatibility is most tested during the inflammatory phase of healing, which ultimately dictates the foreign body response and degree of fibrous encapsulation. Upon interaction with blood and plasma exudate, a layer of host proteins interact with and adhere to the surface of the biomaterial [93]. The chemistry and physical conformation of the surface play a crucial role in the type of protein adsorbed [94, 95]. Tegoulia et al. reported that protein adsorption was highest in hydrophobic and polar surfaces, whereas leukocyte adhesion was highest on phosphorylcholine rich surfaces[94]. In addition, depending on the surface, these proteins may desorb rapidly, leading to time-dependent delays in activation of the immune response, known as the Vroman effect [96]. Preliminary data has suggested this effect could be responsible for cases of patterned thrombus formation in artificial organs and vasculature applications [97].

The presence of these accumulated proteins, which include compounds such as fibrinogen, vitronectin, fibronectin, and other globulin proteins [98], initiate the process of thrombosis. Activated blood platelets and clotting factors stimulate the production of chemo attractants, such as platelet-derived growth factor (PDGR), transforming growth factor (TGF), and cytokines such as interleukins and leukotrienes [99]. These signaling molecules serve to attract many types of phagocytes (monocytes, macrophages, neutrophils, etc.) to the site of accumulation. Macrophages, in particular, begin to excrete

their own chemo attractants, initiating an immunological recruitment cascade. In addition, localized inflammatory neutrophils begin to attack both foreign material and microorganisms through secretion of oxidative species[100]. These oxidative species play a role in inducing the secretion of other chemokines, as well as possessing the ability to activate circulating immune cells [101]. This cyclic process of recruitment, activation, and stress leads to a propagation of injury and disease states.

Oxidative stress also plays a crucial role in the recruitment of other inflammation cells through the process of chemotaxis. Leukocytes can respond to H_2O_2 gradients, NADPHox activation, and LPS stimulation [102, 103]. When these cells identify a foreign body or unknown pathogen, their response is to initiate an oxidative respiratory burst of superoxide and hydrogen peroxide[104]. This burst of ROS and RNS is utilized to destroy the invading material. While inflammatory cells can protect themselves through increased uptake of glutathione [105], vascular tissue cannot. This leads to a cascading loop of increased oxidative stress in tissue, which stimulates chemotaxis recruitment of more inflammatory cells.

Following the initial phase of inflammation, macrophages can internalize the activated and apoptotic neutrophils and subsequently clear them from the injury site. In the case of implanted materials, these macrophages can adhere to the protein coated implant surface and initiate the foreign body response reaction[17]. Adhered macrophages are able to further fuse together to form foreign body giant cells. While the exact signaling required to initiate this cascade is currently unknown, it has been shown that IL-4 and IL-13 [106-108] along with mannose play critical roles in expression of the required adhesion

molecules to elicit macrophage fusion. These adhered macrophages and foreign body giant cells can subsequently interfere with the intended function of the biomaterial in question.

It becomes obvious that oxidative stress plays an important role throughout all steps in the immune response to foreign or implanted material. The following section shall present some examples of this oxidative stress driven failure of biomaterials.

2.6 Examples in practice

One of the most widely used implant polymers is polyurethane (PU) based. PUs have been utilized in applications such as valve replacements, vascular grafts and stent coverings, and in coatings of silicone breast implants [109]. While PU based polymers typically have ideal mechanical properties and show reasonable blood-material compatibility, it was discovered that long-term stability in tissue was a problem when in contact with vascular tissue. This launched a long reaching investigation into methods of in vivo biodegradation in the late 1980's [110]. Aliphatic esters were observed to be hydrolytically degrading in polyester-urethane systems [111]. In polyether-urethane systems, commonly incorporated in breast implants and valve replacements, a phenomenon of micro-fissure formation was seen, termed environmental stress cracking. This phenomenon occurred whether the implant was subjected to intense mechanical stress or not. Further research concluded that ROS produced from adhered macrophages and foreign body giant cells began to degrade and corrode the system. This effect was even greater when metal compounds were incorporated in the urethane device [111, 112], such as in the case of coated implanted pacemaker leads.

Besides PU cracking, aseptic loosening of orthopedic implants can also be a result of oxidative stress. Total hip arthroplasty is especially susceptible to dislodging and failure.

It has been theorized that a combination of mechanical wear, increased intraarticular pressure due to fibrous encapsulation, and high oxidative stress contributing to localized septic tissue, contribute to premature failure of hip implants [113-115]. Supporting this theory, groups have looked into the involvement of free radicals in localized fibrous tissue around implants. Kinov et al. examined tissues obtained directly from patients with both loosened implants and structurally sound implants. From these tissue samples, the group looked at GSH/GSSH ratios, malondialdehyde, and collagen formation [113].

The results indicated a substantial increase in depleted GSH, lipid oxidation, and excessive collagen formation, all indicative of oxidative stress and overproduction of free radicals, in samples from patients with loosened implants, as compared to both intact implants and controls. FIGURE 1 illustrates a hypothesized model of ROS interaction and fibrous formation.

Besides permanent implants, biodegradable materials can also induce an oxidative stress related inflammatory response. Poly lactic co-glycolic acid (PLGA) has been investigated for its particle formulation capacity, and was perceived as being biocompatible, as its degradation products of lactic and glycolic acid are both naturally found in tissue. Yet, it was found that due to slow hydrolysis and high concentration of localized acidic degradation products, compared to what naturally occurs in tissue [116], PLGA has limited use in clinical applications. Springer et al. had investigated the inflammatory response of PLGA nanoparticles administered to the lungs of rats. The group observed a marked influx of both macrophages and neutrophils into the lung tissue of treated rats [117]. The macrophages had demonstrated the ability to engulf these PLGA particles; however a 40 day half-life of these particle dosages was measured. In addition,

localized areas of acidic environments were measured, which can potentially interfere with drug delivery methods utilizing protein and peptides [118]. Other groups have also demonstrated increases in oxidative stress, via lipid peroxidation and GSH/GSSH assays, with respect to degradation of the polymer.

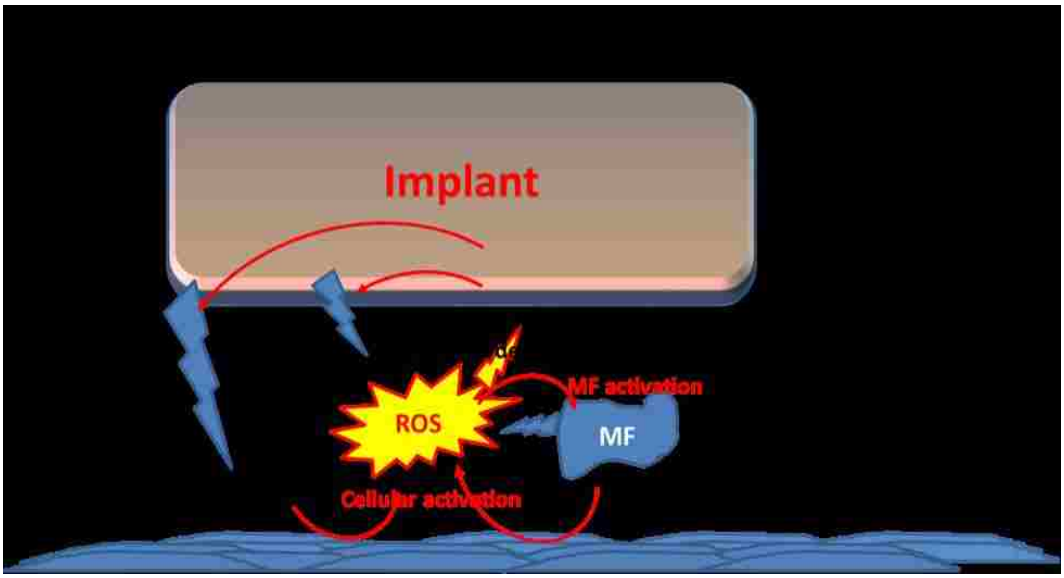

Figure 2-1. A hypothetical model illustrating the mechanism of ROS and implant inflammation

Either mechanical or chemical insults can result in the generation of ROS release. This is either directly from the degradation products, or as a secondary result of the activation of neighboring cells. The release of ROS induces macrophage recruitment and activation. These activated macrophages can also release ROS, further stimulating localized oxidative stress and inflammation. This ROS release also results in potential degradation, mechanical wear and stress cracking of the implant. These responses can all lead to additional oxidative stress, further stimulating localized inflammation. Prolonged effects could lead to fibrosis, implant morbidity and loosening of the implant. MF=Macrophage, ROS = Reactive Oxygen Species.

This indicates that classically biocompatible materials, when subjected to biological conditions, can elicit a relevant host response through the generation of oxidative stress.

2.7 Antioxidant polymers in drug delivery

The relationship between oxidative stress and many diseases, such as Alzheimer's [119] and Parkinson's disease [120], is well documented. And while it stands to reason that antioxidant therapy should provide an effective treatment strategy for these diseases, there exist many limitations, which have prevented their wide scale use. Indeed, conflicting results from many studies confound the beneficial effects of orally delivered antioxidants [121-123]. Direct application or injection of pure antioxidants at the site of interest is also plagued by rapid clearance and nonspecific distribution. Antioxidant polymers are a promising solution to delivering antioxidants, potentially overcoming these problems. Further, antioxidant polymers may also provide supportive benefits to other therapeutic strategies. The following outlines both of these approaches.

2.8 Uses as active pharmaceutical ingredients

Most obviously, antioxidant polymers can be used as a therapeutic alternative to small molecule antioxidants. For instance, trolox, a water soluble analogue of vitamin E, is known to have extensive antioxidant activity. Indeed, trolox is commonly used as a reference standard for total antioxidant potential [124]. Yet, trolox has not seen direct clinical success due to its poor biodistribution and local accumulation. Recently, Poly(trolox) polymers were synthesized, where were demonstrated to undergo enzymatic degradation to release monomers of active trolox. This hydrophobic polymer was formulated into nanoparticles, demonstrating the ability to suppress oxidative damage caused by metal nanoparticle toxicity *in vitro* [22]. Similarly, these antioxidant

nanoparticles also have mitigated the oxidative damage caused by hydrogen peroxide and iron oxide and recovered cellular viability. Perhaps most interestingly about this polymer is not its ability to degrade, nor reduced toxicity attributed to its "polymer" characteristics, but that it possessed the ability to suppress protein carbonyl formation. Overall protein carbonyl and 3-NT levels were suppressed, markers of overall protein damage and damage via RNS respectively. This level of protection was not seen in free trolox, suggesting the route of delivery plays a very important role in therapeutic benefits [45].

Dziubla et. al have also developed a class of poly(beta amino ester) polymers with incorporated phenolic antioxidants such as quercetin and curcumin. Selection of the monomers in formulation gives extensive control over degradation, and subsequent antioxidant release, times via hydrolysis. These polymers have been shown to modulate the oxidative state *in vitro* cell culture models and provide protection against oxidative stress insults, similar to poly(trolox). Some of the advantages provided by this polymer chemistry are that it does not require free-radical polymerization, thereby allowing loading of antioxidant drugs that are susceptible to free-radical damage. In addition, the availability of a large library of commercial diacrylates [125, 126] could be used to tune polymer properties, and that it could be extended to any class of polyphenolic antioxidants. The toxicity profiles observed with the polymers were similar to that of the pure antioxidant, indicating toxicity and activity were functions of the loaded therapeutic content, rather than constituent compounds in the polymer.

Puoci et al. developed a one-step reaction by free radical polymerization to form a PMMA-ferulic acid copolymer. The polymer showed high scavenging activity, with little interference of activity from the PMMA backbone [127]. Application of this material

shows promise in hemodialysis, cosmetic stability, and as preservative agents in food. With the ability to develop limitless classes of high molecular weight antioxidant polymers that exhibit increased stability, decreased toxicity, and tunable delivery rates [45, 128, 129], many of the traditional obstacles involved in direct antioxidant drug delivery can potentially be overcome.

2.9 Uses as pharmaceutical excipients

While developing treatment strategies, it is important to keep in mind that the shelf life and stability of drug formulations are essential in the practical applications of therapeutic systems. The potential for oxidation and decreased efficacy can be seen in both initial formulation, as well as in long term storage. The protection and longevity provided by antioxidant polymers presents an excellent opportunity to increase a biomaterials window of use, even before introduction into the body.

With the increased production (and expense) of protein based therapies such as monoclonal antibodies, hormones, and interleukins, developing methods to increase the shelf life of these compounds has become extremely important. A major pathway of degradation has been identified as oxidation of methionine [130-132]. Strategies to overcome this stability problem have been the addition of chelating agents, chain terminators, or small molecule antioxidants. Common materials utilized are free methionine or sodium thiosulfate [133]. Experiments have shown increased stability of aqueous and lyophilized formulations up to two weeks in dark ambient storage conditions [134] with little loss in activity shown in Figure 2-2.

Expanding on the idea of utilizing slow degrading antioxidant polymers Davis et al. developed a system of carbohydrate-antioxidant (vitamin E) hybrid polymers for prolonged

protection from oxidation in applications of both storage and active delivery of spermatozoa. Their results reported a significant increase in sperm activity utilizing a controllable antioxidant delivery system over time compared to addition of free vitamin E during storage. Additionally, they also saw up to a 20 fold increase of sperm delivery *in vivo* compared to control systems. It was theorized that the protective polymer system was able to protect spermatozoa during the uptake and intracellular trafficking, whereas free vitamin E was quickly leached out and lost during endosome activity [135].

Antioxidant polymers also have applications in long term preserving and prevention of oxidative stress cracking in implant based biomaterials during formulation and storage, which will be discussed in a later section.

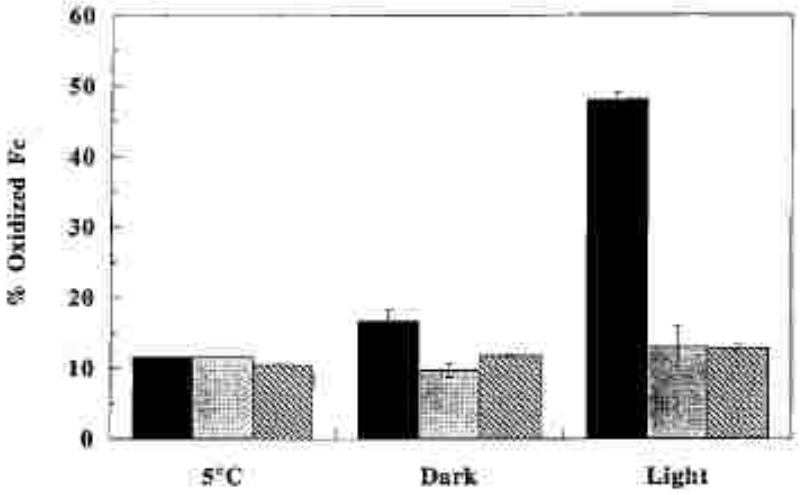

Figure 2-2. Effect of antioxidants on light-induced oxidation of rhuMAb HER2 formulation

Antioxidants were added to the formulation before filling into sample vials. Sample containing no antioxidant (black), 6.3 mM sodium thiosulfate (gray), and 3.5 mM methionine (striped) were stored wrapped (Dark) and unwrapped (Light) in a light box with light intensity of 20 000 lux for 2 weeks. The light box temperature was 27 °C. After light exposure, samples were assessed for methionine oxidation of rhuMAb HER2 by HIC. Results were also compared with the control samples stored in the dark at 5 °C for 2 week. (Figure reproduced from [134])

2.10 Antioxidant polymers in anti-cancer therapies

In addition to direct lipid and DNA damage caused by oxidative stress, endothelial cells can produce cytokines and chemokines that play a role in propagation of the inflammatory response [136] such as interleukin-1 (IL-1), interleukin-6 (IL-6), and tumor necrosis factor alpha (TNF-α) [9, 137]. This inflammatory response can, in turn, induce signal activation of the NF-κB pathway, initiating a cascade of gene activation to regulate antioxidant and immune defenses [138]. Endothelial cells, in response to this pathway activation, begin to secrete and express molecules known as Cellular Adhesion Molecules (CAM) on their surfaces to facilitate leukocyte adhesion, vasodilatation, and transmigration [14].

In recent years, researchers have focused on the cellular mechanisms of tumor cell extravasation and transmigration to other organs and tissues. It has been hypothesized that circulating tumor cells develop cellular adhesion molecule binding ligands specific for E-selectin[139, 140], ICAM-1 [42], and VCAM-1 [42]. Circulating tumor cells of many different origins [141] have been shown to utilize inflammatory response CAMs for adhesion and invasion into downstream vascular beds. Similarly, groups have shown that oxidative stress generation in cell culture experiments through injury agents such as H_2O_2 or TNF-α stimulation can directly stimulate expression of these CAMs, and subsequent studies have shown that circulating tumor cells can firmly adhere to endothelial cells grown in flow culture systems that have been activated by these injury agents, as compared to non-stimulated cells [141]. These results indicate a relationship between oxidative stress generation and cancer formation, either by cytokine stimulation (TNF-α, IL-8, etc.), or supplemental ROS induction (smoking, UV exposure, ionizing radiation). In addition, it has been shown that addition of monoclonal antibodies directed towards E-selectin, ICAM-

1, and VCAM-1 to block current expression in activated endothelial cells can significantly attenuate tumor cell adhesion [141, 142].

New research however has delved into how certain classes of antioxidants modulate cellular responses and pathway activation or deactivation. It has been observed that flavonoids such as quercetin, epicatechin, and curcumin not only reduce oxidative stress, but can suppress inflammatory pathways such as NF-κB and AP-1 through inhibition of specific kinase pathways [35-37]. Interestingly, quercetin is the only reported flavanol with the ability to suppress both ICAM-1 expression and NF-κB activation through JNK pathway inhibition [35]. Flavones on the other hand, have been reported to suppress JNK and ERK pathways, leading to down regulation of ICAM-1, VCAM-1, and E-selectin, along with NF-κB [36], making them great candidates for applications such as cancer metastasis prevention. While the direct mechanism of NF-κB, JNK and ERK pathway suppression is not known, it is theorized that that flavonoids can inhibit transcription by preventing complete phosphorylation of the protein portions required for activation.

Recently, the anti-proliferative effects of curcumin have been of notable interest, owing to its selective cytotoxicity to cancer cell lines, it's antioxidant activity, and low toxicity *in vivo* [143, 144]. Unfortunately, curcumin exhibits poor water solubility and has a therapeutic half-life of under 15 minutes at pH 7.4 [145]. To this end, Tang et al. developed a system of polycurcumins with a range of molecular weights, degradation times, and solubility. One system, labeled PCurc8, was found to be both water soluble and exhibit higher stability than pure curcumin. *In vitro* it was shown to be more cytotoxic by mass than pure curcumin, along with arresting division phases of tumor cells FIGURE 3. *In vivo*,

the easily formulated and injectable system showed remarkable antitumor activity in a xenograph model [146].

This shows promises that direct antioxidant therapy as a biomaterial in of itself, which have demonstrated suppression of these CAMs, can be utilized as a treatment for prevention of tumor formation.

2.11 Antioxidant polymers in wound healing and tissue engineering

In the previous sections the direct and indirect ways oxidative stress plays a role in relation to biomaterial function have been discussed. Free radicals can directly damage a biomaterial, such as in the case of polyurethane coatings and hip implants. Indirect methods of failure can occur such as the degradation of newer generation materials, previously believed to be biocompatible. The following section reviews potential applications of antioxidant polymers to address both these direct and indirect stress mechanisms.

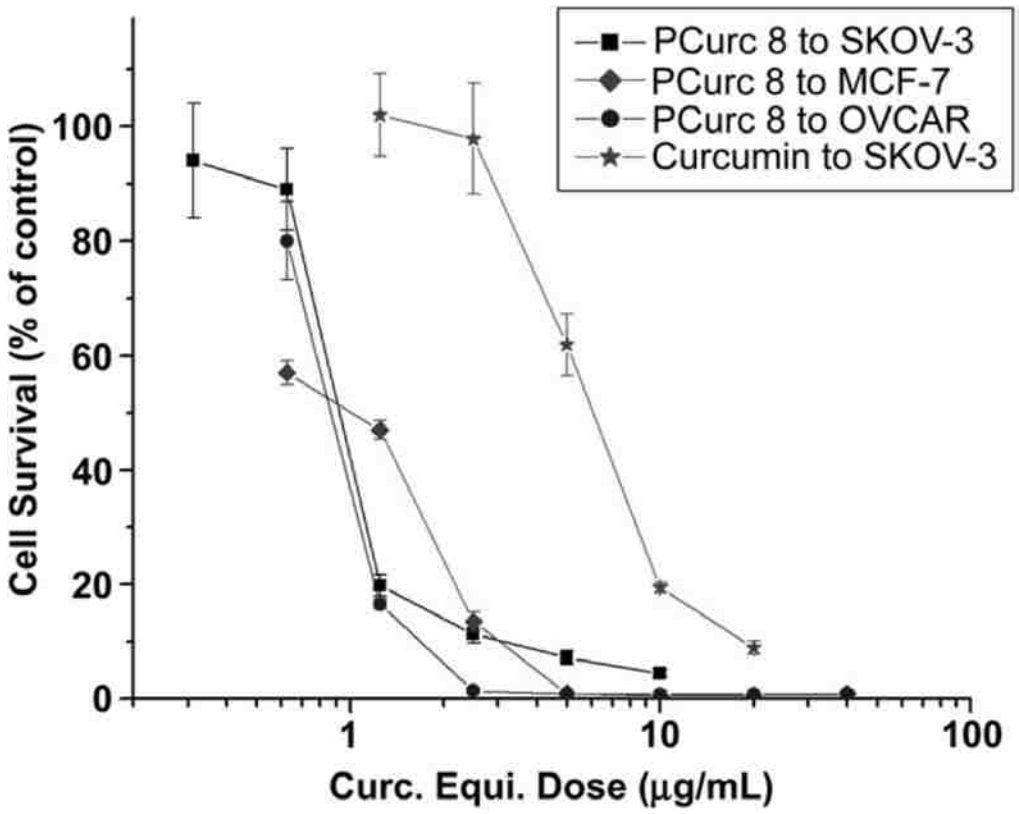

Figure 2-3. Cytotoxicity of PCurc 8 to SKOV-3, OVCAR-3 and MCF-7 cancer cell lines

Cells were treated with PCurc 8 for 72 h followed by 24 h incubation in free medium. (Figure reproduced from [146])

2.12 Antioxidant polymers incorporated into biomaterials

Recently, groups have attempted to mitigate the oxidative stress induced from biomaterial implantations. Initially, research was focused into developing biomaterial platforms that have a neutral host response, such as systems with PEG coatings, or degradable platforms utilizing polyketals[147]. Others have modified existing material selections to incorporate small molecule antioxidants or even enzymatic antioxidants. Strategies to incorporate antioxidants into existing scaffolds or hydrogels have also proven effective in creating artificial diffusion barriers, simulating the effects of a degradable antioxidant polymer system [148]. Initial work with these methods of antioxidant grafting or loading has proven effective *in vivo*.

2.13 Direct prevention of implant failure

Within the past five years, focus has shifted towards prevention of aseptic loosening of implanted materials through the use of antioxidants to mediate damage caused by extensive wear and particulate formation over time. Initially research focused on elimination of oxidized material during creation of the implant[149] using methods such as inert gas irradiation. Even though these methods improved material shelf life, a growing amount of evidence supported the oxidation stress *in vivo* hypothesis. Stemming from this information, a second generation class of implants was developed utilizing antioxidant stabilizing compounds, such as Vitamin E. Vitamin E is typically added in low concentrations during consolidation of the ethylene polymer. Clinical data suggests blended formulations with concentrations less than 0.1% vitamin E maintain the same physical and mechanical properties [150] and can prevention of oxidation up to 24 months post implantation [151]. In addition, preliminary *in vitro* and *in vivo* data using particulate

matter from antioxidant loaded implants indicates a reduction of phagocyte adhesion and activity [152]. Promising results stemming from these initial studies provide a framework for the incorporation of long lasting antioxidant polymers to provide protection over extended periods of biomaterial use. One can also imagine with classes of antioxidant materials exhibiting high mechanical loading capabilities, that higher antioxidant content can theoretically be incorporated into implants as well.

Another example of utilizing antioxidant polymers to improve biocompatibility is in the area of ophthalmology. Cirillo et al. reported on the ability to graft quercetin, a potent flavonoid, into traditional pHEMA hydrogels used in contact lenses through free radical grafting reactions discussed earlier. Quercetin was selected owing to its anti-inflammatory properties and ability to prevent cataract formation in preliminary *in vitro* models. Contact lenses have the potential to induce ocular damage by interrupting the ability of the epithelium to absorb oxygen from the atmosphere [153]. Similarly, UV radiation can propagate the formation of free radicals, which can compound the oxidative stress effect from restriction of oxygen supply to the eye. The results of this study indicated that the Quercetin-HEMA gels exhibited significant antioxidant activity, and an irritancy index of zero, meaning high compatibility and no signs of irritant effects in a chicken embryo chorioallantoic membrane (CAM) model [154] as opposed to unmodified HEMA lenses, which scored an irritancy index of 1 (mild irritant effects, good compatibility). This application of grafting antioxidants into externally applied biomaterials can begin to pave the way to suppressing the damage associated with ocular irritation. Simultaneously, the delivery of quercetin directly to ocular epithelium can help treat existing diseases such as cataracts and glaucoma.

2.14 Mitigation of toxic side effects

While antioxidants show promise in the ability to prevent modes of failure in biomaterial implants such as joint replacements and contacts, it is also important to delve into the ability of these antioxidants to mitigate the eventual damage caused by the degradation of newer classes of biomaterials. In the recent years, many newer generations of materials have been developed with the premise to degrade over time, allowing the body's own wound healing process to coincide with deterioration and infiltrate through the material. Implant systems once thought to be "biocompatible" such as TEGDMA, commonly used as inert coatings on dental implants, PEG, considered the gold standard in immune system masking, and PLA/PLGA, a naturally derived copolymer from lactic and glycolic acid, have all been shown to induce oxidative stress over time (TEGDMA, PLA/PLGA)[155, 156], or elicit a host immune response in the form of antibody synthesis (PEG) [157].

With the advent of these discoveries, it became clear that when developing new classes of biomaterials the entire lifetime of the implant must be taken into account. This not only includes response upon implantation but also during its degradation time. Because of the oxidative nature of these end products, grafting, or blending, antioxidant polymers into the material is an ideal strategy for mitigating this potential damage.

One example is that of dental composites containing HEMA and TEGDMA. These two polymers are an attractive alternative to typical amalgam and gold in classical fillings. Within the past 5 years, implants have shifted to approximately 50% by weight of newer HEMA/TEGDMA bonding resins [158]. It has been shown that as the resin deteriorates from normal wear and tear, particulate matter can lodge in the lung epithelium, and

inducing oxidative stress mediated damage. In cell culture models, particulate matter cultured with human pulp and gingival fibroblasts was associated with depleted GSH and eventual cell apoptosis [159, 160]. Schweikl et al. investigated the effect of increased oxidative stress of both compounds. It was discovered that concentrations of 1 mmol/L in V79 fibroblast cells induced substantial genotoxic effects. Cell cycle disruption was observed, along with significant micronuclei formation, both indications of genotoxic effects. They hypothesized this was due to oxidative stress, and examined the effect of N-acetyl cysteine (NAC) would have on the same cell model. The results demonstrated that concentrations of 10 mmol/L of NAC significantly decreased the micronuclei formation resulting from both HEMA and TEGDMA treatments [161]. This work has set a fundamental basis into the application of antioxidants *in vivo* may be a viable strategy to reduce toxic side effects, and increasing overall biocompatibility.

Another example of polymeric materials utilized to suppress toxic side effect is to utilize enzymatic antioxidants or mimetic. By covalently conjugating super oxide dismutase mimetic (SODm) to the backbone of UHMWPE and PU polymers, a new platform for biomaterial structures was created. These SODm grafted polymers showed potent acute and chronic anti-inflammatory properties *in vivo*. Rat implants showed inhibition of neutrophil infiltration over 3 days. Extended out to 28 days, there was a significant suppression of foreign body giant cells and fibrous encapsulation [162]. Figure 2-4 illustrates the cell count and capsule thickness as a function of SODm conjugation.

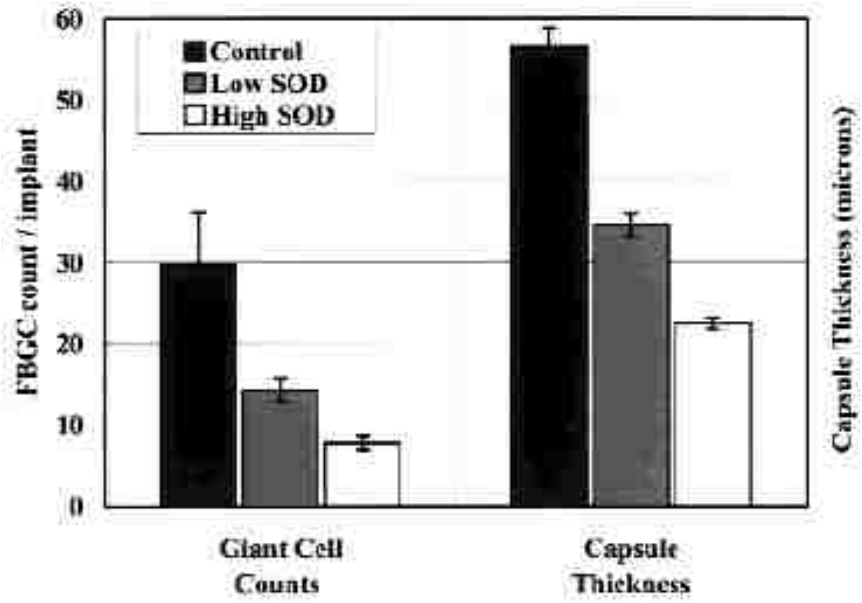

Figure 2-4. Effect of SODm grafting on polymer implants

Graph of FBGCs counts (left) and capsule thickness (right) for control and SODm-treated PE implants at 28 days. (Figure reproduced from [162])

2.15 Stimulation of direct wound healing

In addition to the utilization of antioxidants and antioxidant polymers in biomaterial implants, antioxidants as a direct delivery agent have been shown to possess properties to enhance the body's ability to heal itself. This has obvious advantages in enhancing recovery time from surgical wounds or injury unrelated to biomaterial insertion.

Previously groups have shown that incorporation of natural antioxidants, such as quercetin and curcumin, into 3D hydrogel scaffolds had successfully improved the wound healing response to deliberate dermal injury. The antioxidant loaded scaffolds showed reduction in healing time and dramatically reduced scarring formation [163, 164]. Similarly, carbodymethylcellulose (CMC) gels with entrapped SOD showed similar effects both *in vitro* and *in vivo* [165].

2.16 Conclusions and perspectives

In conclusion, it has become apparent that there are nearly limitless strategies for developing new and novel antioxidants for clinical applications. Table 2-3 consolidates a list of antioxidant polymers and their applications. Additionally, as our knowledge expands on the effects of oxidative stress and how they relate to diseases, so to do our options for utilizing antioxidants in our current treatment strategies, either as direct therapies or in tandem with other biomaterials. By controlling the level and time of delivery through new chemistries and systems, modulating the oxidative state of the body can be accomplished, allowing for greater flexibility and treatment windows in traditional biomaterials. While clinical data and application at this time has been limited due to unknown factors or mechanisms of antioxidant function, the consistently positive results obtained from

ongoing *in vivo* trails will begin to pave the way into a new future of medicine and applications.

Table 2-3: Antioxidant polymers and their applications

Polymer Structure /Backbone	Functional Antioxidant	Administration Method	Application	Mechanism of Action	Ref
Carbohydrate-antioxidant hybrid polymer	α-tocopherol	Mixed in Seminal Fluid	Prolong functional viability and fertility rates of mammalian spermatozoa	Specific uptake of carbohydrate polymer in sperm prevents oxidative damage during storage.	[135]
Poly(Trolox)	Trolox	Nanoparticles	Slow release of trolox through degradation has potential in controlling cell status in biomedical and tissue engineering applications	Poly(Trolox) suppresses oxidative stress levels in cells. In addition, polymeric form has shown to reduce protein carbonyl levels, a feature not seen in free trolox	[45]
Poly(Rutin)	Rutin	Water solubilized	Demonstrated high superoxide scavenging ability and inhibition of LDL oxidation	Antioxidant capability more potent in polymer form. Increased superoxide scavenging along with prevention of cellular damage	[128]
UHMWPE	Superoxide Dismutase Mimic	Implantable Gel	Significant suppression of inflammatory response along with long term inhibition of fibrous encapsulation	SOD reduces superoxide at the biomaterial interface, inhibiting macrophage activation and neutrophil infiltration	[162]
HEMA	Quercetin	Implantable Hydrogel	Contact lenses formed using quercetin-HEMA exhibit irritancy index of zero	Active quercetin mitigates oxidative stress damage caused by oxygen deficiency due to contact lens barrier	[154]

Chapter 3. Research Goals

3.1 Introduction

In this body of work, we have developed antioxidant and anti-inflammatory delivery systems to be used in practical applications, such as the treatment of cancer and arthritis. These delivery devices are in the form of nanoparticles that can be modified to target cell types of interest, or provide long circulation times due to the stealth enhancing properties of PEGylation. We have shown that the antioxidant systems can inhibit free radical damage and restore cellular viability in vivo. Additionally we have demonstrated that these particles of poly(trolox) can be utilized *in vivo* to reduce cytokine levels associated with oxidative stress, and prevent protein oxidation. This is a unique feature not observed in the native form of trolox, conferring an additional level of protection for future studies.

In a similar fashion, our anti-inflammatory particles can suppress the expression of inflammatory markers on the surface of vascular cells, which circulating tumor cells can utilize to attach to the vascular bed. The long term release provided by these polymer nanoparticles can prevent tumor cells from adhering for up to 72 hours, coinciding with the natural inflammation response cascade.

3.2 Objectives and Significance

The overall hypothesis of this work is:

> *Antioxidant and anti-inflammatory polymer systems can be utilized to treat a variety of clinically relevant injuries through the suppression of oxidative stress and inflammation.*

In order to test this hypothesis, three stages of research were planned. Each stage is described in detail below:

3.2.1 Specific Aim 1: Utilization of targeted antioxidant nanoparticles to inhibit iron oxide nanoparticle injury

A. Development of poly(trolox) nanoparticles with a functional antibody coating specific towards PECAM-1, a constitutively expressed protein on the surface of endothelial cells.
B. Quantification of particle specificity, internalization potential, and antioxidant capacity in an endothelial cell culture model.
C. Utilize targeted poly(trolox) nanoparticles to inhibit the toxicity associated with iron oxide nanoparticles.

3.2.1.1 Hypothesis #1

Poly(trolox) nanoparticles can be modified to actively target vascular cells to suppress the oxidative injury from iron oxide nanoparticle accumulation.

3.2.1.2 Significance and Outcome

Chapter 4 highlights the experiments used to test our hypothesis. Poly(trolox) nanoparticles were successfully synthesized using a solvent in solvent nanoprecipitation technique. These particles were then coupled with a targeting antibody directed towards PECAM-1. These nanoparticles adhered to vascular cells, internalized, and significantly reduced background oxidative stress. We then determined the therapeutic efficacy of targeted PTx in an iron oxide nanoparticle injury model. It was found that we could not only inhibit oxidative stress, but also recover cellular viability. This result demonstrates

the ability to not only target nanoparticles to sites of interest, but reveals that antioxidant therapy can be a viable treatment option to prevent injury.

3.2.2 Specific aim 2: Utilize Poly(trolox) nanoparticles to treat the damage caused by rheumatoid arthritis *in vivo*

A. Encapsulate poly(trolox) in a biocompatible polymer that provides stealth properties and long circulation times *in vivo*.
B. Investigate the ability of poly(trolox) nanoparticles to accumulate in inflamed joints and tissue.
C. Study the effects of antioxidant therapy on the deleterious effects in the joints of rheumatoid arthritis

3.2.2.1 Hypothesis #2

The antioxidant protection provided by poly(trolox) nanoparticles can inhibit the oxidative stress and inflammation stemming from rheumatoid arthritis

3.2.2.2 Significance and Outcome

In Chapter 5 we describe how we can utilize our antioxidant nanoparticles into an *in vivo* injury that is clinically relevant. Rheumatoid arthritis is an autoimmune disease that causes localized inflammation, oxidative stress, and damage to joints and cartilage. We found that our particles can accumulate at the inflamed joints due, in part, to the EPR-like effect from the disrupted vasculature. These particles did not appear to reduce the symptoms of arthritis by a visual scoring system. However, upon further analysis it was found that they did in fact reduce oxidative protein damage, recover antioxidant capacity,

and significantly down regulate cytokine levels associated with oxidative stress, such as IL-6 and TNF-α.

3.2.3 Specific Aim 3: Develop a novel anti-inflammatory polymer delivery system to inhibit the incidence of cancer metastasis

A. Synthesize and characterize an anti-inflammatory poly(beta-amino ester) of apigenin
B. Investigate the activity, loading potential, and release characteristics of apigenin PβAE nanoparticles
C. Evaluate the potential of apigenin PβAE nanoparticles to prevent tumor cell adhesion to inflamed vascular beds.

3.2.3.1 Hypothesis #3

Apigenin PβAE nanoparticle systems can be utilized to prevent inflammation-mediated tumor cell adhesion to endothelial cells.

3.2.3.2 Significance and Outcome

A linear chain polymer comprised of apigenin was developed as described in Chapter 6. This polymer was formed into a nanoparticle delivery device similar to other chapters. It was found that the PβAE loaded nanoparticles released active therapeutic for up to 72 hours. The apigenin PβAE was effective in reducing inflammation, as observed through inflammatory CAM analysis. As a benefit of these anti-inflammatory properties, the potential of circulating tumor cells to adhere to vascular cells was reduced.

Chapter 4. Suppression of Iron Oxide Injury

Based on the research article:

> David Cochran, P. Wattamwar, R. Wydra, J.Z. Hilt, K.W. Anderson, R. Eitel, and T. Dziubla. "Suppressing Iron Oxide Nanoparticle Toxicity by Vascular Targeted Antioxidant Polymer Nanoparticles", Biomaterials.

4.1 Introduction

Owing to their superparamagnetic properties [166], iron oxide nanoparticles have seen applications as varied as MRI contrast agents [167], iron supplementation in cases of anemia [168], localized hyperthermia generation for increased drug efficacy, or even direct thermoablation of tumor tissue [169]. Additionally, researchers have exploited the controllable size, shape, and potential surface chemistry of these nanoparticles to develop targeted therapy strategies utilizing the iron oxide core. For example, the core can be modified with a poly(ethylene glycol)-based hydrogel shell that entraps a wide range of therapeutics, or consist of surface-bound targeting ligands such as antibodies or peptides [170, 171]. However, despite clinical acceptance, the use of iron oxide particles has also come under scrutiny owning to their ability to induce cellular toxicity and nephrotoxicity. Due to their size, ultrafine iron oxide nanoparticles, either in a biomedical setting or in an environmental contaminant setting (e.g., miners, industrial manufacturing, *etc.*), are readily internalized within cells, including the vascular endothelium [172, 173]. Toxicity associated with iron oxide nanoparticles stems, in part, from catalytic generation of free radicals through Fenton chemistry [174], leading to oxidative stress. Even iron oxide particles stabilized with coatings such as dextran or citric acid have demonstrated oxidative stress induction [175].

Oxidative stress is a key pathological process in a variety of disease states (ischemia – reperfusion injury [1, 2], acute lung [3] and renal injury [4]) and is characterized by the formation of a wide range of reactive oxygen species (ROS), which can cause severe DNA, protein, and lipid damage leading to cellular dysfunction and death [5, 6]. Theoretically, it should be possible to mitigate iron oxide induced cell injury by delivering antioxidants directly to the site of injury [25-27]. Yet, in order to realize antioxidant therapy for treatment of iron oxide toxicity, it must be possible to deliver active antioxidant directly to the site of action for a sufficient time [28, 29]. In the case of most biomedical applications of iron oxide nanoparticles (e.g., MRI [176] and chemotherapy adjuncts [177]), this site of action is the vascular bed.

Orally administered antioxidants are mostly inactivated through first pass metabolism well before they are able to reach the vascular bed [178]. Indeed, due to the highly labile nature of antioxidants, even direct injection fails to accumulate in the vasculature cells at sufficient levels to be effective. To overcome the stability limitation, we have previously reported on a the development of a degradable antioxidant polymer, poly(trolox) (PTx), which demonstrated the ability to suppress oxidative cellular stress [22]. This polymer is readily synthesized into nanoparticles that can suppress the formation of oxidized cellular products [22]. In this work, we extend this capability by actively targeting poly(trolox) nanoparticles to vascular endothelial cells through surface coating of the nanoparticles with platelet endothelial cellular adhesion molecule-1 (PECAM-1) antibodies.

PECAM-1 is a member of the immunoglobulin superfamily that regulates cell-cell adhesion and transmigration [179-182]. It is an especially useful target for vascular targeting due to its constant expression at cell-cell boarders in the endothelium [180].

PECAM-1 provides an excellent basis for targeting antioxidants to vascular beds, one of the primary residence areas for iron oxide nanoparticles. Previous work has demonstrated the ability to physically absorb targeting antibodies to therapeutic particles for active targeting to specific adhesion molecule groups [183-185]. These targeting antibodies have shown to have higher specificity towards sites of interest, especially in tumors and organs, as compared to non-targeted therapeutics [186, 187].

We hypothesize that by combining antioxidant polymer nanoparticles with the active endothelial targeting provided by antibodies directed towards PECAM-1, an effective therapeutic can be realized that has the capacity to intercept and prevent the free radical damage caused by the accumulation of iron oxide nanoparticles in vasculature used in many applications.

4.2 Materials and Methods

4.2.1 Reagents

All reagents received were used without further purification. Poly(trolox) 1000 and 2500 were synthesized in lab as previously reported [188].

2', 7'-dichlorodihydrofluorescein diacetate (DCF-DA) was purchased from Invitrogen. DyLight 488 antibody labeling kit, anti-mouse IgG counterstain, and 4', 6-diamidino-2-phenylindole (DAPI) nuclear stain, were purchased from Piercenet. Nonspecific mouse IgG was purchased from JacksonImmuno. Mouse anti-human anti-PECAM-1 antibodies were created and purified in house through the use of hybridoma cell lines (cell line designation P2B1) purchased from the Developmental Studies Hybridoma Bank. $Na^{125}I$ (Sodium Iodide) was purchased from Perkin Elmer. Polystyrene

beads were purchased from Polysciences Inc. Gel-clot LAL endotoxin test kits were purchased from Lonza. All other materials and solvents were purchased from Sigma-Aldrich.

4.2.2 Citric acid coated iron oxide nanoparticle formulation

A one-pot co-precipitation method was used to prepare the core citric acid coated iron oxide nanoparticles as previously reported [189]. Briefly, an aqueous solutions of $FeCl_3 \cdot 6H_2O$ and $FeCl_2.4H_2O$ were combined in a 2:1 molar ratio in a sealed three-neck flask under vigorous stirring and an inert N_2 environment. Once 85 °C was reached, NH_4OH was injected into the vessel followed by 2 M citric acid. The reaction was carried out for 1 hour. The particles were washed with ethanol and retrieved with magnetic decanting. Following the wash, the particles were dried and stored under vacuum.

4.2.3 Poly(trolox) nanoparticle formulation and characterization

A single emulsion technique was used to formulate nanoparticles. Initially, poly(trolox) was dissolved in acetone. This solution was then added drop wise into methanol vortexing at 2000 RPM. The final concentration of acetone to methanol was 10% v/v. The nanoparticle solution was then dialyzed against sterile PBS overnight. The dialyzed solution was then centrifuged three separate times at 22,000 RPM for 1 hour and resuspended in fresh sterile DI water to remove all traces of methanol, as confirmed by GC analysis (data not shown). Particle size and zeta potential was measured after centrifugation using dynamic light scattering on Malvern Zetasizer Nano.

4.2.4 Antibody loading and characterization

AntiPECAM-1 and mouse IgG were radiolabeled with ^{125}I using the Iodogen Method (Pierce Chemical) and purified using Bio-Rad Desalting columns, as previously described.[182] Antibody concentrations totaling 10,000 AB/μm^2 were incubated with 1 mg of PTx and Polystyrene nanoparticles (100 nm) overnight at 20ºC. Bovine Serum Albumin (Fisher Scientific) in PBS was then added to a final concentration of 1% BSA to block remaining surface sites for 1 hour before use. Particles were then washed in triplicate by centrifuging at 22,000 RPM for 30 minutes and resuspended in 1% BSA to wash away unbound antibody. Antibody was traced in both supernatant and pellets using a PerkinElmer 2470 Automatic Gamma Counter. Stability was determined by storing nanoparticles at 20ºC for one week, then repeating the centrifugation cycle.

4.2.5 Antibody and particle binding to HUVEC model

HUVECs were obtained by Lonza and cultured in EGM-2 media (Lonza) supplemented with penicillin and streptomycin. HUVECs, passage 4 to 8, were seeded at a density of 25,000 cells/cm^2 and cultured overnight in 24 well plates. Antibody coated particles were then incubated with cells for 30 minutes. Following incubation, HUVECs were rinsed 5 times with PBS. Cells were lysed using a solution of 5% Triton-X 100 and 0.1 N sodium hydroxide in PBS and lysates were analyzed using a gamma counter. Antibody molecules per cell were estimated by the masses recorded and area of the microplate well divided by the average area of a cell, assuming complete confluence.

4.2.6 *In Vitro* iron oxide nanoparticle toxicity assessment

HUVECs were seeded at a density of 25,000 cells/cm^2 were cultured for 24 hours. Iron oxide nanoparticles in media were placed in a sonicating bath for 2 hours to aid in

suspension. Iron oxide nanoparticles were then added to the cells. After 24 hours, cells were washed 3 times using warm media. Viability was determined by incubation of Calcein AM for 30 minutes and fluorescence measured at 495ex/515em. Viability was measured by the following equation, where the control refers to untreated cells:

$$\%\, Viability = \frac{Fluorescence_{sample} - Fluorescence_{blank}}{Fluorescence_{control} - Fluorescence_{blank}}$$

4.2.7 *In Vitro* cellular protection against background oxidative stress

HUVECs seeded at a density of 25,000 cells/cm^2 were cultured for 24 hours. DCF-DA at a concentration of 10 µM was added and one hour later, polymers nanoparticles added. After 30 minutes, the cells are washed 5 times using warm media to remove unbound particles. 24 hours later, fluorescence was measured from bottom at an excitation wavelength of 485 nm and emission wavelength of 528 nm using a GENios Pro fluorescence spectrophotometer. Percent protection from the antioxidant polymer was by the following equation, whereas the control refers to untreated cells that underwent the same washing steps:

$$\%\, Protection = \frac{Fluorescence_{sample} - Fluorescence_{blank}}{Fluorescence_{control} - Fluorescence_{blank}}$$

4.2.8 *In Vitro* cellular protection against iron oxide induced oxidative stress

HUVECs were prepared as in the previous section. AntiPECAM-1/PTx-1000 at 0.5, and 1 mg/mL, AntiPECAM-1/PS, and IgG/PTx 1000 at 1 mg/mL were incubated for 30 minutes. Afterwards, the cells are washed 5 times using warm media to remove unbound particles. Additionally, PTx 1000 without any targeting coating was incubated for the entire duration of the experiment. One hour later, iron oxide nanoparticles were added at

a concentration of 30 µg/mL. After 24 hours, ROS levels were recorded as previously described. Viability was determined by incubation of Calcein AM for 30 minutes and fluorescence measured at 495ex/515em. In order to account for dead cells exhibiting no DCF fluorescence, normalized percent protection from injury by the antioxidant polymer was obtained by the following equation:

$$\%\ Normalized\ Protection = \frac{\%\ Protection}{\%\ Viability}$$

Additionally, to determine endotoxin levels, iron oxide nanoparticles were subjected to gel-clot LAL endotoxin analysis according to manufacturer's instructions.

4.2.9 Determination of particle internalization

HUVECs were seeded on glass slides and grown to confluence. Green fluorescent polystyrene beads (200 nm) were coated and purified with anti-PECAM-1 and IgG as described previously. Antibody coated particles were then added to HUVEC cultures and washed 5 times using warm media after 30 minutes at 37ºC. Cells were than fixed in 2% paraformaldehyde solution either immediately or after 8 hours. Following fixation, cells were labeled with secondary antibody for 30 minutes and washed. Cells were permeabilized and stained with DAPI. Glass slides were than imaged utilizing a fluorescent microscope and analyzed for internalization and particle counts (Nikon Elements 4.2). In short, overlaid images depicting orange (red + green) particles were marked as surface bound, whereas green particles were marked as internalized. Similarly, particle counts per cell were determined by pixel area of all particles divided by the pixel area of a single particle as determined by the Nikon Elements software.

4.3 Results

4.3.1 Poly(trolox) nanoparticle synthesis and characterization

To promote physioabsorption of antibodies onto PTx nanoparticles, a surfactant-free nano-precipitation method was developed. It was found that at the concentrations tested (0.5, 1, 10 mg/mL polymer in solvent phase), the nanoparticle size was independent of the initial polymer concentration (Figure 4-1). Formulations of nanoparticles with solvent concentration of over 10 mg/mL resulted in significant aggregation and inconsistent particle sizes. Particles ranged in size from 150 to 160 nm, within the limit for CAM mediated internalization [190]. Analysis of the zeta potential for both PTx 1000 and 2500 revealed charges between -21 to -32 mV (Figure 4-1). This moderate negative charge promotes the ability for physioabsorption of antibodies to their surface, providing a basis for further targeting modification.

4.3.2 Antibody coating and stability determination

The ability to physically absorb targeting antibodies to the surface of PTx nanoparticles was evaluated through the use of ^{125}I-IgG tracing. Antibodies were radiolabeled as described in the methods section. To aid in complete coverage, antibodies were incubated with the nanoparticles at a solution concentration equivalent to 10,000 antibodies/μm^2 particle surface area, 1.2 times the theoretical monolayer coating based on antibody size and particle area. The particles were then centrifuged to separate solid particles from free antibody. Based upon radiotracing of antibody bound to PTx 1000 and 2500 nanoparticles, we observe 57.04 ± 5.7% (PTx 1000) and 56 ± 4.7% (PTx 2500) surface coverage of antibody, or 826 ± 67 (PTx 1000) and 812 ± 66 (PTx 2500) antibodies / particle (Figure 4-1).

While physiochemical adsorption is a convenient and easy mechanism of nanoparticle surface modification, if the adsorption strength is too low, the antibody coating could potentially be replaced by other proteins found in serum and thereby lose targeting capacity. To test the stability of the antibody coating, the particles were incubated at 4ºC in 1wt% BSA for 7 days of storage. Importantly, it was determined that 94 ± 1.5% (PTx 1000) to 99 ± 1.3% (PTx 2500) of the antibody remained attached to the nanoparticle surface, suggesting stability in storage conditions (Figure 4-1). This is consistent with prior work with antibody coating of polystyrene and poly(lactic glycolic) acid nanoparticles [191].

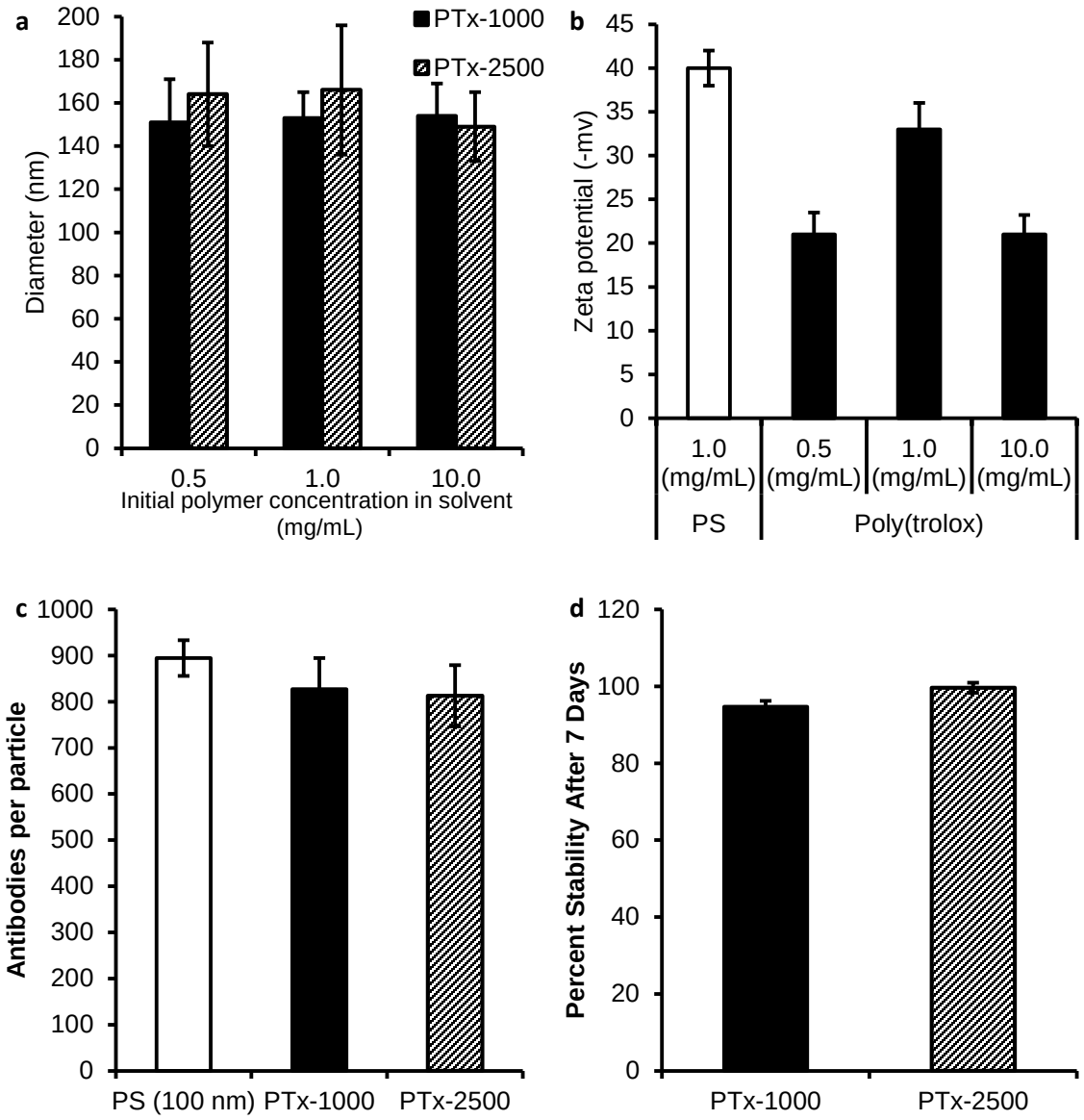

Figure 4-1. Characterization of poly(trolox) nanoparticles

A single step, surfactant free solvent extraction method was used to prepare poly(trolox) nanoparticles. Particle size (A) and zeta potential (B) were measured after centrifugation using dynamic light scattering (M ± SD, n=3). Poly(trolox)-1000 and Polystyrene nanoparticles were antibody coated using physioabsorption, with extent of adsorption determined using 125I Radiolabeled IgG. Theoretical loading was determined as a ratio of the surface area of the particle divided by the surface area of the Fc base fragment of

the antibody (C) (approximately 3 nm x 3 nm) (M ± SD, n=3). Stability of antibody coating was determined by monitoring the extent of antibody coating remaining on the particle after 1 week incubation. Particles were then centrifuged for 30 minutes and pellet examined in gamma counter to determine viability of antibody coating. Near 100% of the antibody coating is retained after one week (D) (M ± SD, n=3).

4.3.3 Iron oxide nanoparticles exhibit toxicity and ROS generation in Human Umbilical Vein Endothelial Cells (HUVEC)

Although iron oxide nanoparticles have been formulated with many types of coatings to inhibit either toxic effects or improve stability, they still are able to induce oxidative stress within cells. Specifically, citric acid coated nanoparticles were tested due to their emerging prevalence in early clinical trial biomedical applications, owing to their hydrophilic properties and stability in aqueous media [192, 193]. These nanoparticles can be easily produced and coated in a one-step synthesis reaction from the reduction of iron salt in citric acid buffer.

While these particles are generally referred to as chemically unreactive, they directly react with viability stains, such as MTT and MTS, which rely upon reduction to measure cell activity [194]. To avoid this artifact, cell viability was assessed using Calcein AM (live) stain, which relies upon esterase activity as a means of determining intact cells. In this work, we observed a concentration dependent toxicity and ROS generation over a period of 24 hours. The LD50 of iron oxide was determined to be 35 μg/mL. This toxicity was related to the ability of the particles to induce oxidative stress as measured by a 2', 7'-dichlorodihydrofluorescein (DCF) fluorescence assay. At 15 μg/mL, the DCF fluorescence was 307 ± 33% over control at 24 hours (Figure 4-2). At increasing concentrations of iron oxide nanoparticles, DCF fluorescence decreases due to significant cellular death and detachment of cells.

4.3.4 AntiPECAM-1 and AntiPECAM-1/PTx nanoparticles, but not IgG, bind specifically to HUVECs

In order to evaluate the ability of antiPECAM-1/PTx to adhere to vasculature, a HUVEC cell culture model was once again employed. Binding of free antiPECAM-1

antibody and antiPECAM-1/PTx were tested against nonspecific mouse IgG. In antiPECAM-1/PTx studies, to eliminate the possible artifact of detached antiPECAM-1 adhering to the cell surface, antiPECAM-1/PTx binding was evaluated using a non-specific 5wt% ^{125}I-IgG tracer.

Concentration dependent binding profiles of both free antibody and coated particles were observed and compared to the non-specific binding observed from IgG controls.

The antiPECAM-1/PTx nanoparticles exhibit an order of magnitude higher specificity and adhesion with 350 particles/cell compared to 40 particles/cell for IgG coated particles at an initial incubation concentration of 0.8 mg/mL.

It is interesting to note that in each concentration of the targeted antioxidant nanoparticles, we conclude that 1/10th of incubated particles adhered to the cell monolayer following five wash cycles (Figure 4-3).

4.3.5 Antioxidant function of AntiPECAM-1/PTx nanoparticles in HUVECs

To verify if antiPECAM-1/PTx nanoparticles are capable of inhibiting cellular oxidative stress, a DCF assay was used. For PTx 1000, a dose dependent decrease in ROS levels was observed, reaching a maximum of 19% reduction at 0.6 mg/ml.

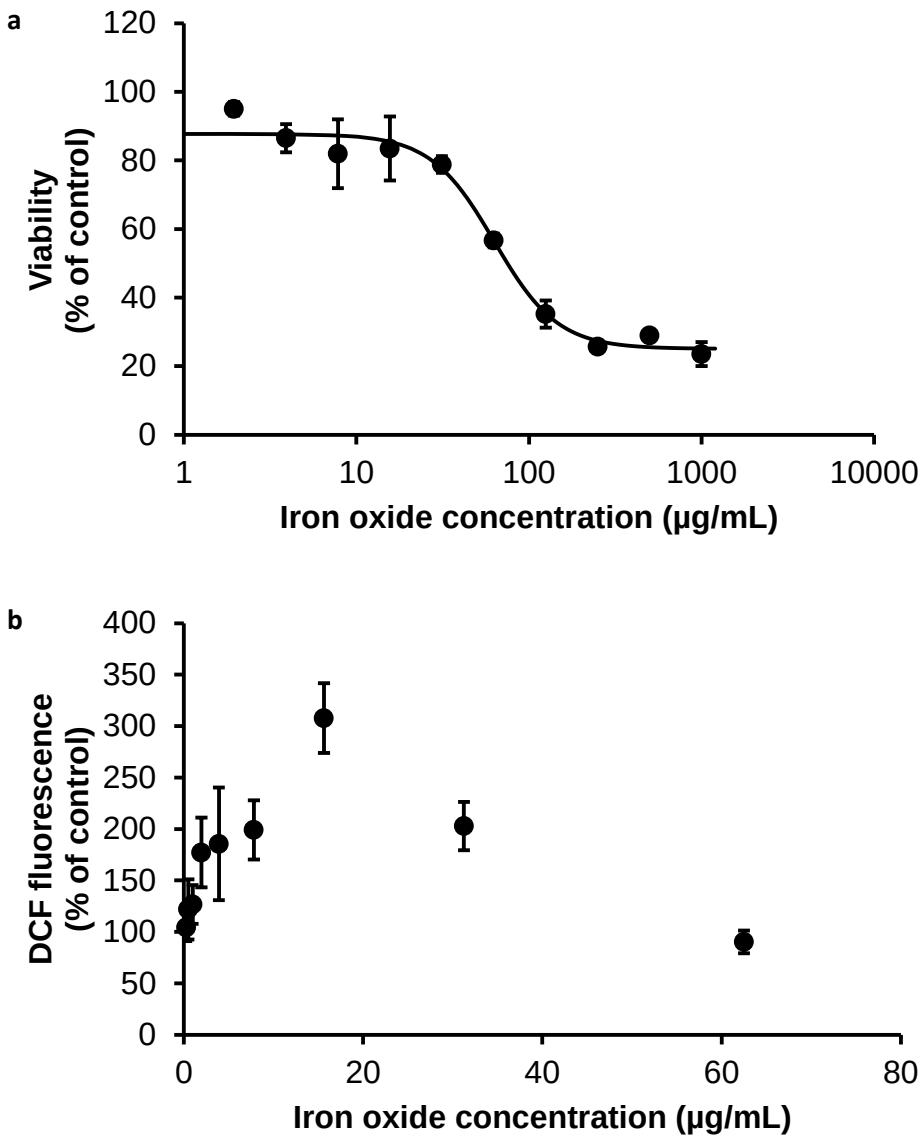

Figure 4-2. Iron oxide toxicity and ROS in HUVECs

HUVECs were incubated with iron oxide nanoparticles in a range of concentrations for 24 hours to determine viability and ROS levels. From the viability (A), the LD50 was determined to be 35 µg/mL. A close-up view of ROS levels near this concentration are shown in (B). ROS levels peak at 300% over background at a sub-lethal concentration of 15 µg/mL followed by a decline in level as significant cellular death occurs.

In the case of PTx 2500, the 0.8 mg/mL concentration had an 18% reduction of background oxidation, with no therapeutic benefit at lower concentrations. It is hypothesized that this is due to the smaller molecular weight chains degrading faster, thereby exhibiting a slight antioxidant effect, compared to the slower degradation of the higher molecular weight species that are likely to be overcome by natural redox signaling inside of the cell. In each concentration, the IgG/PTx shows no suppression of ROS. ROS level is measured as a percent of control, HUVECs that were not exposed to any treatment (Figure 4-3).

This MW behavior and dose dependence correlates well with previously published results [45]. Comparing the level of suppression in relation to mass bound ($1/10^{th}$ of incubated 1 mg/mL dose as determined in Figure 4-3) corresponds to previously published literature for ROS suppression. In the previous publication, 0.1 mg/mL, the relative mass bound for 1 mg/mL incubation concentration, of PTx 1000 and PTx 2500 exhibited 30% and 20% reduction in ROS respectively [45].

4.3.6 Suppression of iron oxide nanoparticle induced ROS injury through the use of AntiPECAM-1/PTx

To determine if targeted poly(trolox) nanoparticles can prevent iron oxide toxicity, 1.0 and 0.5 mg/mL of antiPECAM-1/PTx and IgG/PTx nanoparticles were prophylactically administered to HUVECs for 1 hour and rinsed 5 times prior to iron oxide nanoparticle exposure.

Iron oxide at a concentration of 35 μg/mL induced a normalized ROS response that was 180 ± 11% over untreated cells with a viability of 52 ± 7.2%. As non-targeted particles do not significantly bind to HUVECs, IgG/PTx treatments did not provide protection against iron oxide nanoparticle injury. For antiPECAM-1/PTx we observe

43.5% suppression in ROS levels at 1 mg/mL and 47.7% at 0.5 mg/mL (Figure 4-4). Interestingly, we see a dose dependent increase in viability, with a recovery of 92 ± 10.1% at 1 mg/mL dosage, and 65 ± 8.0% recovery at 0.5 mg/mL (Figure 4-4).

4.3.7 Determination of iron oxide nanoparticle injury suppression mechanism

It is proposed that the mechanism of iron oxide toxicity is due to the generation of free radicals due to Fenton reactions. In the presence of hydrogen peroxide, Fe^{2+} can undergo oxidation and Fe^{3+} can undergo reduction. The byproducts of this are highly reactive hydroxyl and peroxyl radicals. We theorize that the antioxidant potential of AntiPECAM-1/PTx nanoparticles can intercept these radicals, thereby attenuating damage caused by iron oxide nanoparticles.

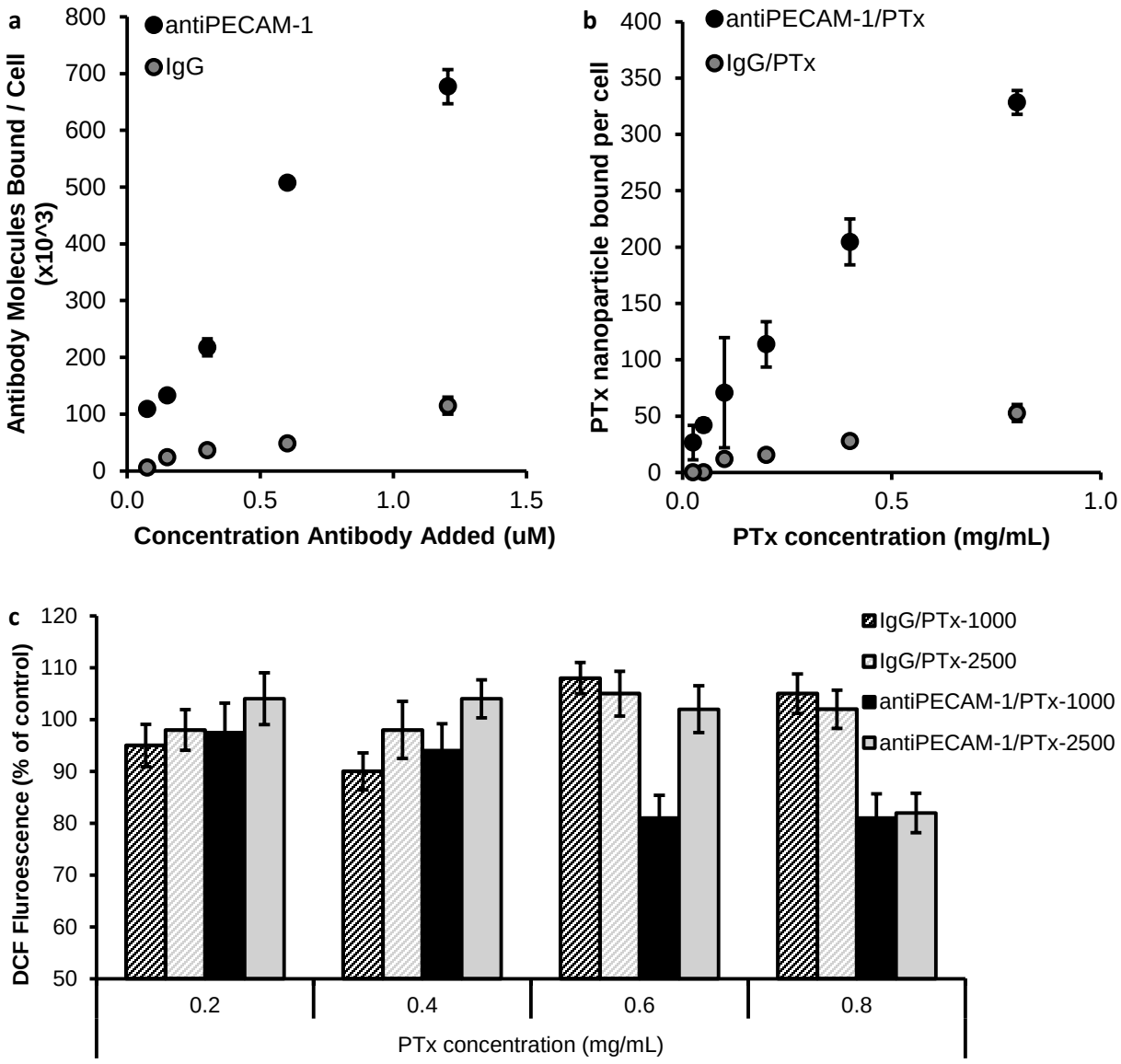

Figure 4-3. Antibody and particle binding to cellular model with suppression of background ROS

Free antibody and poly(trolox) nanoparticles were incubated with HUVEC cells in varying doses. Antibody (A) and particles (B) were incubated for 30 minutes, followed by 5 washes in warm media. AntiPECAM-1 and antiPECAM-1/PTx possessed an order of magnitude higher binding to cells as compared to the non-specific IgG controls. Approximately 10% of particles incubated stay adhered after washing (M± SD, n=3). Oxidative stress was measured using DCF as a fluorescent probe. DCF was added to

HUVECs for one hour prior to administration of antioxidant nanoparticles. Particles were incubated for 30 minutes followed by 5 washings in warm media. Nonspecific IgG coated nanoparticles show no suppression of oxidative stress as compared to the control in each formulation. PTx 1000 shows a dose dependent decrease in oxidation. PTx 2500 shows an effect at 0.8 mg/ml, but no significant protection thereafter. This can be attributed to the slow degradation of PTx 2500 due to its higher molecular weight (C) (M± SD, n=3).

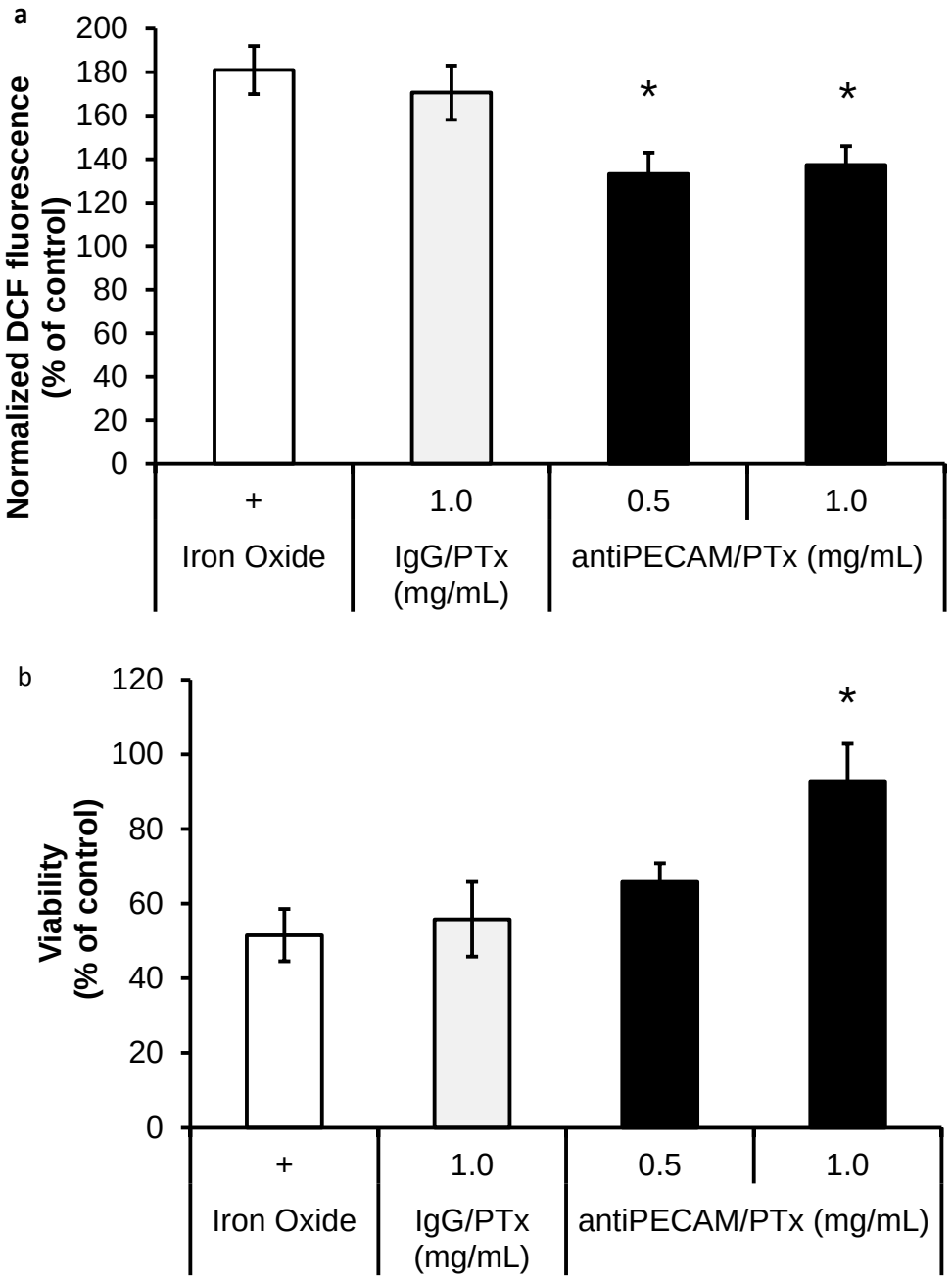

Figure 4-4. Suppression of iron oxide injury

HUVECs were incubated with DCF for one hour then removed. Afterwards, antioxidant nanoparticles were incubated 1 hour before introduction of iron oxide nanoparticles at a concentration of 30 µg/ml. (A) DCF Fluorescence was measured 24 hours after injury. (B) After DCF measurement, Calcein AM at 5 µM was incubated for 20 minutes, and

fluorescence subsequently measured. IgG/PTx shows no significant protection from ROS, or exhibit an increase in viability. AntiPECAM-1/PTx particles show suppression of ROS levels as compared to control, however it does not appear to be dose dependent. Viability for AntiPECAM-1/PTx however shows a dose dependent increase in viability, indicating mitigation of iron oxide toxicity. (M± SE, n=3, * = $p<0.05$).

However, it was not certain if the observed results in Figure 4-4 were due to the antioxidant activity or if it was due to physically blocking/occupying possible internalization routes, which would likely reduce the uptake of iron oxide. To determine if this is a concern, the study was repeated using the targeted, but non antioxidant antiPECAM-1/Polystyrene (PS) beads. As a comparison group cells were also incubated with PTx-1000 nanoparticles that were not rinsed.

After a 24 hour incubation period of iron oxide, the AntiPECAM-1/PS treatment showed no significant reduction in either viability or ROS levels; however 1.0 mg/mL PTx 1000 nanoparticles exhibited 87.6 ± 3.4% recovery in viability, and significant reduction in ROS levels (Figure 5). This indicates the protection mechanism is a linked to the antioxidant potential of the targeted treatment, rather than inhibition of internalization routes utilizing an active targeting method.

4.3.8 AntiPECAM-1 coated fluorescent particles exhibit significant internalization following incubation

To determine if antiPECAM-1 antibody coated particles possess the ability to internalize into a cell, an expected prerequisite for function, a fluorescent microscopy approach was utilized. HUVECs were incubated with antibody coated green fluorescent polystyrene beads for 30 minutes then washed as described before. Targeted particles were then both fixed and counterstained with a Texas Red labeled goat anti-mouse IgG either immediately or after an 8 hour incubation period to allow for cellular endocytosis to occur.

Membrane bound particles will fluoresce both green (polystyrene) and red (Texas Red secondary antibody stain) that, when overlaid, appear yellow. Particles that have been internalized will be inaccessible to the secondary stain due to cell membrane

fixation. These internalized particles will remain green. AntiPECAM-1 coated particles showed an expected increase of internalization over the 8 hour time period, from 20% to over 80% internalized, indicating significant internalization and delivery of particles to the endothelial cells (Figure 4-6).

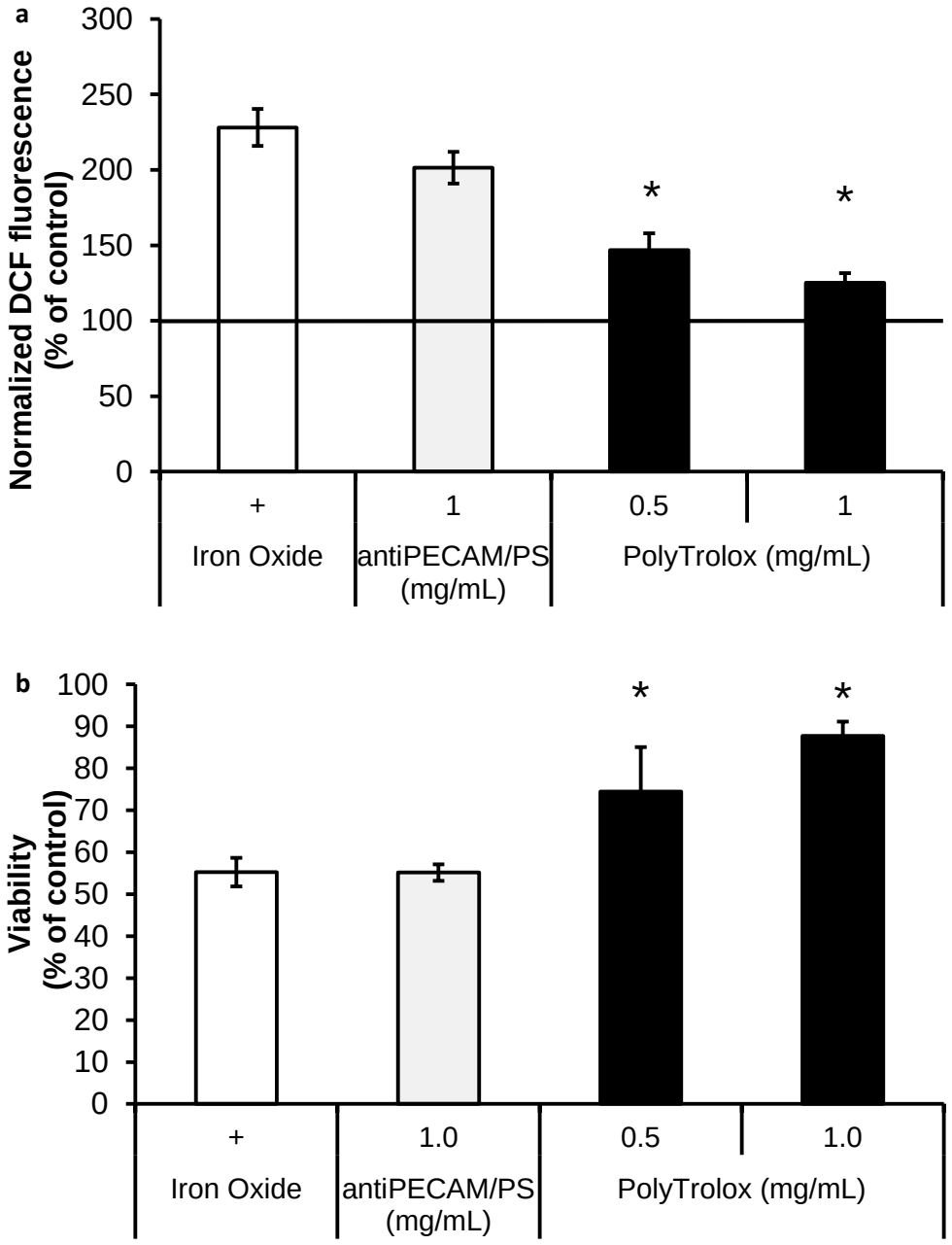

Figure 4-5. Determination of protection mechanism

HUVECs were incubated with DCF for one hour then removed. Afterwards, targeted polystyrene particles were incubated for 30 minutes then washed 5 times to remove unbound particles. Conversely, poly(trolox) particles incubated for the entirety of the

experiment. One hour after incubation iron oxide nanoparticles at a concentration of 30 µg/ml were introduced. DCF Fluorescence was measured 24 hours after injury. Black bar represents background ROS levels (A). After DCF measurement, Calcein AM at 5 µM was incubated for 20 minutes, and fluorescence subsequently measured (B). Targeted polystyrene particles show no therapeutic effect towards iron oxide injury regarding viability or ROS measurements. Poly(trolox) incubated for the duration of the experiment shows a significant viability recovery and reduction in ROS levels, indicating protection is a result of antioxidant capability. (M± SE, n=3, * = $p<0.05$ from control).

4.4 Discussion

As motivation to this study, we hypothesized that targeted antioxidant nanoparticles could suppress cellular injury associated with iron oxide nanoparticle use. By injecting these particles either prior to or in tandem with iron oxide administration, it should be possible to block associated vascular damage. In our prior work, poly(trolox) nanoparticles were shown to degrade in the presence of cellular esterases and release active antioxidant, which is capable of suppressing cellular oxidation. We have also shown that this polymer has a unique ability to inhibit the formation of cellular oxidation products that is not seen in the native free antioxidant [45]. However, these studies centered on non-targeted free particles that, due to expected clear mechanisms, would not accumulate in the vasculature *in vivo*. To accommodate antibody coating onto the particle surface, the formulation approach was changed to eliminate surfactant. The surface charges of these particles are complimentary to surface absorption of various proteins allowing the ability to tailor the targeting antibody to multiple applications.

Using simple physioadsorption methods, the antioxidant nanoparticles were coated with greater than 500 antibodies/carrier, permitting sufficient multimer binding and observed affinity in cell culture. Protein coating on nanoparticles can serve to stabilize them from aggregation. To this end, antibody nanoparticles were suspended and stored in 1wt% BSA. Importantly, it is possible that this BSA could over time replace the antibody from the surface of particles during storage. However, it was found that there was no statistically significant decrease in antibody coating over one week storage in refrigerator conditions. When added to an endothelial cell culture model, these PECAM-1/PTx particles were then shown to significantly adhere to the surface of the cells. The method

of adhesion was shown to be antibody-antigen based, as particles coated in nonspecific IgG had no inherent capacity to adhere to the cell layer.

Based upon prior work of poly(trolox), with esterase dependent hydrolysis, it was assumed that antioxidant function would require cellular internalization into lysozymes [22]. While it has been shown that antiPECAM-1 antibodies are not internalized [195], antiPECAM-1 conjugates can indeed be taken up through CAM mediated pathways and is typically independent of the substrate particle [190]. It is observed here that the polystyrene particles, over the course of 8 hours, are internalized, and trafficked towards the nucleus in lysosomes. This compartmentalization can enhance the degradation of the antioxidant particles, leading to the release of active therapeutic. Indeed, the targeted antioxidant particles exhibit the ability to suppress background ROS generation with no detrimental effect on cellular viability.

The antioxidant properties of this polymer may be highly beneficial in the biomedical field, especially with the emerging use of transition metal based nanoparticles that can cause free radical formation such as iron, zinc, cerium, and titanium [196] and the overarching theme of safety in biocompatibility. The mantra of small size and high surface, and subsequently reactive, area of metal nanoparticles has led to a paradigm of monitoring oxidative injury as it pertains to cytotoxicity.

In medical applications of iron oxide nanoparticles, direct IV injections are the traditional route of administration. As such, the vasculature epithelium becomes the first point of contact for these particles, and thus a crucial area to study toxic and oxidative interactions. Similarly for environmental exposure, the pulmonary endothelium becomes the settling area for inhaled particles, which can cause significant inflammation and tissue

damage. Not only is the endothelium the first point of contact in iron oxide exposure, it has also been demonstrated that these cells are highly prone to oxidative damage and injury [197]. Therefore, if protective particles are injected prior to iron oxide administration, it should be possible to mitigate its observed toxicity.

To test this iron oxide-based toxicity, we studied the dose dependent ROS generation and subsequent toxicity of iron oxide nanoparticles. While we observe a sharp decline in the free radical generation with higher concentration of iron oxide, it is hypothesized this is due to detachment and membrane disruption of the cell monolayer, causing the fluorescent DCF probe to leak out of the cells, only to be removed following washing steps involved in the procedure. Due to this phenomenon, subsequent analysis of free radical generation is normalized against the viability, in order to observe the ROS level in the remaining living population. It should be noted that this toxicity could also be caused by endotoxin load of the formulation, as endotoxin has been shown to cause oxidative stress related cellular activation [198]. While we do not have endotoxin calculations for the exact particles used in this study, a similarly prepared batch that has been in storage for 2 months was assayed. Endotoxin values were found to be below detectable levels, or less than 0.015 endotoxin units (EU) per milligram of iron oxide nanoparticles. At this level, endotoxin would be well below needed values to elicit a ROS response, reported to occur as low as 150 EUs [199, 200]. Further, the toxicity and ROS generation exhibited by iron oxide nanoparticles correlates with results found by other groups [201], and provides a sound basis for evaluating the ability of antioxidant polymers to mitigate this damage.

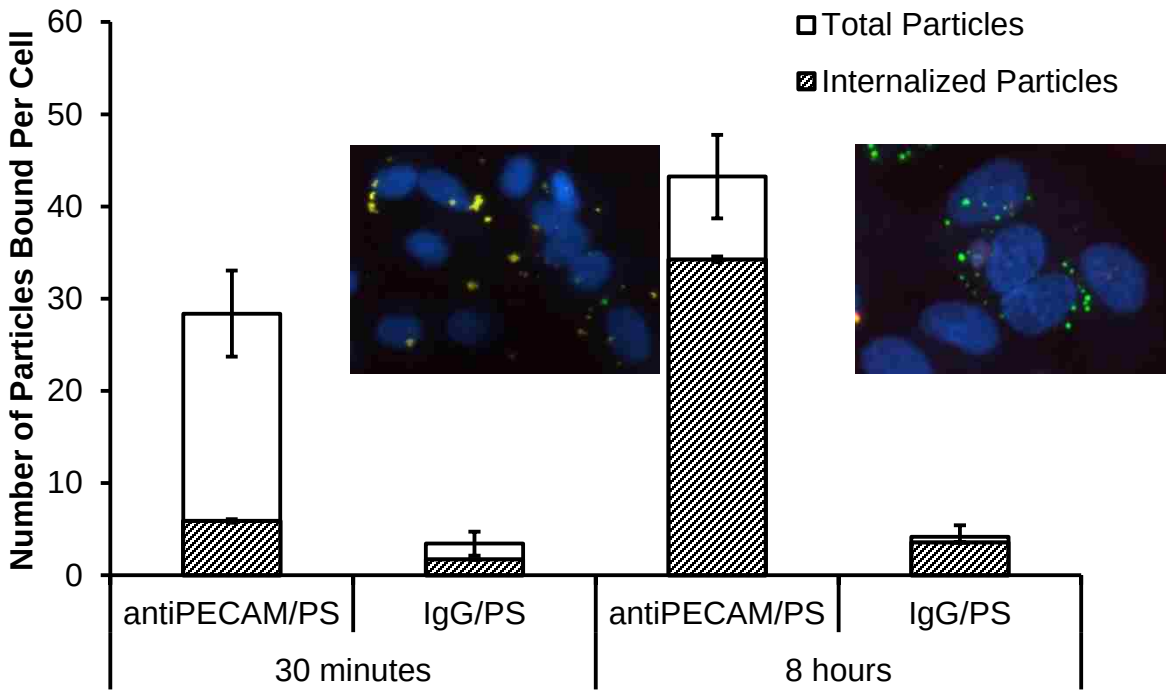

Figure 4-6. Particle adherence and internalization

HUVECs were incubated with antibody coated green fluorescent polystyrene beads for 30 minutes. Following removal of unbound particles, cells were fixed either immediately or after 8 hours of incubation. Cells were then labeled with red secondary for 30 minutes, washed, then permeabilized and stained with DAPI nuclear stain. Imaging was done utilizing a fluorescent microscope, and analyzed utilizing Nikon Elements. Particles that appear yellow (red + green) are said to be bound to the outside of a cell. Particles that appear green are said to be internalized. Particle counts per cell were also obtained utilizing Nikon tracking software. 30 minutes after incubation, 20% internalization is observed, after 8 hours this increases to over 80%. Particles adhered per cell for antiPECAM-1 targeting were an order of magnitude higher than IgG coated (fluorescent image not shown), similar to radiolabeling results in Figure 2. (M± SE, n=10).

When the antiPECAM-1 PTx particles are added to cells before introduction of the iron oxide nanoparticles, a significant recovery in both viability and ROS generation is seen. Particles with a nonspecific IgG coating show no statistically significant effect on viability. This is to be expected considering the adhesion data, where no accumulation of nanoparticles is seen with the IgG coated particles. From this data, we concluded two possibilities of protection, either that the adhered nanoparticles are physically blocking the internalization pathway of the iron oxide or the antioxidant potential of the nanoparticles is indeed protecting the cells (Figure 4-7). In order to elucidate the actual protection mechanism, non-targeted PTx nanoparticles and targeted polystyrene particles were employed. If the polystyrene particles, being the same size and having no intrinsic therapeutic value, prevented cytotoxicity then it could be concluded that the protection mechanism is due to the prevention of iron oxide from reaching the cell. However, we observed that the polystyrene particles offer no protection, whereas the non-targeted antioxidant particles once again recovered cellular viability, strongly indicating the therapeutic efficacy of trolox.

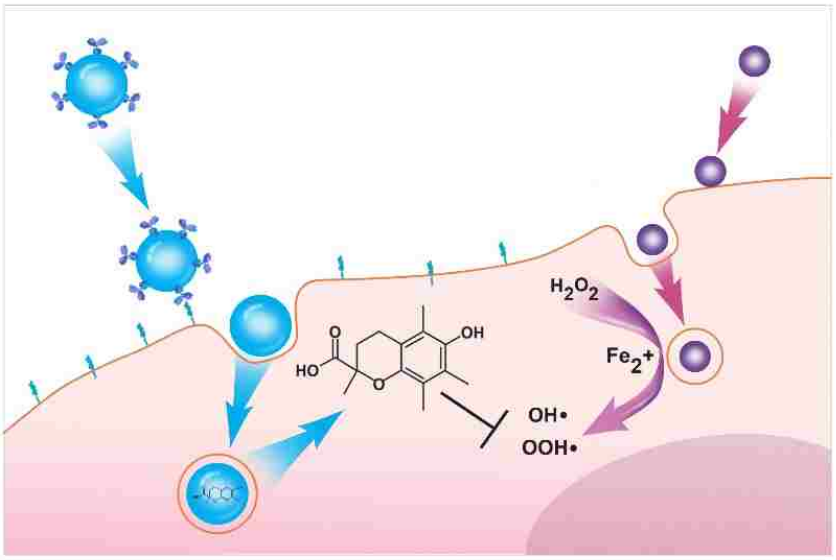

Figure 4-7. Proposed protection mechanism of antiPECAM-1/PTx nanoparticles

A cartoon depicting the proposed protection mechanism provided by antiPECAM-1/PTx nanoparticles. On the left: Bound antiPECAM-1/PTx nanoparticles (green) adhere to the surface of the cell. These nanoparticles are then internalized, where cellular esterase degrade the PTx nanoparticle into the active antioxidant trolox. On the right: Iron oxide nanoparticles are internalized, where they undergo Fenton reactions. Endogenous hydrogen peroxide reacts with Fe2+ and Fe3+ to form hydroxyl and peroxyl radicals, which induce oxidative stress. Trolox can intercept these free radicals, mitigating the damage caused.

4.5 Conclusions

The antioxidant polymer poly(trolox) was successfully formulated into nanoparticles coated with an antibody directed towards PECAM-1. These active targeting nanoparticles have shown to adhere to HUVEC cells, internalize, and reduce oxidative stress in both static and iron oxide mediated ROS injury type models. This targeted delivery system shows great promise as a prophylactic or possibly tandem delivery system to vascular beds, the common final destination of therapeutic iron oxide nanoparticles, in order to mitigate the growing concern of toxicity.

Chapter 5. Inhibition of inflammation-mediated rheumatoid arthritis

Based on the research article:

> David Cochran, L. Gray, K.W. Anderson, and T. Dziubla. "Encapsulated Apigenin-based Polymers for the Prevention of Tumor Cell Adhesion and Metastasis" (*In review*).

5.1 Introduction

In the previous chapter, we have demonstrated the link between oxidative stress and injury through the use of iron oxide as a vascular injury agent. To further test the ability of poly(trolox) to inhibit injury, we have utilized an *in vivo* injury consisting of rheumatoid arthritis (RA). It is an autoimmune disease that primarily affects the joints of the hands [202]. In RA, a host of immune cells such as T cells, B cells, and macrophages infiltrate the pannus surrounding joints and begin to digest and injure articular cartilage and bone [203]. It has been shown that reactive oxygen and nitrogen species are produced at the site of synovitis [10]. This buildup can contribute further to the inflammation and activation of immune complexes, resulting in increased damage to bone and tissue [15, 41]. In fact, researchers have reported that oxidative stress in RA leads to reduced antioxidant capacity in tissues [42]. In regards to therapy options, other groups have reported on the utilization of supplemental antioxidant therapy to inhibit injury with mixed results [35, 204], with the prime cause of treatment failure pointed towards ineffectual delivery and accumulation [205]. In separate studies, it's been shown that vitamin E can also inhibit inflammation via prostaglandin E_2 down regulation [206].

Our polymer nanoparticle systems have the ability to overcome the issues of premature oxidation and non-selective delivery. Indeed, it has been shown that nano-emulsions of vitamin E have increased bioavailability and accumulation in other *in vivo* inflammation models [207]. With the unique oxidation suppression provided by

poly(trolox) over trolox [45], it's feasible that a controlled delivery system thereof, capable of accumulating in inflamed joints, could potentially be used to inhibit or prevent the progression of rheumatoid arthritis *in vivo*.

5.2 Materials and Methods

5.2.1 Polymer synthesis

mPEG-PLA: DL-lactide was initially recrystallized in anhydrous ether to remove residual water and impurities. The purified DL-lactide was then stoichiometrically mixed with mPEG and 1% stannous 2-ethyl-hexanoate in dichloromethane (DCM) to form a polymer of a final molecular weight of 55,000. The resulting solution was heated to 90°C under continuous nitrogen purge until all solvent was evaporated. Following this, the ring-opening polymerization reaction proceeded for 6 hours at 120°C. The polymer was then cooled overnight, dissolved in DCM, precipitated in cold diethyl ether, and freeze-dried then stored till further use.

5.2.2 Nanoparticle formulation and characterization

Formulation: mPEG-PLA and poly(trolox) were dissolved in acetone (10 and 5 mg/mL, respectively, 1 mL total). The mixture was added drop-wise to 20 mL of deionized water mixing at 2000 RPM. Solvent was allowed to evaporate by stirring overnight, and the solution was filtered through a 1 µm filter and centrifuged at 40,000*g* for 15 minutes. This was followed by resuspension in sterile PBS with 1% BSA added. Nanoparticle recovery was determined using a PEG-barium iodide complex assay. Briefly, a known mass of nanoparticles were dissolved in 200 µL of 5 M NaOH for 4 hours at 80°C then neutralized with 5 M HCl. The solution was then mixed with a

solution barium iodide, the absorbance was determined at 550 nm. This was then compared against PEG standards, and compared to initial PEG content before formulation.

Nanoparticle size: Particle size and polydispersity (PDI) were investigated using dynamic light scattering (DLS). Nanoparticles were diluted in PBS at 25°C to a concentration of 0.1 mg/mL then measured for size.

Drug loading: To determine total drug loading, nanoparticles were formulated as described above with a slight exception. After the initial centrifugation, the supernatant and nanoparticle mass were freeze-dried overnight, then dissolved in acetone. The absorbance was then measured and compared against standards of poly(trolox) in acetone at 370 nm. Encapsulation efficiency and drug loading was determined by the mass in the supernatant compared to the mass in the nanoparticles:

$$Encapsulation\ efficency = \frac{Mass\ of\ poly(trolox)\ in\ nanoparticles}{Total\ mass\ of\ poly(trolox)\ added} * 100\%$$

$$Drug\ Loading = \frac{Mass\ of\ poly(trolox)}{Total\ nanoparticle\ mass} * 100\%$$

5.2.3 Induction of arthritis *in vivo* and treatment regimen

Arthritis was induced in wild-type DBA/1 LacJ mice through the use of a Collagen Antibody-Induced Arthritis model (CAIA) according to manufacturers supplied protocols (Chondrex, Inc). In brief, mice were given an intraperitoneal injection of 2 mg of

collagen antibody. Three days later this is followed by an intraperitoneal injection of 50 µg lipid polysaccharide (LPS). Animals were treated daily on day 3 on with mPEG-PLA/PTx nanoparticles (125 µL at a 50 mg/kg concentration) or 1% BSA in PBS as control for a total of 5 days via the tail-vein.

Extent of injury was assessed each day for a period of 7 days following initial antibody injection by a visual-based scoring system provided by the manufacturer, along with tracking of animal weight. Following the 7^{th} day, the animals were sacrificed and tissues collected for further analysis.

5.2.4 Assessment of nanoparticle accumulation *in vivo*

On day 7, the animals were injected with a slightly modified treatment. For mPEG-PLA/PTx treatment, a near IR fluorescent dye Cy 5.5, obtained from Lumiprobe (Hallandale Beach, FL), was incorporated into the nanoparticle formulation at a final concentration of 2 wt%. Control group animals received an identical concentration of Cy 5.5 in saline.

After sacrifice, the whole animal and excised paws were imaged utilizing an IVIS Spectrum imaging system (Caliper Life Sciences) at a wavelength of 673/707 ex/em. Fluorescent intensity of the animal cavities and paws were recorded and exported for analysis in ImageJ.

5.2.5 Determination of endogenous antioxidant activity in liver.

Following sacrifice, the whole animal liver was collected and homogenized in PBS. A Myoglobin based colorized antioxidant equivalence content assay was utilized to determine antioxidant activity. A mixture of myoglobin (Sigma) and potassium

ferricyanide was added in PBS, and allowed to react in the dark for 5 minutes. The oxidized myoglobin was separated from the potassium ferricyanide through the use of a Sephadex spin column (Biorad) and diluted in PBS to a concentration of 6 µM. Next, 8 µL of liver homogenate, 100 µL of the 6 µM myoglobin solution, and 100 µL of 2, 2'-azino-bis (3-ethylbenzothiazoline-5-sulphonic acid) (ABTS) at 0.8 mg/mL were added to a 96 well plate and well mixed. The assay was started when 40 µL of 250 µM hydrogen peroxide was added. After 6 minutes, the colorization of the ABTS was measured at 734 nm, and plotted against a generated calibration curve of trolox. Trolox equivalence was then normalized to a known mass of tissue homogenate and compared.

5.2.6 Protein oxidation of paw tissue

To measure the effect of oxidative stress and injury in paw tissue, a 2, 4-dinitrophenylhydrazine based protein carbonyl colorimetric assay was used according to manufacturer protocols (Cayman Chemical). In brief, whole paws were homogenized in MES buffer and solids centrifuged and removed. The protein containing solution was then mixed with a solution of 2,4-Dinitrophenylhydrazine (DNPH) and hydrochloric acid. After reaction on ice for 15 minutes, the protein was precipitated in a solution of trichloroacetic acid and excess DNPH removed. Finally, the protein pellet is resuspended in guanidine hydrochloride and absorbance measured at 370 nm using a plate reader. Carbonyl content was measured per milligram of total protein content as measured by a Bradford assay.

5.3 Results

5.3.1 Nanoparticle formulation and characterization

To formulate a biocompatible delivery system for poly(trolox), a single-step nanoprecipitation method was utilized. Table 6.1 outlines the size, encapsulation efficiency, and final drug loading of each formulation. Blank mPEG-PLA nanoparticles were determined to be 144.1 ± 13.5 nm with a polydispersity index (PDI) of 0.176 by DLS. Nanoparticles with incorporated poly(trolox) were slightly larger at 163.1 ± 11.7 nm, a PDI of 0.313, with a final drug loading of 24.8 ± 2.08%.

5.3.2 Assessment of mPEG-PLA/PTx nanoparticles to suppress rheumatoid arthritis

To evaluate if mPEG-PLA/PTx nanoparticles possess the capacity to inhibit oxidative stress and inflammation *in vivo*, mice were subjected to a CAIA arthritis model. After a booster shot of LPS on the third day after antibody injection, treatment began with daily tail-vein injections of mPEG-PLA/PTx nanoparticles or saline. The animal paws were evaluated each day utilizing a scoring system provided by the manufacturer, ranked depending on severity of swelling. Figure 5-1 outlines the scoring trend and body weight of the animals over time. Animals in the control group demonstrated a sharp rise in incident score after 3 days of 4.3 ± 2.1, and continued to climb as expected, hitting a plateau of 10.3 ± 1.3 at 6 days. Animals treated with mPEG-PLA/PTx nanoparticles experienced a delay in arthritis symptoms, taking 5 days to reach a significant scoring level of 3.0 ± 1.5. Symptoms plateaued after 6 days, similar to the control group, at a scoring of 6.7 ± 2.0.

Analysis of body weight over time indicated a decline in weight following LPS booster at

day 3, with a weight loss of 5%. Animals from both groups declined in an identical fashion, a symptom of illness, to a maximum of 15% weight loss after a period of 7 days.

Table 5-1 Properties of mPEG-PLA nanoparticles

Nanoparticles without any incorporated PTx are 144.1 nm in size with a relatively monodispersity. Poly(trolox) loaded particles are slightly larger at 163 nm and less monodisperse. Encapsulation efficiency was determined to be 51%, with a total drug loading of 24.8% (N=3, M±SD).

Drug loaded Core	Size (nm)	PDI	Encapsulation efficiency (%)	Drug loading (%)
-	144.1 ± 13.5	0.176	N/A	N/A
PTx	163.1 ± 11.7	0.313	51 ± 1.04	24.8 ± 2.08

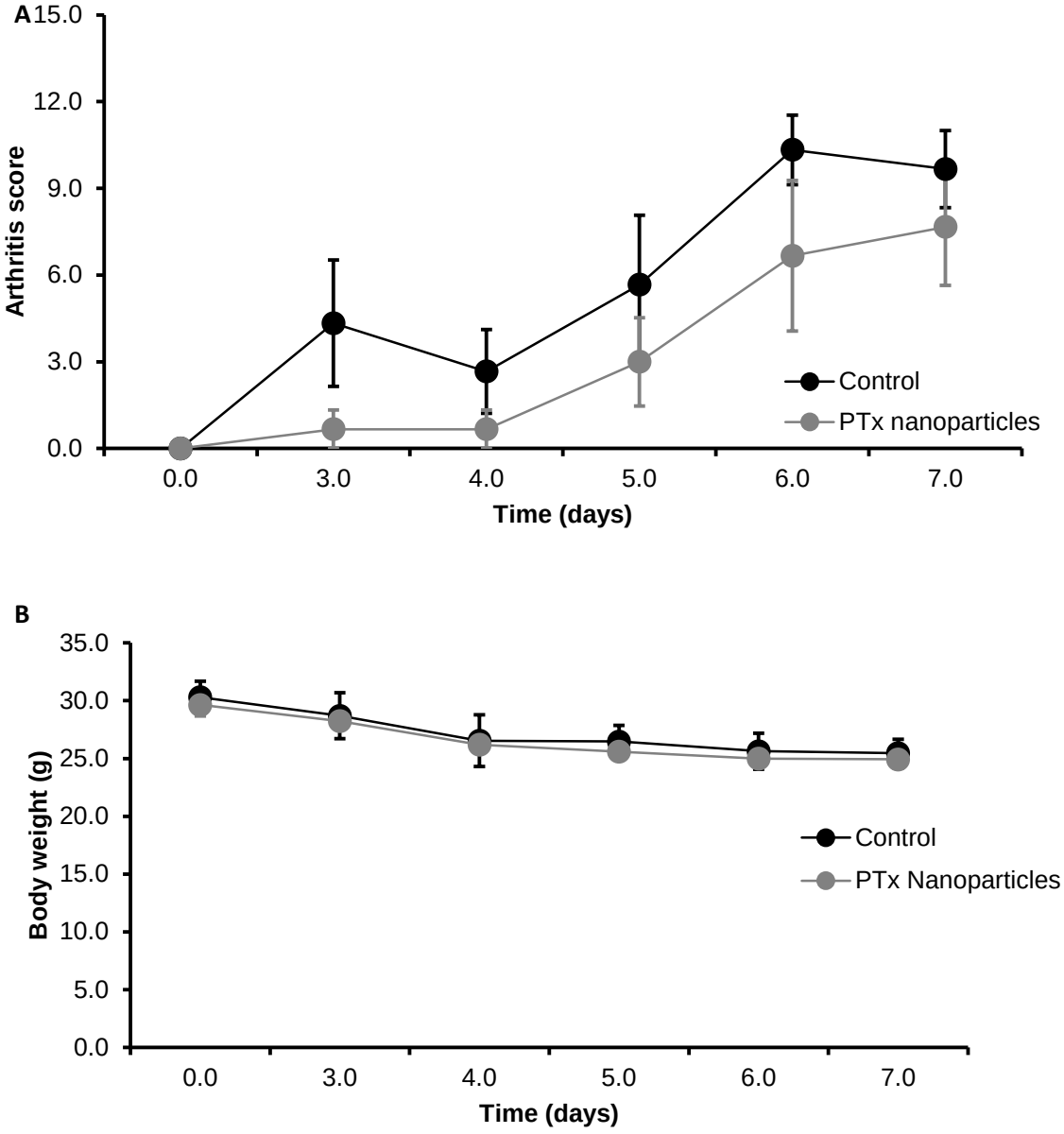

Figure 5-1: Analysis of arthritis score and animal weight over time

Arthritis score and weight were recorded over a 7 day period. (A) Animals treated with PTx nanoparticles showed a lag time between treatment and generation of symptoms compared to control group. Both groups plateaued in score after 6 days. Body weight, however, declined at identical rates for both groups (B) (N=3, M±SD).

5.3.3 mPEG-PLA/PTx nanoparticles accumulate in organs and joints

In order to test if mPEG-PLA/PTx nanoparticles can accumulate at the site of inflammation, an important prerequisite to effectual therapy, a modification to the nanoparticle formulation was made for the final day of delivery. A fluorescent dye, Cy5.5, was added to the synthesis step to allow for particle imaging in an IVIS Spectrum imaging system. Control animals were given an identical mass of dye in saline.

Mice treated with mPEG-PLA/PTx nanoparticles showed significant accumulation of particles in the liver and kidneys with over 40 fold increase compared to free dye (Figure 5-2a). As expected, the animals in the control group quickly cleared and excreted the free dye. Most interestingly, analysis of the excised paws of mPEG-PLA/PTx treated animals revealed a 267% increase over controls. This suggests a significant effect of accumulation in the inflamed tissue (Figure 5-2b).

5.3.4 Endogenous antioxidant activity is recovered through the use of mPEG-PLA/PTx nanoparticles

A myoglobin based TEAC assay was employed to determine if supplemental antioxidant therapy can restore normal antioxidant function, and thus inhibit the oxidative stress and inflammation due to rheumatoid arthritis. Liver tissue was selected for analysis over paw tissue, due to the large relative differences in mass and overall sensitivity of the assay. Figure 5-3 shows the antioxidant levels of the mice. The control group had an antioxidant equivalence of 1.93 ± .019 mM trolox per mg of tissue. Animals treated with mPEG-PLA/PTx recovered to 2.43 ± 0.03 mM trolox per mg of tissue. For reference, baseline levels of antioxidant capacity in non-arthritic mice have been reported to be between 2.5-3.5 mM trolox per mg of tissue.

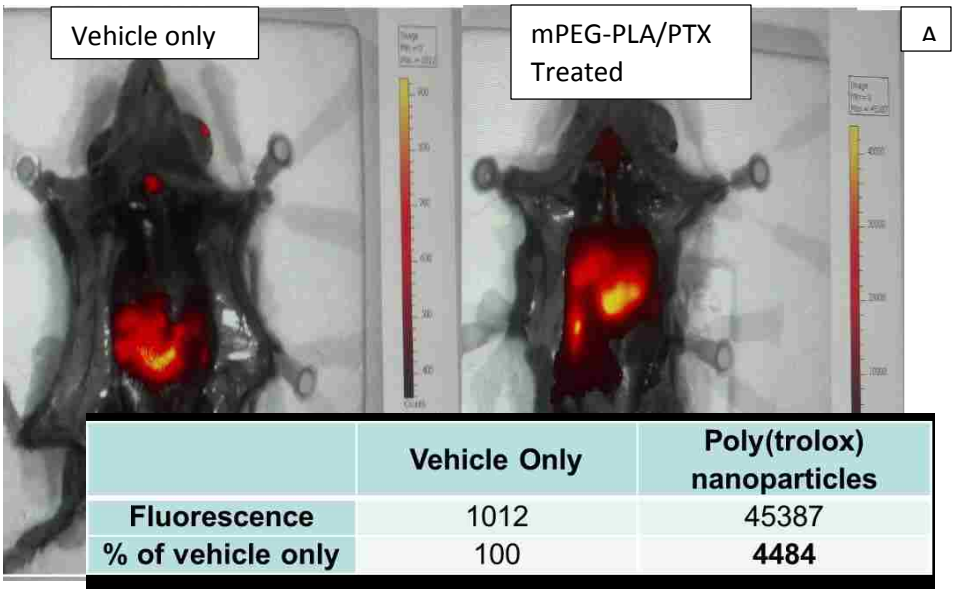

	Vehicle Only	Poly(trolox) nanoparticles
Fluorescence	1012	45387
% of vehicle only	100	**4484**

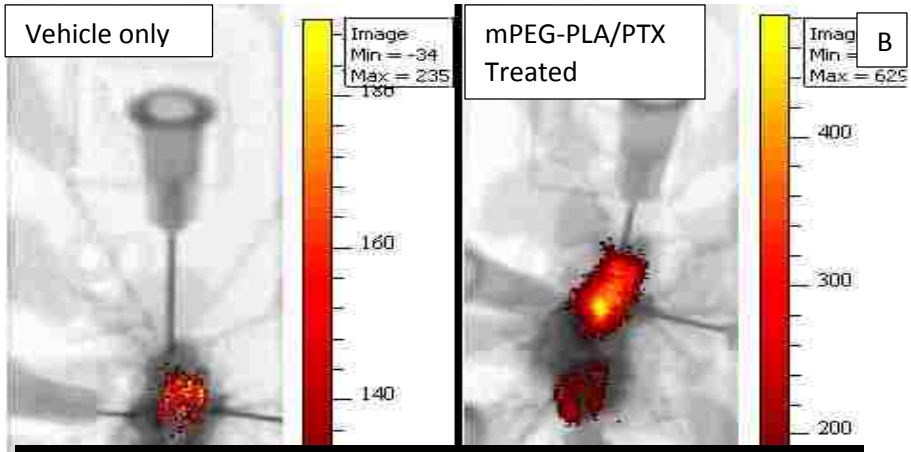

	Vehicle Only	Poly(trolox) nanoparticles
Fluorescence	235	629
% of vehicle only	100	**267.65**

Figure 5-2: Fluorescent images of nanoparticle accumulation *in vivo*

mPEG-PLA/PTx nanoparticles were formulated with a fluorescent dye to track accumulation *in vivo*. Control groups were given a dose matching of dye. Treated animals had a 40 fold increase of accumulation in liver and kidneys (A). In excised paw tissue, a 267% increase of accumulation over free dye was observed (B).

5.3.5 mPEG-PLA/PTx significantly inhibits protein carbonyl content in the paws of arthritic mice.

Utilizing a DNPH based protein carbonyl content assay, we looked at the ability of mPEG-PLA/PTx to inhibit protein oxidation, a major sign of oxidative stress. Whole paws were excised and washed in DI water to remove excess blood or clots. Protein was then extracted and tested. Figure 5-4 outlines the levels of protein carbonyl content. The control group contained 5.37 ± 1.07 nmol carbonyl per mg of total protein. This level is significantly higher than baseline levels of non-arthritic mice. The group treated with mPEG-PLA/PTx was vastly reduced down to 0.25 ± .025 nmol carbonyl content per mg of protein. This level is suppression is even lower than reported basal levels of 2.5-3.5 nmol per mg of protein.

5.3.6 Antioxidant nanoparticles reduce levels of inflammatory cytokines associated with oxidative stress

Tissue recovered from animal paws were subjected to PCR and RNA analysis to determine levels of cytokine expression. Four cytokines were analyzed; IL-6, Cox-2, IL-8, and TNF-α. There were no differences in IL-6 or Cox-2 expression between controls and treated animals. However, levels of IL-8 expression were reduced by 54%, and TNF-α expression by 81%.

5.4 Discussion

In previous chapters, we have discussed the ability of the novel antioxidant polymer Poly(trolox) to suppress oxidative stress mediated-injury. In this work we have further expanded this polymer platform to elucidate the connection between oxidative stress and inflammation in a relevant

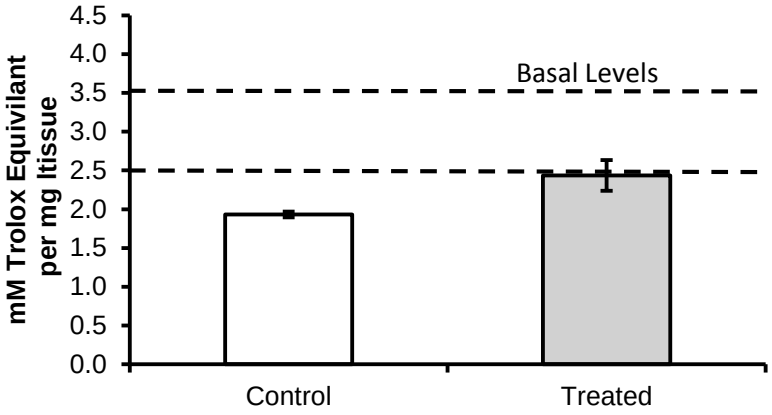

Figure 5-3: Ability of mPEG-PLA/PTx to recover antioxidant capacity

Untreated animals have a suppressed antioxidant capacity, due to inflammation and oxidative stress stemming from RA. Animals treated with mPEG-PLA/PTx nanoparticles experienced a recovery in antioxidant capacity, back up to basal levels. (N=3, M±SD)

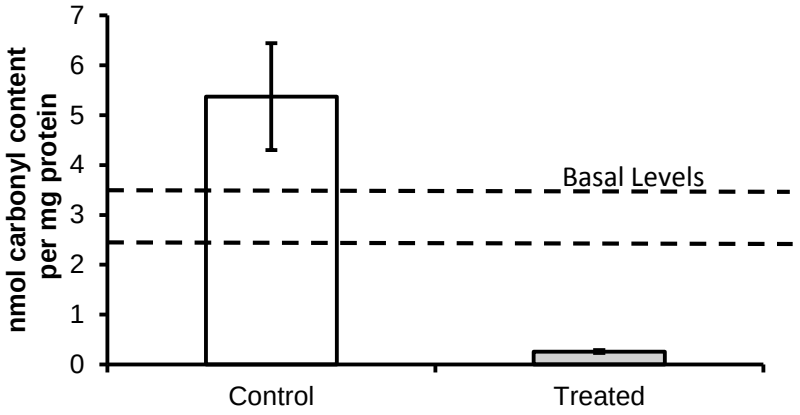

Figure 5-4: Suppression of protein carbonyl content of paw tissue

Arthritic animals had significantly elevated levels of carbonyl content of 5.37 ± 1.07 nmol carbonyl. In contrast carbonyl content was eliminated in treated animals, a feature observed in previous publications with PTx. (N=3, M±SD)

disease model of rheumatoid arthritis. By encapsulating PTx into a degradable PEGylated polymer, we have developed a biocompatible polymer that offers longer circulation times compared to free PTx alone.

Similar to the delivery system in chapter 5, we have devised a nanoprecipitation strategy to encapsulate PTx into an amphiphilic polymer of mPEG-PLA. The resulting nanoparticles were 163 nm in size, with a drug loading of 25%. This is similar to the results obtained for our apigenin PβAE polymers, which coincidently are similar in molecular weight and hydrophobicity.

In order to test the particles *in vivo*, the CAIA arthritis model was used. From an initial observation of Figure 5-1, it appears clear that animals treated with mPEG-PLA/PTx nanoparticles had inhibited levels of arthritis. However, it is very important to note that treatment did not occur until after scoring on day 3 of the LPS booster. In this situation, the control group of animals were scored significantly higher than the treatment group, despite the treatment group not receiving any nanoparticle dosages yet. Despite this, the increase in scoring between day 4 and 7 appeared identical between both groups.

Similarly, the decrease in body weight between both groups were also identical, indicative of the progression of the disease. From a visual scoring system, it appears that our antioxidant nanoparticles offer no protective effects. Several suggestions in further studies have been proposed, such as recording of pain thresholds, gait analysis, and synovial fluid analysis to further elucidate the effect of treatment.

For the last day of treatment, the animals were given a formulation that incorporated a fluorescent tag. After sacrifice, it was observed that the nanoparticles had significantly

accumulated in the liver and kidneys as expected for nanoparticles of this size. Most interestingly however, was that these nanoparticles also accumulated in the paw tissue of the inflamed joints. It is hypothesized this is due to an EPR-like effect, where disrupted vasculature, poor circulation, and retained fluid allow for these nanoparticles to deposit and accumulate.

After it was determined the antioxidant particles provided no therapeutic effects by visual examination, we had addressed the chemical effects. First, the antioxidant capacity of liver homogenate was assessed. Liver tissue was selected due to the prevalence of nanoparticle accumulation via imaging, the size of the organ, and sensitivity of the antioxidant assay. It was found that the control group had a suppressed level of antioxidant capacity, which is to be expected. The animals in the treatment group, however, had recovered to a healthy basal level of capacity.

Next the level of protein oxidation, a symptom of oxidative stress and inflammation, was evaluated. Tissue from the paw region was removed and protein extracted. The levels of carbonyl content were significantly elevated in the control group of arthritic animals, at nearly 2x the basal level. Animals treated with mPEG-PLA/PTx had almost zero carbonyl content (Less than 0.5 nmol/mg protein, approaching the minimum sensitivity limit of the assay). This result is reinforced from a previous publication where it was demonstrated PTx had the ability to suppress protein carbonyl content, a feature not observed in the monomeric form of trolox [45].

To elucidate the connection between inflammation and oxidative stress, a series of cytokine markers were examined. Utilizing RNA expression, we observed the levels of IL-6, Cox-2, IL-8, and TNF-α. It was found that the levels of IL-6 and Cox-2 were not

different between treated and control groups. It has been reported in literature that these two cytokines are highly dependent on inflammation signals as opposed to only oxidative stress [208-210], which can explain why no difference was observed. IL-8 was reduced, and TNF-α expression completely eliminated. In a similar fashion, it has been reported that IL-8 is selectively up regulated from oxidative stress injury [211, 212], whereas TNF-α is a ubiquitously expressed cytokine in response to a multitude of injuries.

5.5 Conclusions

A single-step nanoprecipitation method to encapsulate the antioxidant polymer Poly(trolox) was developed. By encapsulating PTx in the polymer mPEG-PLA, we have created a stealth biocompatible polymer that is long circulating and can be used to treat injury and disease *in vivo*. These mPEG-PLA/PTx nanoparticles served to reduce cytokine markers stemming from oxidative stress and replenish total antioxidant content in the organs of mice in an arthritic mouse model. Fluorescent imaging analysis of the organs indicates significant accumulation over a 5 day period as compared to control mice. Most importantly, imaging analysis suggests higher accumulation of nanoparticles in the inflamed joints possibly due in part to enhanced permeation and disruption of vasculature in the limbs.

These nanoparticles also served to significantly reduce the levels of oxidized protein in the limbs, a marker of downstream damage due to inflammation. This preliminary data serves as a potential therapeutic delivery system for the treatment of rheumatoid arthritis and the accompanying inflammation-mediated damage caused.

Chapter 6. Interrupting the Metastatic Cascade: Apigenin-based Polymer Nanoparticles Inhibit Cancer Cell Adhesion

Based on the research article:

> David Cochran, L. Gray, K.W. Anderson, and T. Dziubla. "Encapsulated Apigenin-based Polymers for the Prevention of Tumor Cell Adhesion and Metastasis" (*in review*).

6.1 Introduction

Relationships between cancer pathology and inflammation have been observed for nearly a full century [213]. Researchers have linked the rates of cancer progression with inflammation in order to understand the connection between the two. One study reported cancer rates of individuals suffering from bronchitis are as high as 24% [214]. Another reported asbestosis cancer rates of 15% [215]. Even individuals undergoing chronic UV exposure (eg. Sunburns, tanning, etc.) have cancer rates of up to 11% [216].

In addition, metastasis has been shown to occur in approximately 20-40% of patients diagnosed with breast and testicular cancer, leaving patients with a typical median survival time of 18-24 months [217, 218]. A recent study revealed that in 2009 an estimated 58,000 women developed metastatic tumors as a direct result of breast cancer [219]. The average healthcare cost was placed at $128,556 per patient, for a total cost of over $7.4 billion per year [219]. Current treatments for metastatic tumors include systemic therapy (i.e. chemotherapy or hormonal therapy) or local therapy (i.e. surgery or radiation) [220]; however, there are currently no FDA-approved treatments for the prevention of metastasis in metastatic-prone patients. In fact, the latest drug application of Xgeva for inhibition of metastasis was rejected by the FDA [221].

Stresses such as the mechanical forces involved during surgery have been shown to initiate a cascade of signaling events which includes the production of pro-inflammatory cytokines TNF-α [222], interleukins [223], and chemokines [224] that lead to localized inflammation and the surface expression of Cellular Adhesion Molecules (CAMs).[225] Subsequently, circulating tumor cells such as breast cancer and lymphomas have been shown to utilize inflammatory CAMs (e.g. ICAM, VCAM, ELAM) for extravasation, which then can lead to metastasis of these cancers [226, 227].

While the connection between metastasis and inflammation is well-known, NSAIDs are usually avoided postoperatively due to the potential for increased risk of hemorrhaging and immunosuppressive effects [228, 229]. Studies from the Baylor College of Medicine have reported that nearly 5% of patients experience post-operative hemorrhaging, and an overall increase of general surgical complications by 2.4x [230]. Furthermore, glucocorticoids (GCs) such as dexamethasone are contraindicated in patients with osteoporosis, a common side effect of chemotherapy treatment [231]. Additionally, systemic administrations of GCs have a relevant immunosuppressant action which has been hypothesized to increase the metastatic potential of shed tumor cells [232].

This mechanism of immunosuppression is believed to be due to GC binding to specific intracellular GC receptors (GR) in both vascular and immune system cells [233]. This complex then binds to multiple transcription factors and DNA motifs such as activator protein 1 (AP-1) and inhibits NF-κB activation by induction of the protein Iκβ [234]. Additionally, recent studies point to GC-induced modulation of other pathways such as Lck and Fyn, along with protein kinase B and C [233]. This wide range of

pathway modulation not only affects CAM expression, but also inhibits cytokine, prostaglandin, and nitric oxide production [235, 236] which confers a significant immunosuppressive reaction [237].

Flavones, notably the potent compound apigenin, have been reported to suppress JNK, ERK, and AP-1 pathways by inhibiting phosphorylation of kinases [44, 238] or pathway inhibitor proteins such as IκBα and IKK [239, 240], although the mechanism is not fully elucidated. This inhibition of phosphorylation effectively arrests pathway activation and stimulation, leading to the down regulation of ICAM-1, VCAM-1, and E-Selectin, along with NF-κB, [36, 37] making them potential candidates as therapeutic compounds for the prevention of cancer metastasis. Additionally, *in vivo* studies indicate little to no systemic toxicity, nor compromising of immune system function in large dosages as seen in GC and NSAID therapies, [241] potentially indicating safe usage after surgery. It is believed this is the result of a more specific pathway of modulation [242], as opposed to the "shotgun" levels of suppression from GC's. Previous research groups have published on the ability of apigenin to suppress monocyte adhesion [36] and tumor cell adhesion [243] in endothelial cells. As a result, apigenin has been selected as the molecule of interest to formulate into a promising drug delivery system.

The largest obstacle in flavonoid delivery is that in their natural form they exhibit poor solubility and limited bioavailability [244]. Widespread studies of oral consumption of both flavonoid-rich food and concentrated extract indicate little to no active form survives the GI tract [245]. A study in flavonoid absorption involving healthy ileostomy patients indicated less than 17% of a 100 mg oral dosage of pure flavonoid compound was recovered even before GI tract entry. Furthermore, analysis of blood plasma peaked at 90

ng/mL after 4 hour, or less than 0.38% of the initial dose [246]. In order to overcome this drawback, we have developed a class of degradable polymer systems based on beta amino ester (PβAE) chemistry. This chemistry allows for incorporation of flavonoids into the backbone of the polymer, creating a tunable release system while additionally protecting the active groups on flavonoids from premature oxidation.[188] As the polymer degrades, the active form of apigenin is recovered. Additionally, by developing a nanoparticle encapsulation delivery method, based on the biodegradable diblock copolymers methyoxypoly(ethylene glycol)-poly(lactide) (mPEG-PLA), both apigenin and apigenin PβAE polymers demonstrate slower release and high activity of active apigenin that can potentially overcome the limits presented by poor solubility and stability, and potentially provide a long-term delivery system. The benefits of incorporating a nanoparticle delivery system in tandem with slow releasing polymer include; enhanced solubility and bioavailability [247, 248], a delivery platform that can facilitate co-delivery of other therapeutics, or modification of the nanoparticle surface to include targeting ligands such as peptides or antibodies [249].

We hypothesize and report on that a novel delivery system containing a polymeric form of apigenin can overcome the problems of poor solubility and stability while still retaining the potential to prevent tumor cell metastasis.

6.2 Materials and Methods

6.2.1 Polymer synthesis

mPEG-PLA: DL-lactide was initially recrystallized in anhydrous ether to remove residual water and impurities. The purified DL-lactide was then stoichiometrically mixed with mPEG and 1% stannous 2-ethyl-hexanoate in dichloromethane (DCM) to form a polymer of a final molecular weight of 55,000. The resulting solution was heated to 90°C under continuous nitrogen purge until all solvent was evaporated. Following this, the ring-opening polymerization reaction proceeded for 6 hours at 120°C. The polymer was then cooled overnight, dissolved in DCM, precipitated in cold diethyl ether, and freeze-dried then stored till further use.

Apigenin multiacrylate: One gram of apigenin was dissolved in 100 mL of dimethyl sulfoxide (DMSO). To this solution, triethylamine was added at a molar ratio of 3:1 and mixed at 500 RPM. Next acryloyl chloride was added drop-wise with the solution placed in an ice bath at a molar ratio of 3.5:1. The reaction mixture was left stirring at room temperature for 12 hours. Precipitated triethylamine hydrochloride salt was removed by vacuum filtration in a separation flask. Distilled water at 20-fold excess was added to the reaction solution to precipitate the apigenin multiacrylate and it was subsequently refiltered. The powered apigenin was once again dissolved in DMSO and precipitated using 0.1 M K_2CO_3 to remove any potential unreacted acryloyl chloride. After the final wash step, the power was freeze-dried and stored at -20°C. Conversion of phenolic –OH groups was determined utilizing ^{1}H-NMR, HPLC, and FT-IR.

Apigenin poly (β-amino ester) (PβAE): Two forms of apigenin PβAE were formulated: a highly cross-linked film and a dispersible oligomeric form. To formulate the PβAE film, a single-step addition polymerization of 50:50 wt% poly(ethylene glycol 400 diacrylate) (PEG400DA) and apigenin multiacrylate with the primary diamine 4,7,10-Trioxatridecane-1,13-diamine (TTD) was completed as previously published[188]. To formulate the oligomeric form, PEG400DA was first mixed with the secondary diamine *N, N'*-Dimethyl-1, 3-propanediamine (NNDA) at a total molar acrylate to amine ratio of 0.9:1 and allowed to react for 4 hours at 60°C. Following incubation, apigenin multiacrylate in DCM (100% by weight of apigenin multiacrylate) was added to make a final ratio of 80:20 wt% apigenin multiacrylate: PEG400DA and reacted for a further 12 hours at 60°C. Polymerization was monitored through FT-IR, and molecular weight via GPC.

6.2.2 Degradation of apigenin PβAE films

To determine the activity of the pure PβAE polymer, films were placed in PBS (pH 7.4) at 37°C for 48 hours. The resulting solution was then freeze-dried, weighed, and then dissolved in DMSO at known concentrations and stored at -20°C until further use in cell culture assays.

6.2.3 Nanoparticle formulation and characterization

Formulation: mPEG-PLA and apigenin/apigenin PβAE polymers were dissolved in acetone with 5% DMSO (10 and 5 mg/mL, respectively, 1 mL total). The mixture was added drop-wise to 20 mL of deionized water with mixing at 1000 RPM. Solvent was allowed to evaporate and the solution was filtered through a 1 μm filter and centrifuged at

40,000g for 15 minutes followed by resuspension in an appropriate buffer; either PBS or complete cell culture media. Nanoparticle recovery was determined using a PEG-barium iodide complex assay. Briefly, a known mass of nanoparticles were dissolved in 200 µL of 5 M NaOH for 4 hours at 80°C then neutralized with 5 M HCl. The solution was then mixed with barium iodide, the absorbance was determined at 550 nm, and this was then compared against PEG standards.

Nanoparticle size: Particle size and polydispersity (PDI) was investigated using dynamic light scattering (DLS). After initial centrifugation, the nanoparticles were resuspended in PBS at 25°C at a concentration of 0.1 mg/mL then measured for size.

Drug loading: To determine apigenin drug loading, nanoparticles were formulated above with a slight exception. After the initial centrifugation, the supernatant and nanoparticle mass were freeze-dried overnight, then dispersed in DMSO. The absorbance was then measured and compared against standards of pure apigenin at 270 nm. Encapsulation efficiency and drug loading was determined by the mass of drug in the nanoparticles compared to the total mass added:

$$Encapsulation\ efficency = \frac{Mass\ of\ drug\ in\ nanoparticles}{Total\ mass\ of\ drug\ added} * 100\%$$

$$Drug\ Loading = \frac{Mass\ of\ drug\ in\ nanoparticles}{Total\ nanoparticle\ mass} * 100\%$$

6.2.4 *In vitro* drug release

To determine the rate of release of apigenin and apigenin PβAE from the mPEG-PLA nanoparticles, the following approach was utilized. The nanoparticles were suspended in 1 mL of PBS (pH 7.4) at 37°C at a concentration of 0.1 mg/mL and placed in a shaking water bath. At pre-determined time intervals, the nanoparticles were centrifuged at 40,000g for 15 minutes, and the supernatant absorbance was measured at 270 nm. The buffer solution was then replaced with fresh buffer to maintain sink conditions.

6.2.5 Cell culture

All cell lines were cultured at 37°C with 5% CO_2 and 95% humidity. Single donor human umbilical vein endothelial cells (HUVECs) were obtained from Lonza (St. Hopkinton, MA) and cultured in EGM-2 media (Lonza) supplemented with penicillin and streptomycin. HUVECs (passage 4 to 8) were seeded at a density of 50,000 cells/cm^2 and cultured overnight in 12 or 24 well plates. Human breast adenocarcinoma cells, MDA-MB-231, were obtained from ATCC (Manassas, VA) and cultured with Leibovitz's L-15 medium (ATCC) supplemented with 10% fetal bovine serum (FBS), penicillin, and streptomycin. MDA-MB-231's were seeded at a concentration of 25,000 cells/cm^2 for all adhesion studies. CellTracker Orange and Calcein AM were from Invitrogen Life Technologies (Grand Island, NY). TNF-α was obtained from Promega (Madison WI). Mouse anti-human VCAM-1 and DyLight 594 goat anti-mouse IgG antibody were obtained from Millipore (Billerica, MA).

6.2.6 Cell viability

HUVECs were seeded as described above and grown to confluence. The cells were treated with either free apigenin, degraded apigenin PβAE (both in a final concentration of 1% DMSO, along with appropriate controls), or directly with nanoparticles for 24 hours. Following this incubation period, the monolayers were washed once with media then viability was determined through the use of Calcein AM according to manufacturer protocols in a spectrophotometric plate reader. All treatment groups were compared to non-treated control cells.

6.2.7 Determination of tumor cell adhesion in cell culture

HUVECs were initially seeded in well plates as described above and grown to confluence. Cells were treated with the desired drug platform (free apigenin or apigenin PβAE with 1% DMSO) at various concentrations for 20 hours. After incubation, TNF-α at 10 ng/mL was added to induce inflammation for 4 hours. Following all treatments, HUVECs were stained using Calcein AM according to manufacturer protocols. In parallel, MDA-MB-231's were trypsinized and stained with CellTracker Orange according to the manufacturer's protocol. After staining, the MDA-MB-231's were centrifuged and washed to remove excess dye, then diluted to working concentrations of 25,000 cells/mL in HUVEC media. The media from the HUVECs was subsequently removed and replaced with MDA-MB-231-laden media and allowed to sit for 30 minutes to allow for adhesion to the cellular monolayer. After removing the media, HUVEC monolayers were then washed 3 times with fresh media to remove unbound tumor cells and the fluorescence of the bound MDA-MB-231 and HUVEC cells was measured (Calcein AM Ex/Em: 490 nm/ 520 nm, CellTracker Orange Ex/Em: 541 nm / 565 nm)

utilizing the fluorescent plate reader. Sample images were also obtained utilizing a fluorescent microscope. Tumor cell adhesion was determined against non-inflamed controls as a function of tumor cell fluorescence (TCf) by HUVEC fluorescence (Hf):

$$Tumor\ cell\ adhesion = \frac{TCf - TCf_{control}}{Hf - Hf_{control}} * 100$$

6.2.8 Time-dependent apigenin PβAE release in cell culture

Apigenin PβAE nanoparticles were suspended into HUVEC media at a concentration of 1 mg/mL. This solution was then incubated in a sealed sterile container in an incubator at 37°C for 24, 48, or 72 hours. The nanoparticles were centrifuged and the apigenin-containing media was utilized for the previously described tumor cell adhesion assay. Non-loaded nanoparticles and pure media were also subjected to these time course incubations as controls.

6.2.9 Quantification of inflammation suppression

HUVECs were seeded in well plates and grown to confluence. The cells were treated with free apigenin or nanoparticle formulations (unloaded, apigenin loaded, apigenin PβAE loaded) for 20 hours. Following this, the cells were washed once with media and TNF-α at a concentration of 10 ng/mL was added for 4 hours. Cells were fixed using cold 2% paraformaldehyde in DPBS for 10 minutes. The primary antiICAM-1 antibody was then added and allowed to sit for 45 minutes. After thorough washing with DPBS, the secondary fluorescent antibody was added for 45 minutes and washed once more. CAM expression was measured via fluorescence in a spectrophotometer.

6.3 Results

6.3.1 Characterization of apigenin multiacrylate

Figure 6-1 outlines the reaction sequence of apigenin to apigenin multiacrylate. NMR analysis reveals the disappearance of phenolic –OH peaks at 4.2 ppm (Figure 1) in the acrylated form of apigenin, indicating successful conversion. The FT-IR spectra of both apigenin and apigenin multiacrylate reveal the formation of a characteristic ester peak at 1740 cm^{-1}, resulting from –C=O bonds (Figure 2). Analysis of multiacrylate injection in HPLC indicated over 80% conversion to the acrylate form (data not shown).

6.3.2 Apigenin PβAE polymerization and characterization

Using a single step Michael addition polymerization scheme resulted in a dispersible oligimeric form of apigenin (Figure 6-2). FT-IR analysis indicates the disappearance of the acrylate C=C bond at 1620 and 1670 cm^{-1}, with preservation of the ester peak at 1740 cm^{-1} (Figure 6-5). GPC confirms an average molecular weight of 2110 with approximately 5.4 mers per polymer unit.

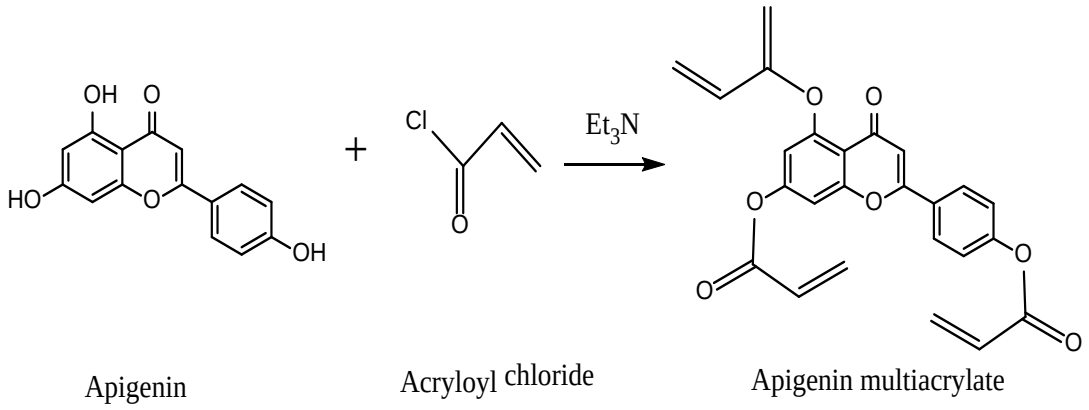

Figure 6-1: Reaction schematic of apigenin to apigenin multiacrylate

Apigenin reacts with acryoyl chloride in the presence of triethylamine to form apigenin multiacrylate.

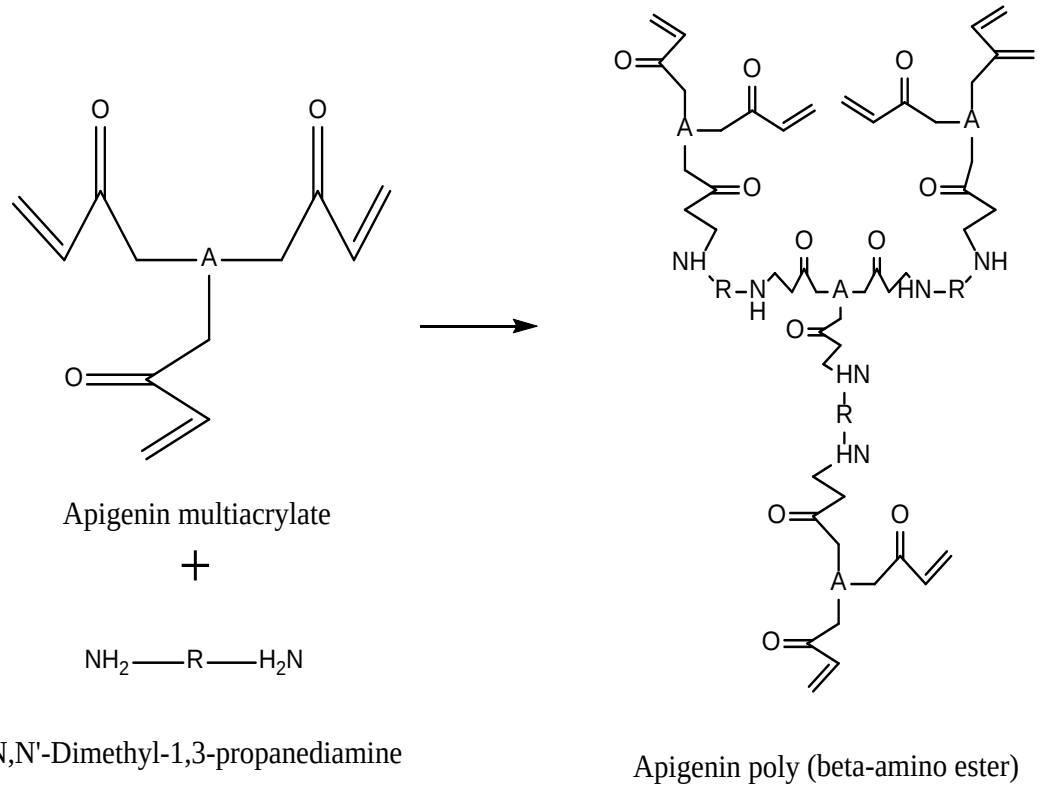

Figure 6-2: Reaction schematic for creation of apigenin PβAE

Apigenin reacts with NNDA to form a low molecular weight branched chain polymer.

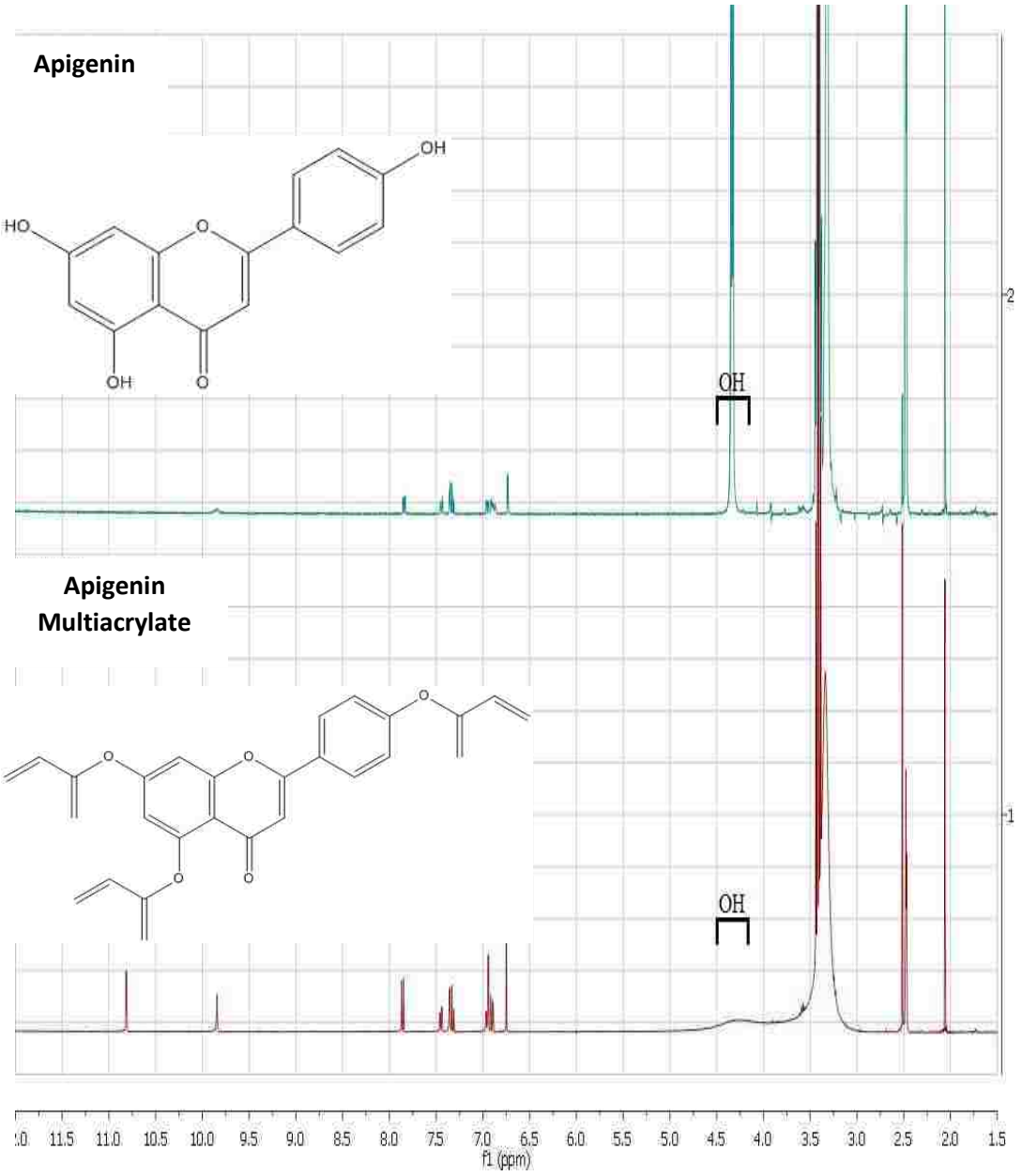

Figure 6-3: ^{1}H-NMR analysis of apigenin and apigenin multiacrylate

Structure of apigenin and apigenin multiacrylate. Apigenin was reacted with acryloyl chloride and purified. NMR scan reveal the disappearance of the phenolic –OH groups at 4.3 ppm, signifying successful conversion to acrylate groups.

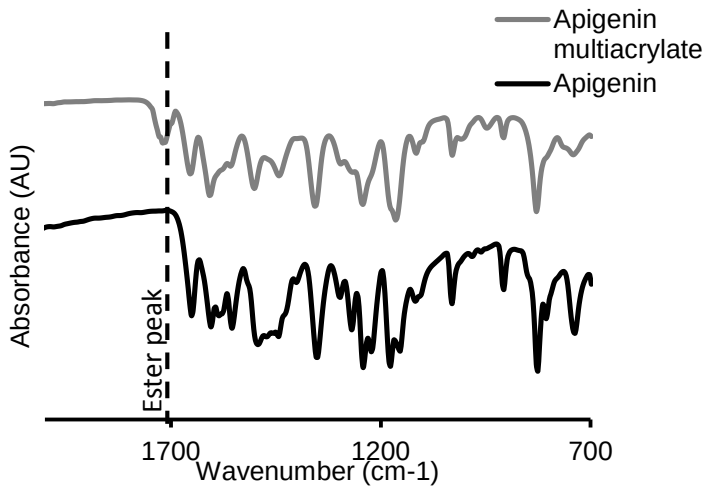

Figure 6-4: FT-IR analysis of apigenin and apigenin multiacrylate

Presence of the peak (dotted line) at ~1740 cm^{-1} of apigenin multiacrylate is a characteristic signal of ester groups, signifying successful conversion of apigenin to apigenin multiacrylate

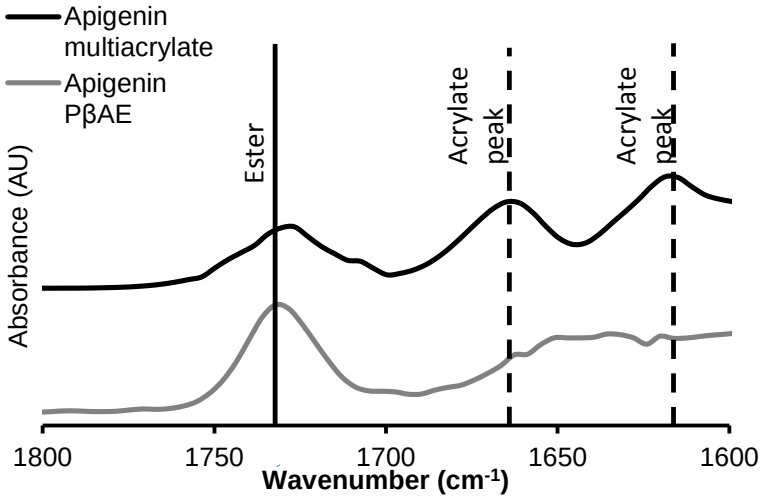

Figure 6-5: FT-IR analysis of apigenin multiacrylate and the polymer apigenin PβAE

The C=C peak at 1670 and 1620 cm^{-1}, characteristic of acrylate groups, disappear indicating reaction with the diamine NNDA. The ester peak at 1720 cm^{-1} remains in the final PβAE polymer, indicative of successful polymerization.

6.3.3 Characterization of nanoparticle formulations and release profiles

To formulate a delivery system for the highly hydrophobic apigenin and apigenin PβAE, a single-step nanoprecipitation method was utilized. Table 5.1 outlines the size, encapsulation efficiency, and final drug loading of each formulation. Blank mPEG-PLA nanoparticles were the smallest at 144.1 ± 13.5 nm. Pure apigenin-loaded particles were 211.8 ± 20.8 nm with a final drug loading of 25 ± 1.8%. Apigenin PβAE-loaded particles were larger at 256.0 ± 9.3 nm, with a slightly reduced loading at 19.2 ± 2.0%.

Outlined in Figure 6-6 are the release profiles of apigenin and apigenin PβAE from the mPEG-PLA nanoparticles. Apigenin-loaded nanoparticles exhibit a large and significant burst release within 4 hours of 54 ± 0.3%, a common occurrence for polymeric nanoparticles [250]. The apigenin-PβAE loaded nanoparticles however showed a marked suppression of this release, with only 35 ± 0.9% release within the first 4 hours.

Pure apigenin-loaded nanoparticles nearly release their full payload (over 80%) after 24 hours, whereas apigenin PβAE-loaded nanoparticles have released only 41% of their payload, and continue to steadily release for up to 120 hours.

6.3.4 Evaluation of apigenin and apigenin PβAE toxicity and tumor suppression capability

To evaluate whether apigenin or the degradation products of apigenin PβAE could protect inflamed endothelium from tumor cell adhesion, a well plate-based tumor adhesion model was developed. First, to find acceptable working concentrations of apigenin, the toxicity of apigenin was determined (Figure 6-6a). Extrapolating from the

viability data, a 4 Parameter Logistic (4PL) regression model was fitted. From the model, the 50% inhibitory concentration (IC50) was 88 µM, in range of toxicity defined in literature [251]. The onset of toxicity began at 50 µM. The degradation products of a 50:50 PEG:apigenin PβAE had an onset of toxicity at an equivalent apigenin concentration of 27 µM, with an IC50 of 60 µM (Figure 6-6). The results indicate that the medication and degradation products associated with the apigenin PβAE do not result in potentially toxic byproducts.

Following this, HUVECs were incubated with 5, 10, and 20 µM of apigenin and the equivalent apigenin concentration of 10 and 20 µM from the PβAE degradation products, followed by treatment with TNF-α for 4 hours. It was observed that cells treated with TNF-α had over 82% more adhered tumor cells compared to cells without TNF-α treatment. This finding has been previously published by our group [252]. With each concentration of pure apigenin treatment, the tumor cell adhesion percentage reduced to background levels, with no statistical ($P > 0.05$) concentration dependence observed (Figure 6-7a). The degradation products of apigenin PβAE did exhibit a concentration-dependent suppression effect, with 10 µM at 129 ± 7.0 % and 20 µM at 106 ± 5.1 % adhesion over uninflamed controls (Figure 6-7b).

Additionally, cells treated with apigenin, but without TNF-α, showed no statistical effect ($P > 0.05$) on tumor cell adhesion possibly indicative of the anti-inflammatory mediated function of adhesion suppression. Due to this result, all further treatment experiments were done in the presence of TNF-α.

Table 6-1: Nanoparticle characterization summary.

Pure apigenin-loaded particles show higher entrapment efficiency (EE), lower size, and drug loading (DL) efficiencies as compared to apigenin PβAE, possibly due to size differences between the monomer and polymer forms (N=3, M±SD).

Drug-loaded Core	Size (nm)	PDI	EE (%)	DL (%)
Unloaded	144.1 ± 13.5	0.176	N/A	N/A
Apigenin	211.8 ± 20.8	0.412	49.0 ± 3.7	25.0 ± 1.8
Apigenin PβAE	256.0 ± 9.3	0.299	38.4 ± 4.1	19.2 ± 2.0

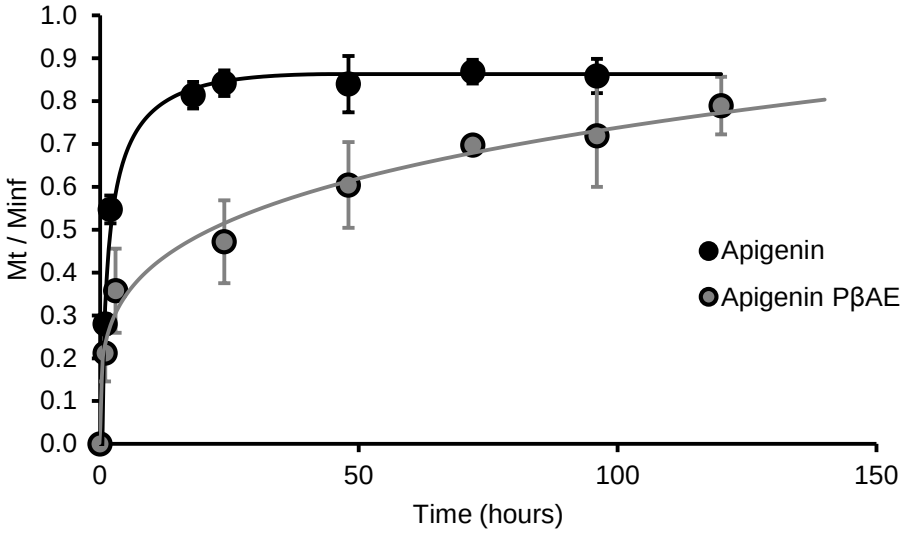

Figure 6-6: Nanoparticle in-vitro release profile

Apigenin-loaded nanoparticles have a high burst effect, followed by near complete release after 24 hours. Apigenin PβAE-loaded nanoparticles by contrast exhibit a smaller burst release followed by a linear release profile up to 120 hours (N=3, M±SD).

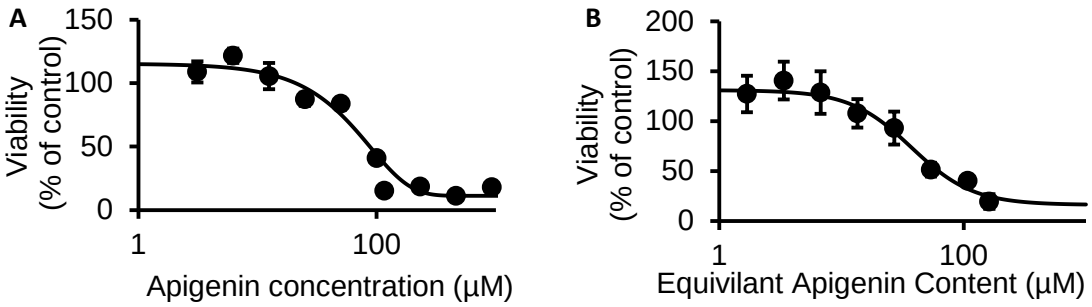

Figure 6-7: Apigenin and apigenin PβAE degradation product toxicity

(A) After 24 hours, the IC50 of apigenin is 88 µM, similar to previously published literature. (B) The degradation products of apigenin PβAE demonstrate an IC50 of 60 µM (N=3, M±SE).

6.3.5 Apigenin and apigenin PβAE nanoparticles retain tumor cell adhesion suppression capacity

Drug-loaded nanoparticles ranging from 0.3 mg/mL to 5 mg/mL were suspended in HUVEC media and directly added to HUVECs without the addition of solubilization agents. A 4PL regression model was fitted to the toxicity plots. Apigenin and apigenin PβAE-loaded nanoparticles were determined to have IC50 values of 4.4 and 3.08 mg/mL, respectively. Blank nanoparticles showed no toxicity over 5 mg/mL (Figure 6-9a).By transforming the data to examine apigenin content only, the IC50 for apigenin is 855 μM compared to 395 μM for apigenin PβAE (Figure 6-9b). Apigenin-loaded nanoparticles retain their anti-inflammatory effect and suppress tumor cell adhesion, as observed in its free form. At a nanoparticle concentration of 0.25 mg/mL a maximum suppression is seen at 118 ± 9.4% adhesion over unstimulated controls (Figure 6-10). At 0.5 and 1 mg/mL an unexpected increase of adhesion is observed. Correlating the dosage to the toxicity plot, we observe the onset of toxicity coinciding at 0.5 mg/mL. Apigenin PβAE nanoparticles show a similar trend with a maximum suppression at 0.5 mg/mL (117 ± 14.1%). The higher dosage required is due to the combination of lower loading (19.2% versus 25%) along with the polymer composition (80% apigenin multiacrylate:20% PEG) Blank nanoparticles show no statistical effect ($P > 0.05$) on tumor cell adhesion, again confirming the therapeutic activity to come from the apigenin payload.

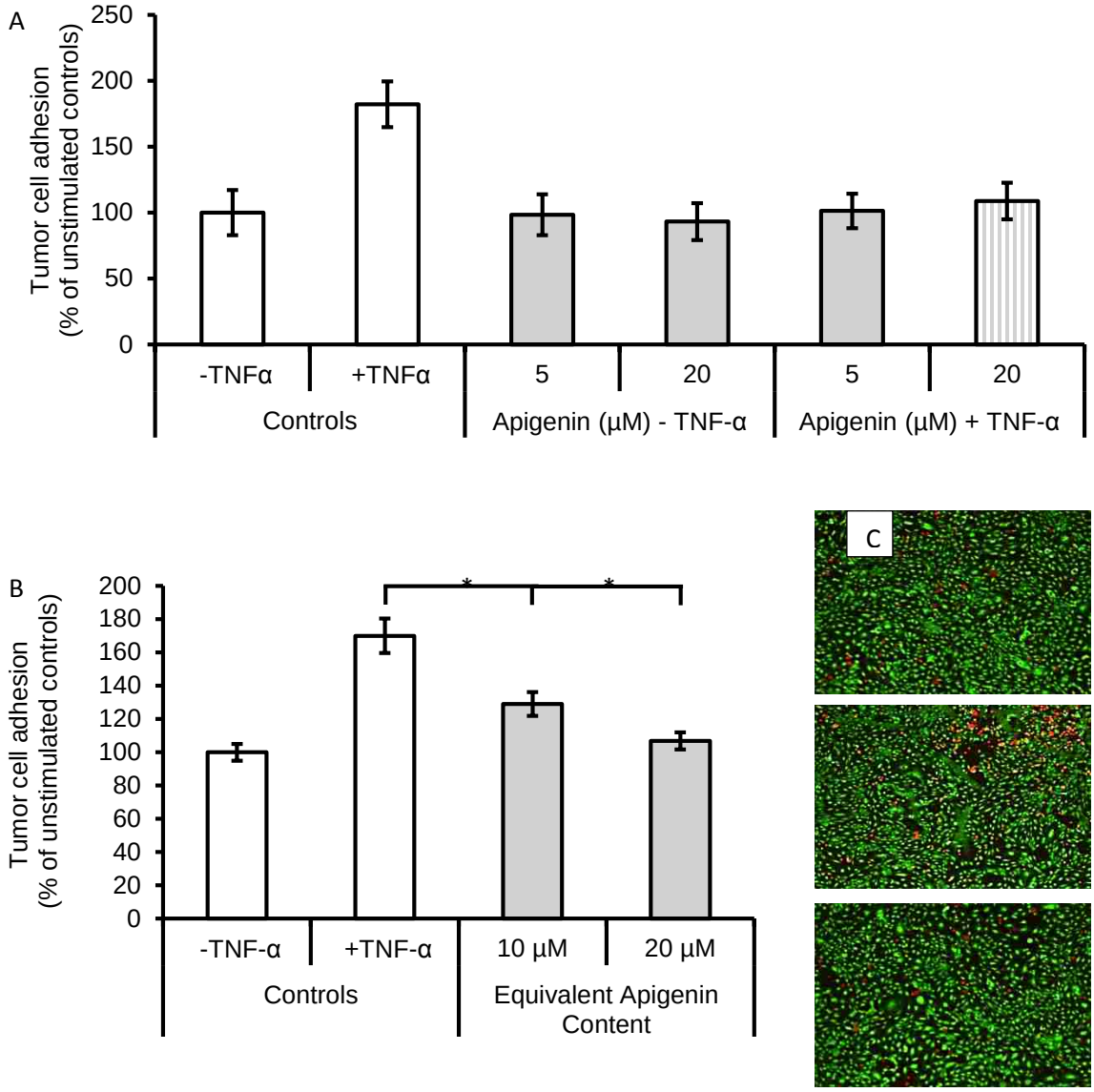

Figure 6-8: Apigenin and Apigenin PβAE tumor cell suppression activity: (A) Pure apigenin suppressed tumor cell adhesion to non-stimulated control levels. Apigenin also does not elicit further suppression response in HUVECs not treated with TNF-α. (B) Apigenin PβAE products still retain suppression activity after degradation. (C) Fluorescent micrographs of tumor cell adhesion. (Top) Calcein AM stained unstimulated HUVECs with cell tracker orange MDA-MB-231 tumor cells. (Middle) TNF-α treated cells show a marked increase in tumor cell adhesion. (Bottom) Apigenin treated cells reduce adhesion levels to background. (*$p < 0.05$, N=3, M±SE).

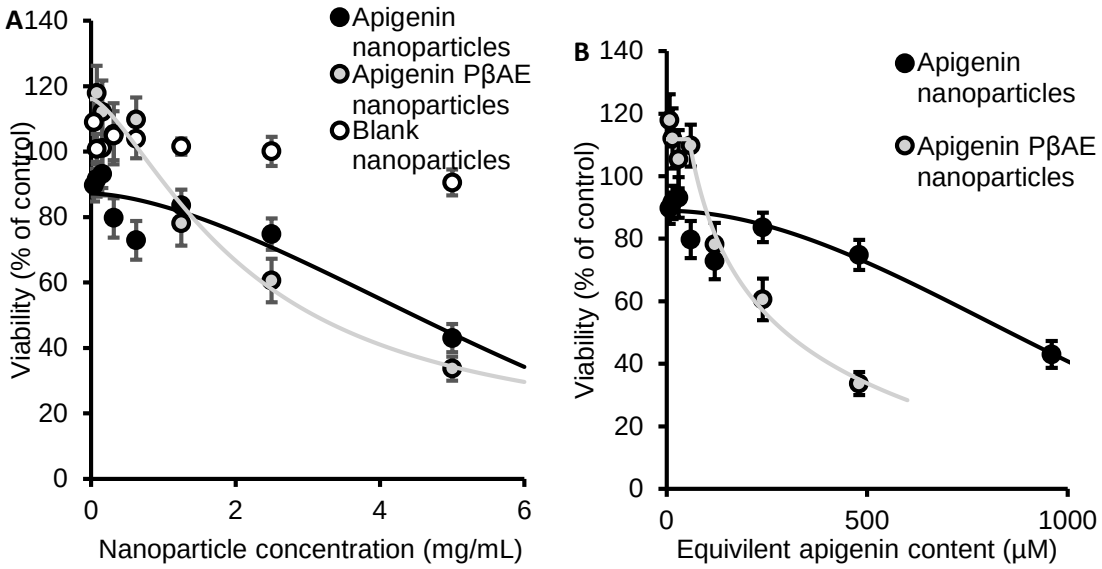

Figure 6-9: Apigenin and apigenin PβAE nanoparticle toxicity profile

(A) Blank nanoparticles show no toxicity up to 5 mg/mL whereas apigenin and apigenin PβAE nanoparticles have IC50 values of 4.4 mg/mL and 3.08 mg/mL respectively. (B) Both apigenin and apigenin PβAE-loaded nanoparticles have an order of magnitude higher toxicity than their free form counterparts (855 µM and 395 µM respectively) (N=3, M±SE).

6.3.6 Extended release of apigenin PβAE nanoparticles provides potential long term tumor cell adhesion suppression

Apigenin PβAE-loaded nanoparticles demonstrated continual release over a 120 hour period. To test the hypothesis that these nanoparticles would release the active compound over this time frame they were incubated in media at 37°C for up to 72 hours. The supernatant, containing released apigenin was then utilized directly. The apigenin PβAE-loaded particles continued to show increasing levels of activity over time. At 72 hours, tumor cell adhesion decreased from 181 ± 6% to 123 ± 12% (Figure 6-11a). Extrapolating from the release curves, at 72 hours, approximately 67% of the drug payload was released, correlating with suppression levels of direct nanoparticle treatment at 0.5 mg/mL. In order to rule out the possibility of suppression due to other factors, blank nanoparticles and media were incubated for the same time frame and tested, with no statistical difference in suppression (Figure 6-11b).

6.3.7 Evaluation of inflammatory intracellular adhesion molecule (ICAM-1) expression

Cells treated with TNF-α at a 10 ng/mL concentration for 4 hours had an elevated level of ICAM-1 expression, 202 ± 25% above untreated cells. Treatment with pure apigenin at 10 μM reduced ICAM-1 levels to 65 ± 8.5%. The nanoparticle therapies of apigenin and apigenin PβAE reduced expression levels to 80 ± 9.3% and 97 ± 16% of unstimulated controls. The unloaded nanoparticles demonstrated no therapeutic efficacy (Figure 6-12).

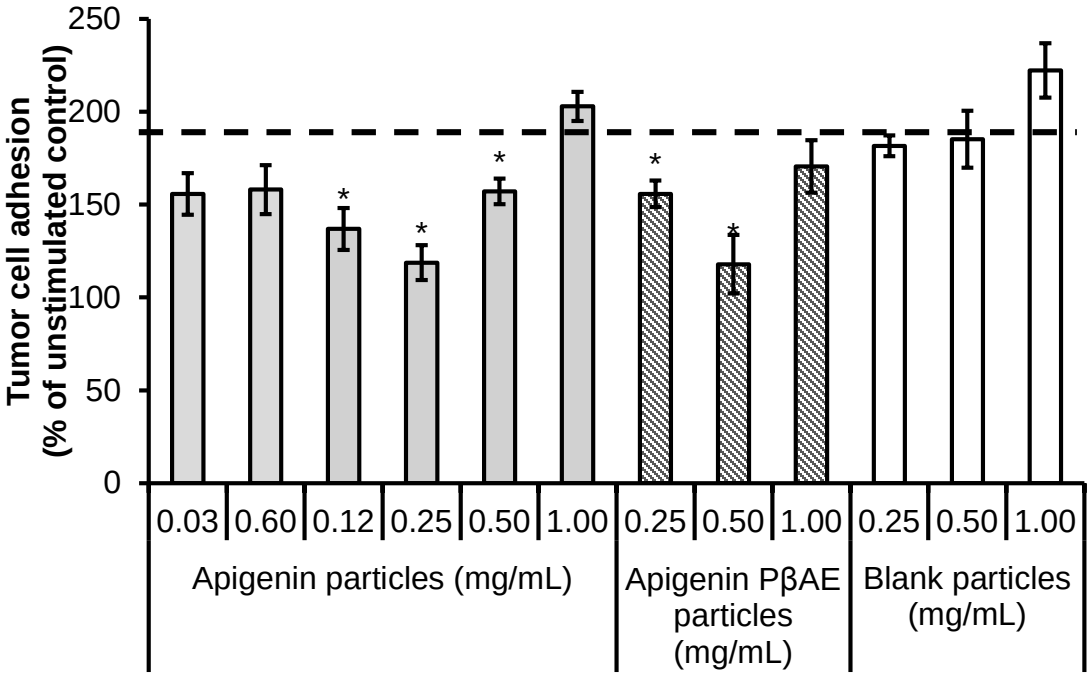

Figure 6-10: Apigenin and apigenin PβAE nanoparticle tumor cell suppression activity

Both forms of nanoparticles demonstrate similar suppression activity whereas blank nanoparticles have no effect. Apigenin PβAE nanoparticles show a shifted suppression ability due to lower overall loading. After the onset of toxicity higher levels of tumor cell adhesion are recorded. Dotted line indicates level of tumor cell adhesion in TNF-α activated controls (*$p < 0.05$, N=3, M±SE).

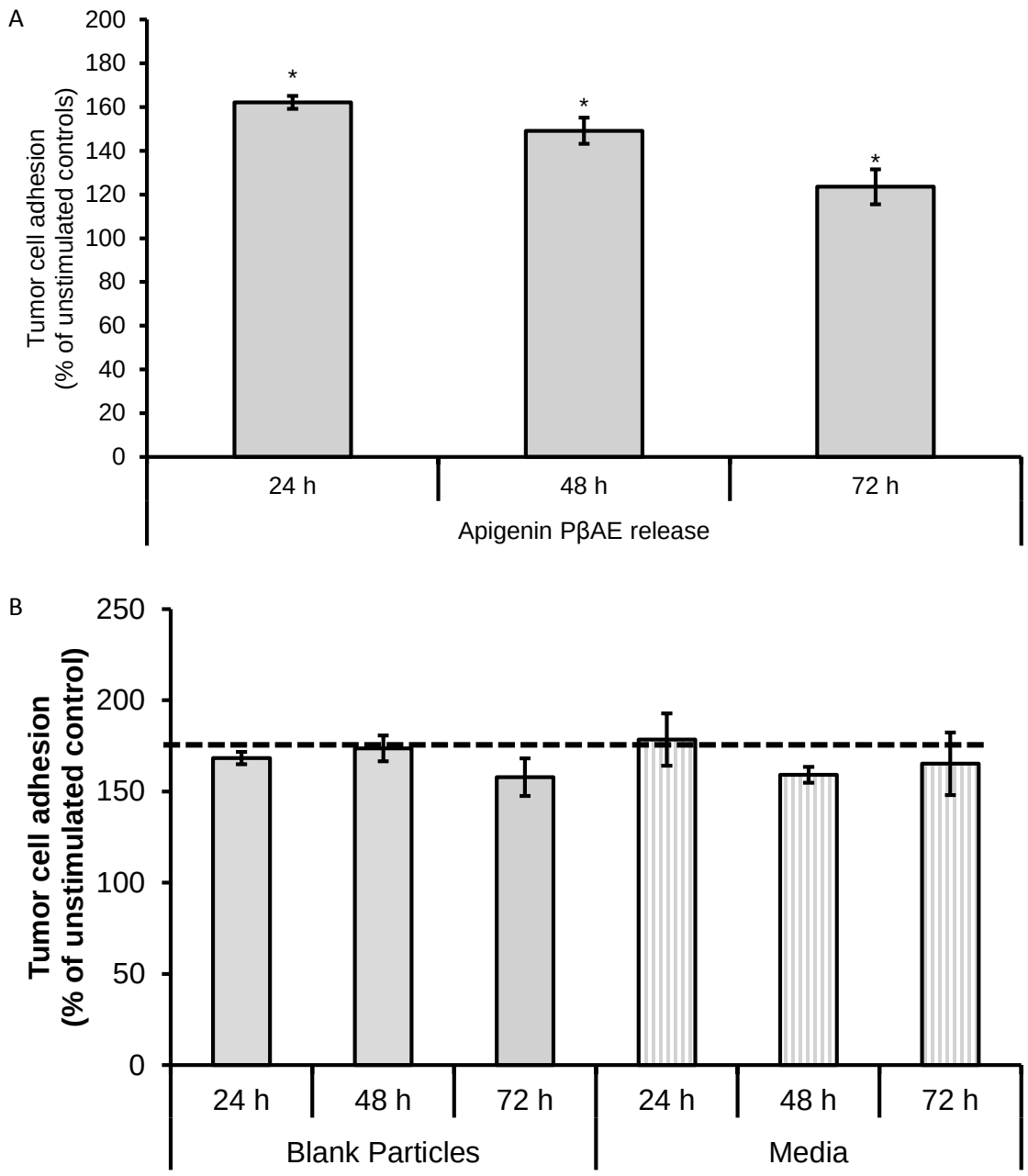

Figure 6-11: Long-term release of apigenin PβAE and tumor suppression activity

(A) Apigenin PβAE nanoparticles have a time-dependent activity due to their long-term release profile. (B) Blank particles and pure media show no statistically significant suppression ability. Dotted line indicates level of tumor cell adhesion in TNF-α stimulated controls (*$p < 0.05$, N=3, M±SE).

6.4 Discussion

As mentioned previously, the anti-inflammatory [253] and antioxidant [254] activity of naturally-derived flavones provides a promising *in vitro* treatment avenue and these materials are applicable in many types of injuries [255] and disease states [256]. Despite this, using flavones as a therapeutic regime has been plagued by issues translating to *in vivo* work due to, in part, by poor solubility, stability, and pharmacokinetics. To address the issue of stability we have developed a non-free radical-based polymerization scheme for antioxidants and anti-inflammatories such as quercetin, curcumin, and apigenin. In their polymeric form these compounds are protected from premature oxidation, and through careful selection of commonly used reagents in the reaction process, can achieve desirable delivery rates following degradation. The new apigenin-based PβAE polymer outlined in this work has been shown to retain activity after complete degradation.

The degradation products of apigenin PβAE do not, however, retain the full activity. The possible explanation for this could be that the degradation products do not fully regain their anti-inflammatory properties, either due to incomplete degradation of the PβAE chains or apigenin

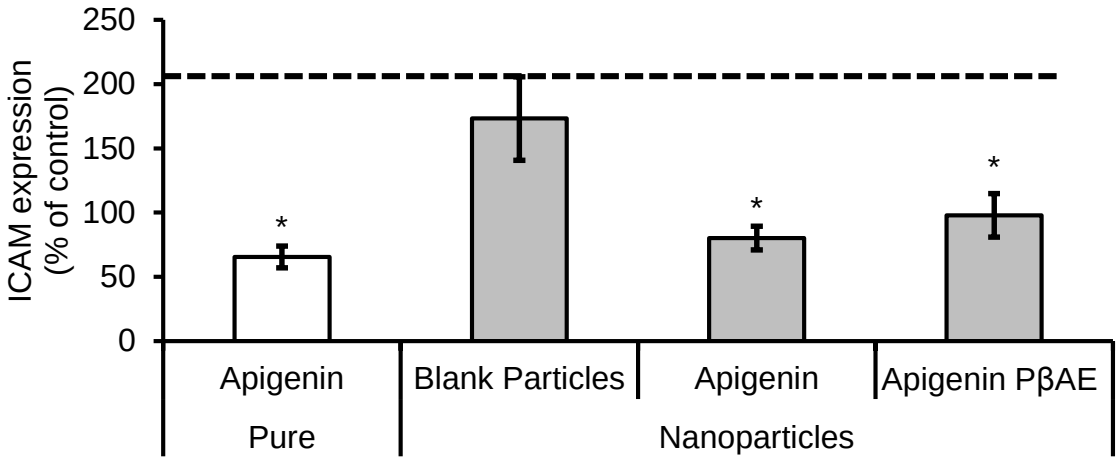

Figure 6-12: Inflammatory CAM expression in HUVECs

Both pure apigenin and nanoparticle formulations significantly reduce ICAM-1 expression in TNF-α treated HUVECs. Blank nanoparticles provide no therapeutic benefit. Dotted line indicates level of tumor cell adhesion in TNF-α activated controls (*$p < 0.05$, N=5, M±SE).

multiacrylate to apigenin. This phenomenon has been observed in a previous publication utilizing antioxidant PβAE polymers [188]. Most interestingly is that our experiments demonstrate that apigenin has no tumor cell adhesion suppression effect in uninflamed endothelial cells, lending credence to the link between inflammation, tumor metastasis, and the ability of flavones to suppress cell adhesion.

To formulate a delivery system for the highly hydrophobic apigenin and apigenin PβAE, a single-step nanoprecipitation method was utilized. By encapsulating apigenin and the apigenin PβAE into a nanoparticle formulation, we can confer advantageous drug delivery properties, such as increased solubility, controllable release, and improved pharmacokinetics through the masking of PEG moieties. The developed nanoparticles range in size between 200-250 nm, which is within the generally accepted size to encourage cellular uptake and internalization [257], with drug loading rates of up to 25%.

Initial cell culture results indicate an order of magnitude decrease in the toxicity between free apigenin and encapsulated apigenin in particle form (80 μM versus 855 μM, respectively). This marks an order of magnitude lower threshold of toxicity, due to the longer term drug release and protection inside a normally inert nanoparticle, compared to a large bolus application in the free drug form. Also, the unloaded nanoparticles demonstrated no toxicity up to 5 mg/mL, indicative that the toxicity of these nanoparticles stems solely from the loaded drug.

Our toxicity model suggests the apigenin PβAE nanoparticles exhibit slightly higher toxicity (400 μM), possibly due in part to impurities from unreacted amines during polymer formulation. However, both formulations retain their adhesion suppression potential. Interestingly, at the highest concentrations of both formulations, the tumor cell

adhesion increases. We believe that at this dosage, the toxic effects begin to overcome the anti-inflammatory benefits provided by apigenin. This toxicity at high concentrations has been observed with our previous antioxidant work [45]. While apigenin PβAE nanoparticles required a higher incubation concentration to achieve the same effect as apigenin, it is important to note that the active drug loading content is 41% lower.

Comparing the release kinetics of apigenin and apigenin PβAE nanoparticles, we observe the most notable trend. Pure apigenin-loaded particles released the majority of their payload within 18-24 hours, with a significant burst release effect within the first hour, a common characteristic with PLA/PLGA based systems [258]. In the scenario of the apigenin PβAE-loaded nanoparticles, a less pronounced burst release is seen, followed by a sequential linear release for up to 120 hours, a stark contrast from the free form of apigenin. It is theorized that the diffusion out of the particles is hindered due to the higher molecular weight of the PβAE. However, it is unclear at this time whether the enhanced release is due to the possibility of PβAE release then subsequent degradation to active apigenin in solution or if the PβAE is degrading within the nanoparticle, followed by diffusing outwards.

To evaluate the potency of this longer term release mechanism, the nanoparticles were incubated in media at normal cell culture conditions over a 72 hour period of time. The particles were then separated from the therapeutic-containing media and cells were dosed with this media. Our results show time-dependent release results with a decrease in tumor cell adhesion. After 72 hours, cell adhesion is reduced to nearly background levels (123 ± 12%). Correlating the previous release data with the time-dependent suppression potential, there is a strong correlation with the whole nanoparticle incubation results. This

points to a potentially viable drug delivery platform that could provide a long circulating and releasing therapeutic to inhibit inflammation-mediated cancer metastasis.

Lastly, in order to derive a link between inflammation and tumor cell adhesion, we examined the expression levels of the inflammatory marker ICAM-1. As expected, we observe a pronounced increase in expression levels of HUVECs treated with TNF-α. Cells treated with pure apigenin do demonstrate the highest level of CAM and tumor cell adhesion suppression, however a viable treatment utilizing the compound alone would prove difficult at best, for reasons explained previously. The apigenin and apigenin PβAE loaded nanoparticles also significantly reduce ICAM-1 expression, down to lower than constitutive expression in fact, while also retaining the ability to inhibit tumor cell adhesion with a higher toxicity threshold, and a demonstration of enhanced release properties with the apigenin PβAE nanoparticles. Figure 6-13 links the correlation to ICAM-1 expression and tumor cell adhesion suppression. We see that for each therapeutic treatment, a near linear relationship is formed, while leaning slightly on the side of higher ICAM-1 suppression. These results suggest a link between the two properties, and further strengthens the discussion of links between metastasis and inflammation.

6.5 Conclusions

This work has demonstrated that a novel flavone-based polymeric nanoparticle system can be used to provide the extended release of active anti-inflammatory compounds. These nanoparticles have been shown to inhibit tumor cell adhesion to inflamed endothelial cells through the delivery of viable apigenin. Future work in the development of targeted nanoparticles through the use of targeting peptides or antibodies

can potentially enhance the ability to suppress inflammation exclusively at sites of interest, such as localized chemotherapy or surgical sites.

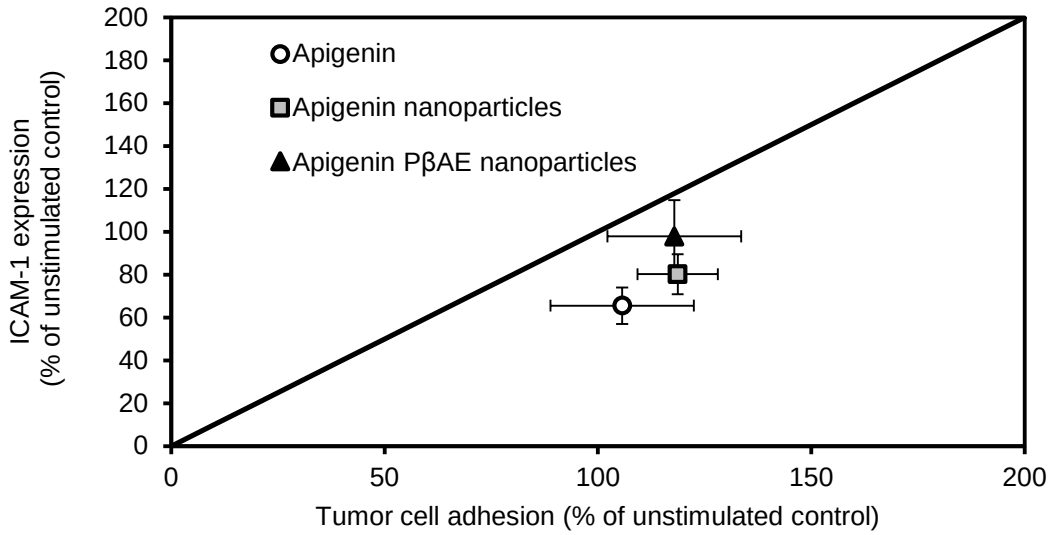

Figure 6-13: Tumor cell adhesion verses ICAM-1 expression

Analysis of therapeutic treatment options demonstrates a near linear link between ICAM-1 expression levels and the ability for tumor cells to firmly adhere to the HUVEC monolayer surface. (N = 3 for x: 5 for y, M±SE)

Chapter 7. Conclusions

In this work, we have developed antioxidant polymers and delivery systems to create practical therapeutics to treat a variety of injuries and diseases. Initially, we have utilized nanoparticles of our novel antioxidant polymer, poly(trolox), and modified their surfaces with monoclonal antibodies. This surface-modification allows for the nanoparticles to be directed to sites of interest. To use this therapeutic in a practical application, we investigated the toxicity associated with iron oxide nanoparticles. These particles are currently being used as MRI contrast agents, drug delivery devices, and chemotherapy adjuvants. Although these nanoparticles have been regarded as non-toxic, a growing body of evidence has pointed towards toxicity stemming from free radical generation and oxidative stress.

We first created antibodies directed towards platelet endothelial cellular adhesion molecules, a constitutive protein expressed primarily in vascular endothelial cells. These PTx adhered and internalized specifically to HUVECs and it was found to suppress the damaging effects of iron oxide nanoparticles. Not only did PTx reduce levels of free radicals, but it also fully recovered cell viability.

In order to understand the link between oxidative stress and injury further, we employed PTx again in an *in vivo* model. By utilizing an inflammation-mediated arthritis injury in mice, we could further elucidate the connection between inflammation, oxidative stress, and disease. It was found that PTx did not have any apparent effect on the arthritic injuries in mice. However, we did observe a significant recovery of antioxidant capacity and suppression of protein carbonyl content, a marker for oxidative stress and injury. In addition, PTx also suppressed cytokine expression known to be

associated with oxidative stress. Further study will be required to tease out the connection to injury and discrepancy between physical and chemical cues.

With the link between metastasis potential and inflammation well-established, we hypothesized that our polymers could be used to inhibit the progression of cancer. In our final study, we utilized our unique poly(beta-amino ester) chemistry to develop a long term delivery system of anti-inflammatory polymers.

Linear chain polymers of apigenin were encapsulated in mPEG-PLA to form a biocompatible polymer capable of delivering active apigenin over a 72 hour period. These PβAE particles were less toxic and deliverable at higher dose compared to the extremely hydrophobic native apigenin. It was found that these apigenin PβAE nanoparticles were able to inhibit the ability of highly metastatic tumor cells to adhere to healthy vascular cells. The long term release component also allows for continual therapeutic dosing for the entire course of the natural inflammation cascade.
By demonstrating that antioxidant polymer therapy can be utilized to treat relevant injuries and diseases, we come one step closer to realizing far reaching clinical applications.

APPENDIX

Based on the research article:

> Mo Dan, David Cochran, Robert Wydra, Robert Yokel, Thomas Dziubla. "Binding, transcytosis, and biodistribution of anti-PECAM-1 iron oxide nanoparticles for brain-targeted delivery" PLOS ONE.

Introduction

Multifunctional superparamagnetic iron oxide nanoparticles (IONPs) have various applications, such as diagnosis and therapy of the central nervous system (CNS) [259, 260]. For example, IONPs have drawn increasing attention as T2 magnetic resonance imaging (MRI) contrast agents to evaluate blood-brain barrier dysfunction related to tumors and other pathologies such as stroke and carotid atherosclerosis in clinical and preclinical studies [261, 262]. Multifunctional IONPs also provide the possibility to deliver therapeutic agents to the brain and concurrently monitor their tissue distribution using MRI [263, 264]. One of the challenges for CNS applications of IONPs is the ability to cross the highly restricted blood-brain barrier (BBB). Previous research has suggested evidence of IONP flux across the BBB by analyzing whole brain concentration. However, there have been no reports distinguishing between IONPs in the brain vessels and BBB cells [265], or therapeutic efficacy of co-delivered compounds in animal models of brain tumors [266]. To advance the potential applications of multifunctional IONPs in the CNS, there is an urgent need to understand how they associate with, and transcytose across, the BBB *in vitro* and *in vivo*.

Brain capillary endothelial cells cooperate with pericytes, astrocytes, and neurons to generate and maintain the unique barrier properties of the BBB. The BBB plays a crucial

role in safeguarding the brain from endogenous and exogenous compounds, which includes most therapeutics [267]. A recent study evaluated the uptake and flux of IONPs using human brain-derived endothelial cells. IONP flux without targeting moieties on the surface was very limited under normal conditions [268]. A promising strategy to enhance IONP flux across the BBB is to use a BBB targeting moiety. Platelet-endothelial cell adhesion molecule (PECAM-1) (CD31) is a member of the immunoglobulin superfamily that is constitutively expressed on endothelial cell membranes and is involved in transcytosis of activated leukocytes across the BBB in neuroinflammation [269-271]. Furthermore, significant upregulation of PECAM-1 in neuroinflammation provides a potential to target the CNS for the treatment of neurological conditions such as stroke and brain tumor [271]. Pure PECAM-1 antibody has been shown to target the endothelial lumen, but does not internalize into endothelial cells [195]. However, anti-PECAM-1 coated nanocarriers can enter the endothelial cells through a unique vesicular internalization pathway, [190]. Anti-PECAM-1 antibodies conjugated to diverse therapeutic cargoes and nanocarriers provided robust intracellular drug delivery into endothelial cells [183]. However, how anti-PECAM-1 nanocarriers associate with and traffic across the BBB, one of the most important endothelial cell barriers, still needs to be defined.

We hypothesized that PECAM-1 antibody will increase IONP BBB association, trafficking across the BBB, and change its distribution profile *in vitro* and *in vivo*. In this study, we characterized anti-PECAM-1 IONPs for size, adhesion to immortalized human brain capillary endothelial (hCMEC/D3) cells, and stability in blood. We investigated the association, and flux across the BBB over 6 hours, of anti-PECAM-1 IONPs using

hCMEC/D3 cells. Furthermore, anti-PECAM-1 IONP brain accumulation and biodistribution in peripheral organs were studied in Sprague Dawley rats. The capillary depletion method was used to test anti-PECAM-1 IONP *in vivo* distribution between the BBB endothelial cells and brain parenchyma. The results of this study demonstrate the potential of anti-PECAM-1 IONPs to target and transcytose across the BBB and enter into the brain parenchyma, providing valuable insight into the feasibility of anti-PECAM-1 IONP as a brain targeting MRI contrast agent and/or drug delivery system for CNS.

Materials and Methods

Ethics Statement

This study used 21 male Sprague-Dawley rats, weighing 300 ± 25 g (mean ± SD), that were housed individually prior to study in the University of Kentucky Division of Laboratory Animal Resources Facility. Animal work was approved by the University of Kentucky Institutional Animal Care and Use Committee (Protocol 2008-0272). The research was conducted in accordance with the Guiding Principles in the Use of Animals in Toxicology.

Reagents

Mouse anti-human anti-PECAM-1 was created and purified in house through the use of a hybridoma cell line (P2B1) purchased from the Developmental Studies Hybridoma Bank (Iowa City, IA). For *in vivo* studies, a mouse anti-rat anti-PECAM-1 (Clone TLD-3A12) was purchased from Millipore (Billerica, MA). Nonspecific mouse IgG was from Jackson Immuno (West Grove, PA). $Na^{125}I$ was purchased from Perkin Elmer (Boston, MA). All other reagents were from Sigma-Aldrich (St. Louis, MO).

Iron oxide nanoparticle synthesis

IONPs were synthesized using a previously reported method [166]. Briefly, ferric chloride hexahydrate (Fe^{3+}) and ferrous chloride tetrahydrate (Fe^{2+}) were dissolved in deionized water (Fe^{3+} :Fe^{2+} = 2:1), followed by adding ammonium hydroxide dropwise under an N_2 atmosphere at 85 ºC. After 1 h, the solution was placed on a magnet to collect black brown particles, which were washed repeatedly using pure ethanol [189, 272]. IONPs were dried overnight in a vacuum drying oven. Properties, such as size and zeta potential of the IONPs, were determined in our laboratories. All of the methods have been previously reported [273].

Protein iodination for antibody tracing

IgG and the anti-PECAM-1 antibody were labeled with $Na^{125}I$ using the Iodogen method. In brief, 100 µg of antibody was mixed with 15 µCi of $Na^{125}I$ for 5 minutes in glass tubes coated with Iodogen reagent. Following the reaction, the now-labeled protein was purified using Bio-Rad Labs packed spin columns (Hercules, CA). The extent of iodination was determined by protein precipitation followed by analysis of radioactivity in the pellet and supernatant [274].

Preparation and characterization of antibody-modified iron oxide surfaces

Iron oxide nanoparticles were suspended in PBS and sonicated with a probe sonicator at a power output of 10 W for 1 minute, then transferred to a sonication bath for 30 minutes prior to surface coating. To couple anti-PECAM-1 or IgG antibody to iron oxide nanoparticles, a physioabsorption technique was employed. Either anti-PECAM-1 or IgG antibodies were incubated with the nanoparticles at a solution concentration equivalent to

10,000 antibodies/μm^2 particle surface area, 1.2 times the theoretical monolayer coating based on antibody size and particle surface area. Radiolabeled anti-PECAM-1 or IgG in PBS was added to the suspended nanoparticles and incubated for 1 hour at 25°C. Particles were washed 3 times by centrifugation for 30 minutes at 22,000*g* and suspended in 1% BSA-PBS. The antibody was traced in both supernatant and pellets using a PerkinElmer 2470 Automatic Gamma Counter to determine the extent of surface coverage.

Antibody-modified iron oxide nanoparticle stability in blood

To determine coating stability *in vivo,* particles were incubated in heparin-treated whole rat blood at 37°C for 24 h at equivalent concentrations utilized *in vivo* (blood to nanoparticles, 0.015 mg/ml). At pre-determined time points, aliquots of whole blood were centrifuged and separated from the nanoparticles and analyzed on the gamma counter.

Cell lines and culture conditions

Immortalized human brain capillary endothelial cells (hCMEC/D3) were obtained under license from INSERM, France. The cells were maintained in endothelial growth medium-2 supplemented with 2.5% fetal bovine serum, 1% penicillin and streptomycin, 0.1% fibroblast growth factor, 0.01% hydrocortisone and 0.025% vascular endothelial growth factor, insulin-like growth factor and endothelial growth factor, under 37°C and 5% CO_2. Cells were passaged into collagenated culture flasks every 3-4 days when they reached approximately 85%-95% confluence [275-277].

PECAM-1 antibody binding affinity to the human brain endothelial cell line hCMEC/D3

hCMEC/D3 cells were seeded on 36 well plates at a density of 50,000 cells/cm^2. They were incubated with serial dilutions from 0.78 to 100 nM of ^{125}I anti-PECAM-1 or ^{125}I IgG antibodies for 2 h (n = 3). Donor chamber supernatant was collected and the cells were washed 3 times with PBS at 4 °C. The hCMEC/D3 monolayer was lysed with 1% Triton X-100 in 1.0 N NaOH. The cell lysate and supernatant (including the washing solution) radioactivity were measured using a Wallac 1470 Wizard™ gamma counter. B_{max} and K_d were calculated using GraphPad Prism (GraphPad Sofware, San Diego, CA, USA).

Anti-PECAM-1 IONP binding and flux using the human brain endothelial cell line hCMEC/D3 *in vitro* BBB model

hCMEC/D3 cells were seeded on type I collagen pre-coated 6 well Transwell filters (polycarbonate 12 mm, pore size 3.0 µm) at a density of 50,000 cells/cm^2. Flux assays were performed 7-10 days after seeding [275, 276]. The tightness of the hCMEC/D3 monolayer was measured as transepithelial electrical resistance (TEER) using a RMA321-Millicell-ERS voltohmmeter (Millipore Corp, Billerica, MA). To monitor flux through the paracellular pathway, lucifer yellow (LY, 100 µM) was added to the medium on the donor side of the cells. Samples of the medium from the donor chamber were collected at time zero and from the receiving chamber hourly for 6 h for LY concentration analysis. Fluorescence was determined in SpectraMax M5 Multi-Mode Microplate Reader (Molecular devices, Sunnyvale, CA) at $\lambda_{ex}\backslash\lambda_{em}$ = 450/530 nm and compared with a standard of LY in endothelial growth medium-2.

Anti-PECAM-1 and IgG IONPs were introduced into the donor chamber at 0.05 mg/mL, as used in our previous cytotoxicity study on IONPs [273]. Samples (100 µL)

were collected from the donor chamber at time 0 and the receiving chamber hourly for 6 h for iron concentration analysis by inductively coupled plasma mass spectrometry (ICP-MS) (Agilent 7500cx, Santa Clara, CA, USA). The donor chamber was removed and the cells washed 3 times using PBS at 4 °C. The hCMEC/D3 monolayer was lysed with 1% Triton X-100 in 1.0 N NaOH. Iron concentration in the cell lysate and supernatant (including washing solution) were measured using ICP-MS. Flux rates of LY and nanoparticles were calculated by linear regression for the first 6 h. Two-way ANOVA followed by Bonferroni multiple comparisons was used to test for significant flux differences among the treatment groups and times using GraphPad Prism (GraphPad Software, San Diego, CA). Statistical significance was accepted at $p < 0.05$.

Brain targeting and biodistribution by anti-PECAM-1 IONPs

Antibody-coated iron oxide nanoparticles were prepared similarly as before with one exception. Both anti-PECAM-1 and IgG coated particles were incubated with 5% ^{125}I labeled IgG at a concentration of 10 mg/kg. This was done to prevent any detached labeled antibody from accumulating in the vasculature, thus providing a false positive for adhesion. Carotid artery injection was employed to delivery 10 mg/kg ^{125}I anti-PECAM-1 IONPs (n = 3) and ^{125}I IgG IONPs (n = 3). Briefly, the rat was anesthetized under ketamine/xylazine anesthesia (75 and 5 mg/kg), and its left carotid artery exposed. Following ligation of the external carotid, occipital and common carotid arteries, PE60 tubing containing heparin (100 U/ml, in 0.9% NaCl) was inserted into the common carotid. The 10 mg/ml ^{125}I anti-PECAM-1 IONPs and ^{125}I IgG IONPs were injected at 1 ml per min at a dose of 10 mg/kg. All the rats were sacrificed 10 min after infusion. The brain was harvested and cleaned of meninges and surface vessels. Blood and organs such

as the liver, spleen and lung were collected for biodistribution analysis using the gamma counter .The results were compared between ^{125}I anti-PECAM-1 and ^{125}I IgG IONPs using t-test or one-way ANOVA. The localization ratio (LR) was calculated as the percent of the injected dose per gram of tissue divided by percent of the injected dose per gram of blood. The specificity index was calculated as the LR of the targeted formulation (anti-PECAM-1 IONPs) divided by the non-targeted counterpart (IgG IONPs). The specificity index indicates specific targeting to organs, normalized by organ weights and the faction contained in blood [278]. One-way ANOVA followed by Tukey's test was used to test for significant differences of IgG IONP and anti-PECAM-1 IONP biodistribution among different organs. All results are reported as mean ± SD. Statistical significance was accepted at $p < 0.05$.

BBB integrity assessment

Five minutes before termination, the rat was given 6 mg Na fluorescein (334 Da) i.a. in 1 ml saline over 40s as a BBB permeability marker. Postmortem brain cortex was obtained to quantify fluorescein content. Fluorescence was determined in a SpectraMax M5 Multi-Mode Microplate Reader (Molecular devices, Sunnyvale, CA) at $\lambda_{ex}\backslash\lambda_{em}$ = 493/514 nm. The results among control, IgG IONP, and anti-PECAM-1 IONP groups were compared using one-way ANOVA (GraphPad Software, San Diego, CA).

Anti-PECAM-1 IONP distribution between the BBB endothelial cells and brain parenchyma using the capillary depletion assay

The capillary depletion method was used to separate brain parenchyma from capillary tissue [279, 280]. After a 10 mg/kg anti-PECAM-1 IONP injection in 1 ml over 1 min, a

20 s washout was conducted using PBS at a flow rate of 20 ml/min immediately before decapitation [281]. The forebrain from the left hemisphere was isolated from ^{125}I anti-PECAM-1 IONP and ^{125}I IgG IONP treated rats (n = 3) and the lateral ventricle choroid plexus in the perfused hemisphere removed. The tissue was homogenized in 3.5 ml of buffer containing 141 mM NaCl, 4 mM KCl, 2.8 mM $CaCl_2$, 1 mM NaH_2PO_4, 1 mM $MgSO_4$, 10 mM glucose and 10 mM HEPES at pH 7.4. Dextran (70,000 g/mol) was then added to 18% (w/v) and the sample further briefly homogenized. After centrifugation at 5400 x g for 15 min at 4 ºC, the supernatant (brain rich fraction) and pellet (capillary rich fraction) were carefully separated for measurement of ^{125}I by gamma counter. The percentage of the forebrain ^{125}I in the capillary rich fraction is as follows:

$$\left(\frac{Mass\ of\ 125I\ in\ capillary\ rich\ fraction}{Mass\ of\ 125I\ in\ capillary\ rich\ fraction + capilary\ depleted\ fraction}\right) * 100$$

The apparent permeability coefficient

The apparent permeability coefficient (P_{app}, cm/s) of LY, IgG IONPs and anti-PECAM-1 IONPs was calculated using GraphPad Prism. The first 6 h flux data were used with R^2 cutoff > 0.8. The P_{app} in (cm/s) was calculated using the equation: $P_{app} = (\Delta Q/\Delta t)/(area*C_D)$ [282]. $\Delta Q/\Delta t$ is the linear appearance rate obtained from the profile of the transported amount of the substrate against time (mg/s). C_D is the initial donor concentration of LY or nanoparticles (mg/mL). *Area* is the surface area of the cell monolayer (4.67 cm^2 for a 6-well plate).

Results

Anti-PECAM-1/IgG coating efficiency

After removal of unbound antibody, the surface coverage was determined to be 63.6 ± 8.4% (Figure 1A). Based on the primary nanoparticle size of 80 nm (Figure 1B), this corresponds to 19.1 μg antibody/mg of nanoparticle or 105 antibody molecules/nanoparticle. DLS measurements showed the size increased from 80 nm to 130 nm after addition of anti-PECAM-1 (Figure 1B), indicating uniform coating with slight aggregation, as the antibody size is ~15 nm in length. The zeta potential of the nanoparticles decreased from -10 to -8 mV (Figure 1C).

Stability of antibody-coated iron oxide nanoparticles in whole blood

Because anti-PECAM-1 IONPs and IgG IONPs were prepared by surface antibody adsorption, their stability in blood is very important for *in vivo* study. The ^{125}I labeled IgG antibody exhibited minimal detachment from nanoparticles for up to 4 h at 37°C. At 4 h, only 6.4 ± 1.2% of labeled antibody was detected in the heparin-treated blood after centrifugation. Between 4 and 24 h this increased to 46.2 ± 9.5%, likely due to the antibody on the nanoparticle surface being replaced with higher affinity serum proteins (Figure 2). The insignificant coating loss over 4 h suggests these nanoparticle modifications will stay stable throughout the circulation life and time frame of *in vivo* experiments.

PECAM-1 binding affinity to the human endothelial cell hCMEC/D3

hCMEC/D3 is a human BBB cell line developed in 2005. Previous research showed that it expressed PECAM-1 [277]. However, the binding affinity between hCMEC/D3 and PECAM-1 antibody was not known. Figure 3 shows that anti-PECAM-1, but not

non-specific control IgG, adhered specifically to the BBB cell model. The predicted antibody saturation (B_{max}) was determined to be $16.94x10^5$ molecules/cell, with a binding constant (K_d) of 32 nM, which is relatively low compared with a designed PECAM-1 antibody (a paired monoclonal antibody) for vascular targeting, with reported affinities between 0.5-5 nM [283]. However, previous research showed that relatively low affinity antibodies boost brain uptake by transcytosis targeting [284]. In the next experiment, anti-PECAM-1 IONP flux across the human endothelial cell hCMEC/D3 was tested.

CNA-IONP flux and cell association using a hCMEC/D3 *in vitro* BBB model

The TEER of the hCMEC/D3 *in vitro* BBB model (Figure 4) was tested every other day after the cells were seeded. After 7-10 days, the resistances were > 90 Ω/cm^2, similar to previously reported [275]. The permeability coefficient of LY, the indication of paracellular flux, was $2.9 \pm 0.2 \times 10^{-6}$ cm/s.

Anti-PECAM-1 IONP flux was significantly higher than anti-IgG IONPs and LY from 3 h to 6 h. The permeability coefficient after 6 hours of anti-PECAM-1 IONPs was $6.7 \pm 0.2 \times 10^{-6}$ cm/s, versus $4.8 \pm 0.2 \times 10^{-6}$ cm/s for IgG IONPs, and $2.9 \pm 0.2 \times 10^{-6}$ cm/s for LY (Figure 5A). After 6 h, 30% of anti-PECAM-1 IONPs was in the receiving chamber and ~ 45 % of anti-PECAM-1 IONPs was associated with the hCMEC/D3 cells, significantly higher than IgG IONPs (Figure 5B). PECAM-1 antibody significantly enhanced the flux of IONPs across the hCMEC/D3 monolayer *in vitro*. In the next experiment, anti-PECAM-1 IONP brain targeting, accumulation, and biodistribution were studied using Sprague Dawley rats.

Anti-PECAM-1 IONP association and biodistribution in brain and peripheral organs

Using ^{125}I tracing, we tested anti-PECAM-1 IONP targeting ability to brain and peripheral organs. As shown in figure 6A, the % dose per mL of blood in anti-PECAM-1 IONP treated rats was significantly lower than IgG IONP treatment, suggesting increased removal from blood and enhanced tissue accumulation. Ten min after infusion, 0.11 ± 0.01 % of the anti-PECAM-1 IONPs dose was associated with each gram of brain, which was significantly higher than anti-IgG IONPs (Figure 6B). The specificity index (the ratio between targeted and non targeted control) was calculated to test the anti-PECAM-1 IONPs brain targeting ability. Anti-PECAM-1 IONPs specificity in the brain was 5-fold higher than with IgG IONPs (Figure 6C). PECAM-1 targeting did not change anti-PECAM-1 IONP distribution in liver and spleen compared with IgG. However, anti-PECAM-1 IONP accumulation was significantly increased in the lungs (Figure 7).

Effect of Anti-PECAM-1 IONPs on blood-brain barrier integrity

Since anti-PECAM-1 IONP brain association was significantly increased, it was important to determine whether that changed the BBB permeability. Ten min after anti-PECAM-1 IONP injection the concentration of the BBB permeability marker, Fluorescein in the brain, did not change significantly compared with the control and IgG IONP groups (Figure 8).

Anti-PECAM-1 IONP distribution between brain capillary cells and brain parenchyma

For brain delivery systems, determination of whether or not they can enter the brain parenchyma is crucial. Our permeability results showed that anti-PECAM-1 IONPs did not alter BBB permeability. Understanding the anti-PECAM-1 IONP distribution between the brain capillary cells and parenchyma would provide evidence for transcellular flux. The capillary depletion results showed that 10 min after infusion, 82 ± 12% of anti-PECAM-1 IONPs were still associated with the capillary fraction and 17 ± 12% of them entered the brain (Figure 9). The capillary depletion assay was also carried out with brain from IgG IONPs treated rats. However, because of the low brain association of IgG IONPs, all radioactivity level readings were indistinguishable from background radioactivity.

Discussion

The use of vasculature-targeting antibodies, especially against PECAM-1, has been utilized before for lung targeting, injury treatment, [182] and as tumor contrast agents [285]. Anti-PECAM-1 nanocarriers can internalize into the cell through cellular adhesion molecule (CAM)-mediated endocytosis [190], which provides the potential to target the BBB and increase nanocarrier flux across the BBB. Previous research showed that IONPs coupled with affinity moieities targeted to receptors, such as transferin, can facilitate IONP flux across the BBB [286]. However, little is known whether anti-PECAM-1 surface-modified IONPs enhance brain flux across the BBB and change the distribution of IONPs between the BBB and brain parenchyma. In this study, we explored anti-PECAM-1 IONP targeting, transcytosis across the BBB, and biodistribution in the brain and peripheral organs.

We demonstrated that iron oxide nanoparticles can be sufficiently coupled with both IgG and anti-PECAM-1 using a non covalant physioabsorption strategy. It was determined that over 60% of the nanoparticle surface was coated with antibody (105 antibody molecules per single nanoparticle). Previous research has demonsatrated that clustering of the CAM through antibody binding can result in efficient internalization of anti-PECAM-1 nanoparticles, depending upon epitope of binding [190]. Using a non covalant targeting strategy, it was expected that upon contact with serum proteins they would inactivate the targeting coating, lowering the treatment efficacy. Contrary to this, it was seen that the coating on these nanoparticles stays intact for up to 4 h, vastly longer than the circulation half life of up to 2 h for uncoated particles [287]. The IgG IONPs and anti-PECAM-1 we developed have desirable properties to investigate BBB targeting and flux *in vitro* and *in vivo*.

In our *in vitro* flux study, LY showed higher flux at 1 h compared with anti-PECAM-1 IONPs and IgG IONPs. At 2 h, the flux of LY, anti-PECAM-1 IONPs and IgG IONPs were similar. After 2 h, anti-PECAM-1 IONPs flux was significantly higher than LY and IgG IONPs. These results provided evidence that the paracellular pathway was not the major pathway for anti-PECAM-1 IONPs flux. Anti-PECAM-1 IONPs use a different mechanism of flux across the BBB compared with IgG IONPs. There are multiple pathways for internalization involving vesicles < 300 nm in diameter. Clathrin- and caveolea-mediated endocytosis are the two major pathways for nanoparticle internalization [288-291]. IgG IONPs are likely to be taken up through these pathways. Limited transcytosis was observed in our study, which was consistent with a previous study in which the flux of three different surface-charged IONPs was studied across a

human BBB model *in vitro*. Very limited flux was observed over 25 h [268]. On the other hand, clustered PECAM-1 can be internalized by a novel endocytic pathway, CAM endocytosis [190], which was distinct from clathrin and caveolin-mediated endocyosis [292, 293]. Our *in vitro* flux study showed that PECAM-1 antibody surface modification significantly improved BBB targeting and flux across the BBB. Previous research showed that intercellular adhesion molecule 1(ICAM-1)-targeted nanocarriers, which also use the CAM-endocytosis pathway, provide considerable promise to enhance delivery of larger multivalent carriers to the CNS [278]. Another study also showed that anti-PECAM-1 nanocarriers demostrated significantly higher brain association [294]. However, they analyzed whole brain tissue including the BBB, brain parenchyma and the blood in the brain vessels. The present study provides a better understanding of the assocation and flux of anti-PECAM-1 nanoparticles across the BBB *in vitro* and *in vivo*.

In our *in vivo* study, anti-PECAM-1 IONPs did not change BBB permeability, further suggesting that anti-PECAM-1 IONPs crossed the BBB through a transcellular pathway rather than a paracellular pathway. We are not aware of any reports on how anti-PECAM-1 IONPs influence BBB permeability. However, previous research showed that anti-PECAM nanocarriers did not change endothelial monolayer integrity compared with a IgG nanocarrier [294]. The lack of anti-PECAM IONP increased BBB permeability decreases its potential adverse effects related to the BBB.

The level of anti-PECAM-1 IONPs in the blood was significantly lower than IgG IONPs, suggesting enhanced tissue accumulation. The results were consistent with anti-PECAM-1 IONP brain association results. Compared with IgG IONPs, anti-PECAM-1 IONP significantly increased IONP brain association 10 min after infusion. There was

0.11± 0.01 % of the dose associated with a gram of brain tissue 10 min after infusion. For comparison, the brain uptake of morphine, a neuroactive lipid soluble small molecule, is 0.0081± 0.001% of the dose /g rat brain [295]. The uptake of anti-PECAM-1 IONPs was higher than morphine, a regularly administered neuroactive small molecule with the capability of crossing the BBB. This demonstrates the potential application of PECAM-1 antibody for brain delivery. The transferrin receptor is the most studied targeting receptor for brain uptake [296]. Most previous studies of transferrin-surface-modified nanoparticles focused on the improvement of diagnosis and therapeutic effects rather than brain uptake [286, 297]. The brain delivery of the transferrin ligand was less than 0.3% of the dose using a healthy animal model [298]. A recent study compared ICAM-1 antibody and transferrin-surface-modified nanocarriers for brain targeting. It was found that they are both effective, but transferrin showed more advantages on smaller conjugates and ICAM-1 worked better for larger multivalent carriers [24]. In our study anti-PECAM-1 IONPs showed a similar specificity index as previously reported anti-ICAM-1 nanocarriers [278]. We expected PECAM-1 antibody would show similar brain targeting as ICAM-1, however, more research needs to be done to compare PECAM-1, ICAM-1 and transferrin for brain targeting. Furthermore, the actual extent of transferrin transcytosis is still unknown. Some studies showed that only a miniscule amount of transferrin was trancytosed across the brain capillary endothelial cells and accumulated in the brain [299, 300]. Our *in vitro* results provide evidence that anti-PECAM-1 IONPs can transcytose across a human BBB monolayer *in vitro* model.

We investigated the distribution between the BBB and brain parenchyma using the capillary depletion method to better characterize anti-PECAM-1 IONP transcytosis *in*

vivo. Our results showed that 10 min after injection, 17 ± 12% of anti-PECAM-1 IONPs crossed the BBB and associated with brain parenchyma. However, the majority of anti-PECAM-1 IONPs was still associated with the BBB cells. CAM-mediated endocytosis is a relatively slow process. One study investigated anti-PECAM nanocarrier internalization into human endothelial cells over time. After 15 minutes, 20% of anti-PECAM nanocarrier was internalized. However, there is little known about anti-PECAM-1 transcytosis [294]. Our *in vitro* flux study showed that 4.5% of anti-PECAM-1 IONPs flux cross the BBB monolayer over 1 h. Our studies demonstrated the potential of anti-PECAM-1 IONPs to cross the BBB *in vitro* and *in vivo*. However, a longer time point study is required to better understand how effectively anti-PECAM-1 enhances flux across the BBB.

The biodistribution results of anti-PECAM-1 IONPs demostrated that PECAM-1 antibody did not increase anti-PECAM-1 IONP accumulation in the liver and spleen 10 min after injection. More study at longer time point is needed to fully understand the depostion of anti-PECAM-1 IONP in the liver and spleen. However, PECAM-1 antibody significantly increased the IONP accumulation in the lung. This result was consistent with previous reports that an anti-PECAM-1 nanocarrier is a good candidate for pulmonary targeting [301, 302]. This is due to the massive surface area provided by lung capillary beds. For brain targeted delivery, high accumulation in the lung has potential to cause side effects there. However, we can take advantage of this properties for certain diseases. For example, about 15-20% of patients with non-small cell lung cancer (NSCLC) develop brain metastasis [303]. Anti-PECAM-1 nanocarriers can target lung and brain simultaneously and be taken up through the CAM-mediated endocytosis

pathway [294]. Furthermore, recent clinical research showed that PECAM-1 could be a potential prognostic factor and a novel therapeutic target for the effective treatment of NSCLC [304]. Therefore, anti-PECAM-1 IONPs have potential to be used to target lung and NSCLC, while treating potential brain metastasis. More research needs to be conducted to test anti-PECAM-1 IONPs in a brain metastasis model and investigate how they associate with the blood tumor barrier and tumor cells.

Conclusions

This work demostrated that anti-PECAM-1-modified IONPs enhance flux across the BBB *in vitro* and *in vivo,* which holds promise to deliver IONPs or other therapeutic agents to the CNS without compromising BBB permeability. This effect was a result of both the capacity of anti-PECAM-1 IONPs to target the BBB and the ability to transcytose across into the brain. Meanwhile, anti-PECAM-1 IONPs demonstrated increased lung accumulation, which provides the potential to simultaneously target lung and lung cancer derived-brain metastasis. Future studies investigating anti-PECAM-1 IONPs using a lung cancer brain metastasis model *in vivo* should provide evidence on how anti-PECAM-1 IONPs associate with the blood tumor barrier and metastatic brain tumor. Anti-PECAM-1 IONPs have great potential to be employed in the diagnosis and therapy of CNS diseases such as NSCLC-originating brain metastasis.

Figure 1. Surface modification of IONPs by anti-PECAM-1 antibody. Iron oxide nanoparticles were incubated with excess ^{125}I labeled antibody and purified by centifugation. The bound antibody was tested after each centifugation (A). Size of IONPs before and after anti-PECAM-1 antibody surface modification (B). Zeta potential of IONPs before and after anti-PECAM-1 antibody (C). (N = 3, mean ± SD)

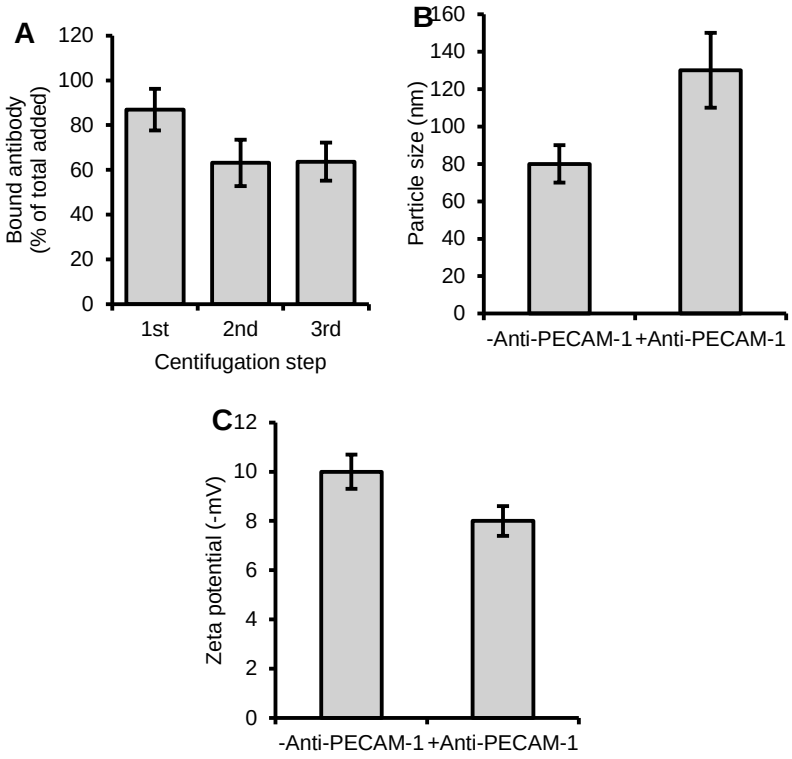

Figure 2. Antibody coating stability in whole blood. ^{125}I labeled nanoparticles show minimal detachment of coating for up to 4 hours, suggesting coating stability and targeting capability *in vivo.* (N = 3, mean ± SD)

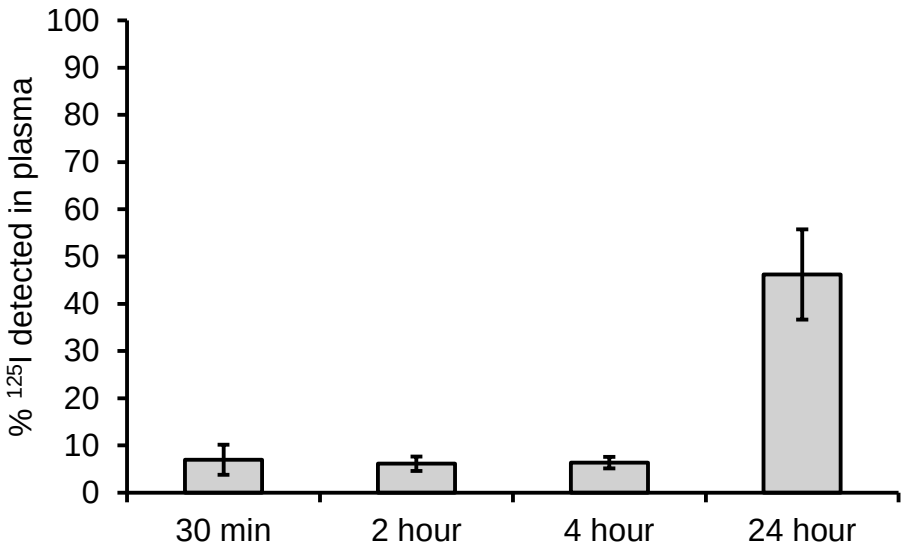

Figure 3: PECAM-1 antibody binding affinity on immortalized human brain endothelial cells (hCMEC/D3). IgG exhibited undetectable levels of binding, whereas anti-PECAM-1 affinity is 32 nM, with a B_{max} of 17 x 10^5 molecules/cell. (N = 3, mean ± SD)

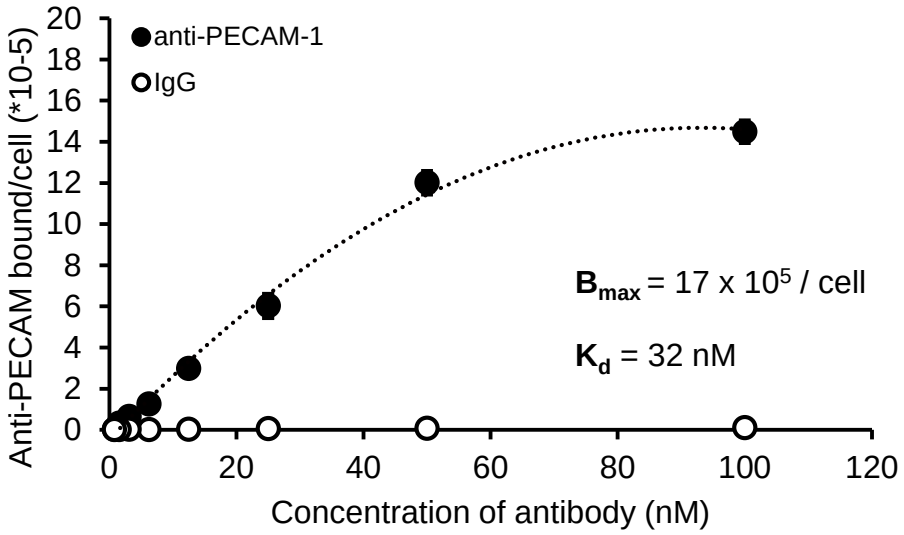

Figure 4. Anti-PECAM-1 IONP flux across hCMEC/D3 cells and cell association results. Anti-PECAM-1 IONP (0.05 mg/ml), IgG IONP (0.05 mg/ml) and LY (100 µM) flux across hCMEC/D3 cells for 6 h (A). Anti-PECAM-1 IONP and IgG IONP distribution in the donor and receiving chambers and hCMEC/D3 cells at 6 h (B). (N = 3, mean ± SD)

* Significantly different compared to IgG IONPs

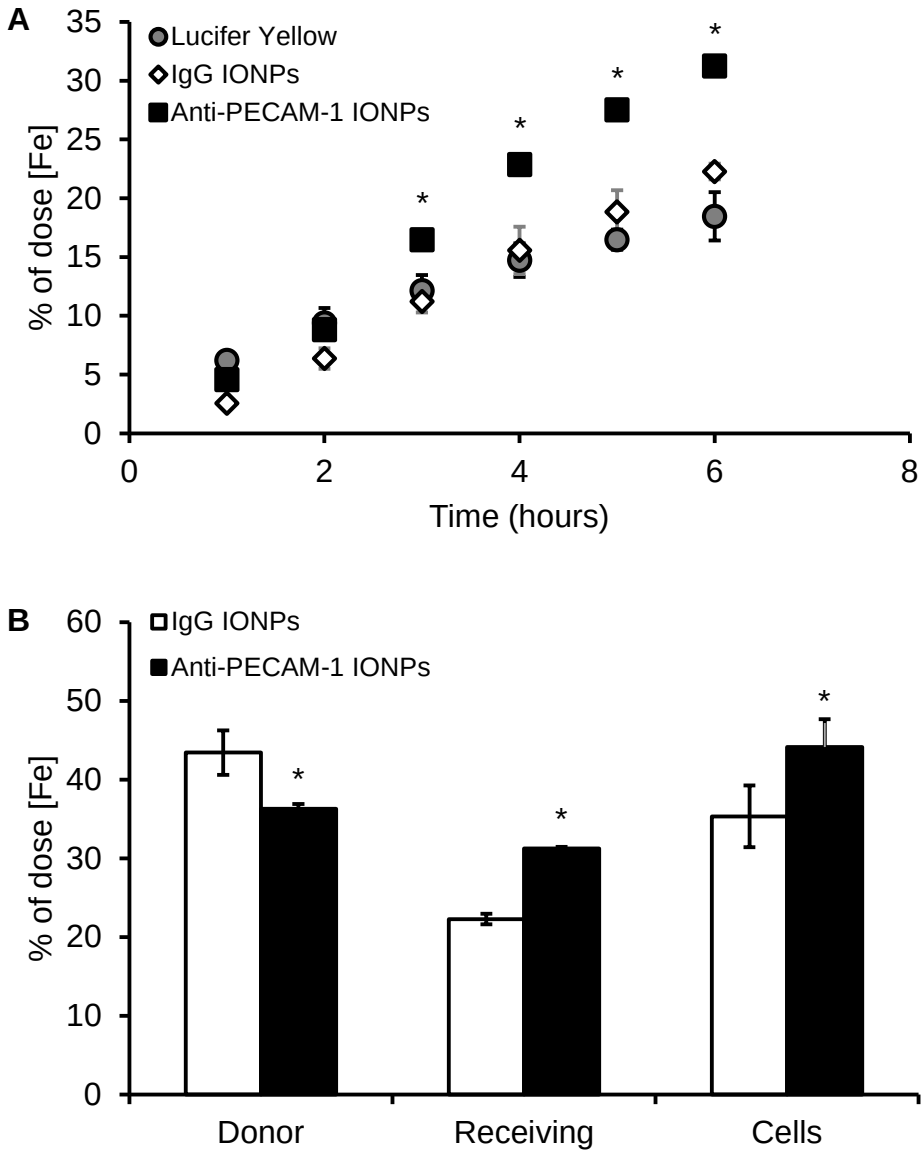

Figure 5: Brain association and blood % of dose of anti-PECAM-1- and IgG IONPs. The brain (A) and blood (B) levels of ^{125}I labeled anti-PECAM-1-IONPs after intra-arterial infusion in rats, expressed as the percentage of injected dose (% Injected Dose (ID), 10 mg/kg). Specific tissue accumulation of anti-PECAM-1 IONPs compared with IgG IONPs in brain, calculated as the specific index (SI). SI values above 1 represent specific targeting in an organ over IgG IONPs (C). * Significantly different. (N = 3, mean ± SD)

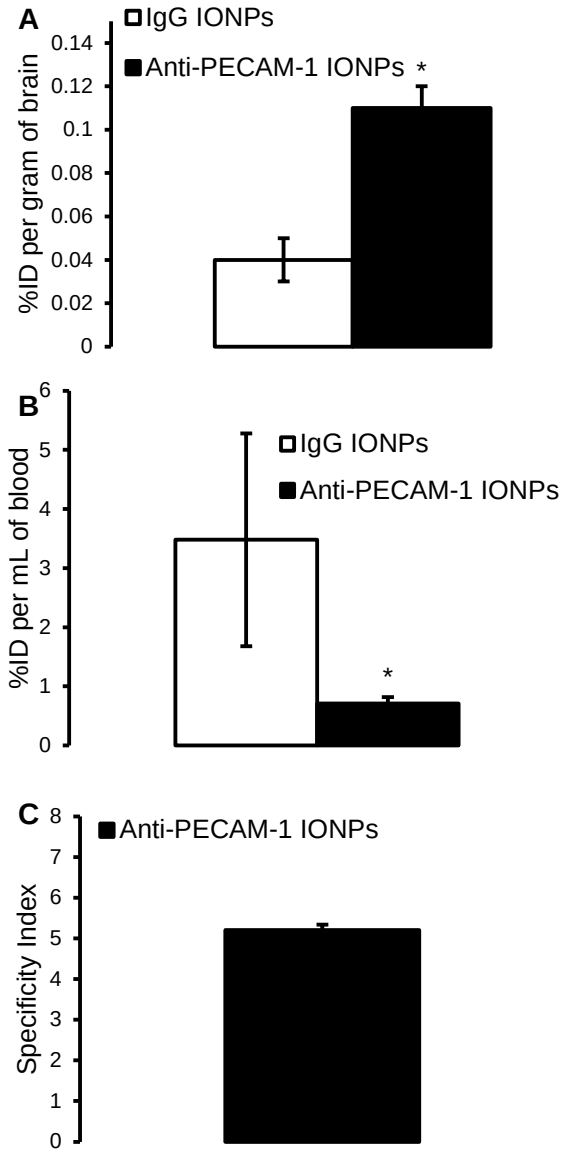

Figure 6: Biodistribution of IgG IONPs and anti-PECAM-1 IONPs in rats. The liver, spleen and lung levels of ^{125}I labeled anti-PECAM-1 IONPs measured 10 min after intra-arterial infusion in rats, expressed as the percentage of injected dose (%ID, 10 mg/kg). * Significantly different. (N = 3, mean ± SD)

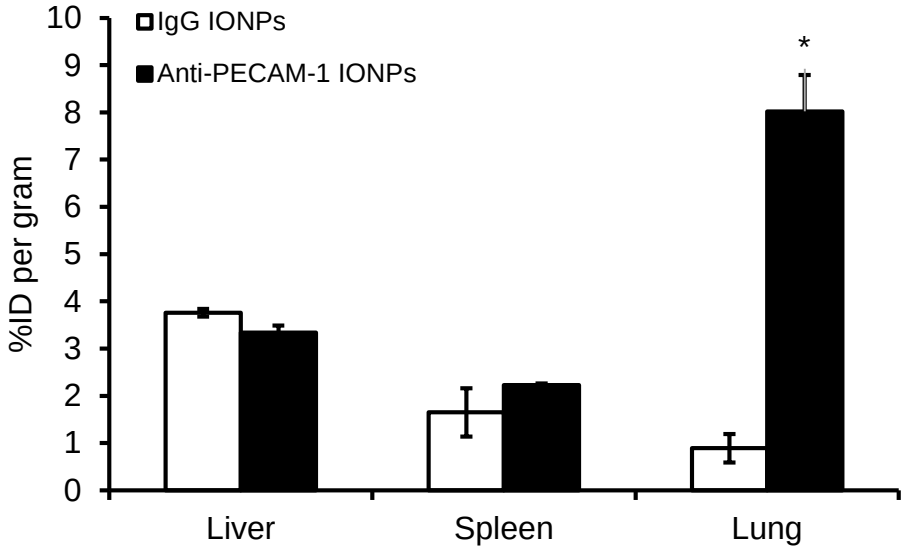

Figure 7: BBB permeability measured by fluorescein concentration 10 min after completion of intra-arterial infusion in rats. Rats received saline, 10 mg/kg IgG IONPs, or 10 mg/kg anti-PECAM-1 IONPs and were terminated 10 min after infusion. (N = 3, mean ± SD)

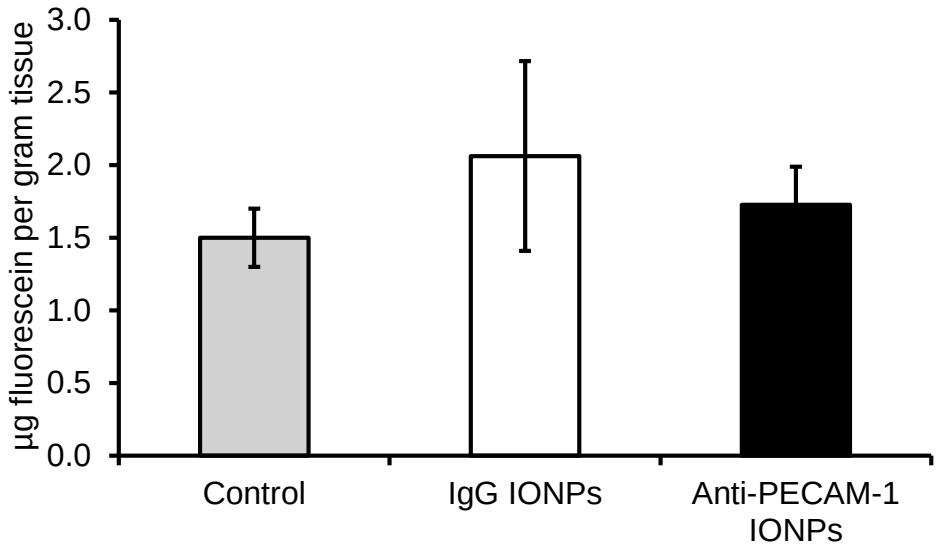

Figure 8: Capillary depletion results. The level of anti-PECAM-1 IONPs and IgG IONPs concentrations in the capillary-rich fraction and brain-rich fraction. (N = 3, mean ± SD). BDL : Below detectable limits.

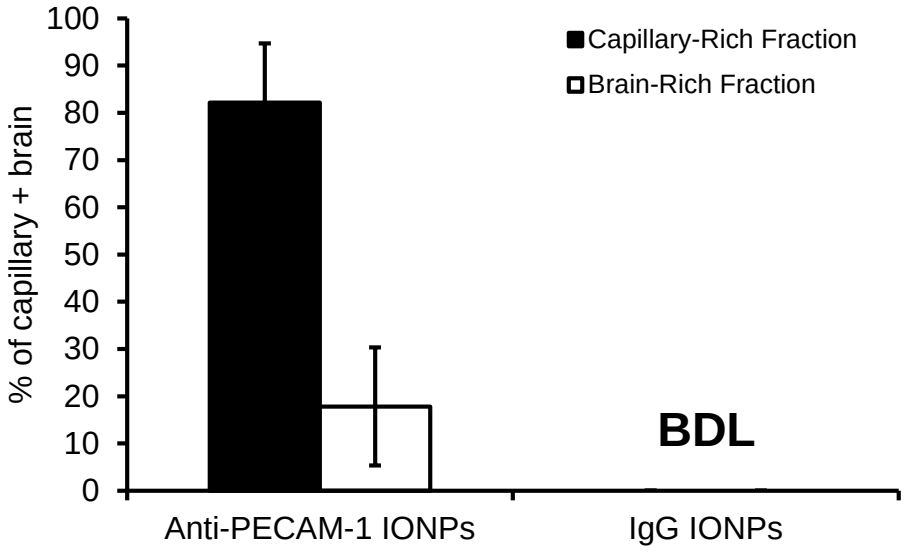

REFERENCES

1. Sasaki M, Joh T: Oxidative stress and ischemia-reperfusion injury in gastrointestinal tract and antioxidant, protective agents. *Journal of clinical biochemistry and nutrition* 40(1), 1 (2007).
2. Halliwell B, Gutteridge J, Cross C: Free radicals, antioxidants, and human disease: where are we now? *The Journal of laboratory and clinical medicine* 119(6), 598 (1992).
3. Kalra J, Chaudhary A, Prasad K: Increased production of oxygen free radicals in cigarette smokers. *International journal of experimental pathology* 72(1), 1 (1991).
4. Comporti M: Lipid peroxidation and cellular damage in toxic liver injury. *Laboratory investigation* 53(6), 599-623 (1985).
5. Macdonald J, Galley H, Webster N: Oxidative stress and gene expression in sepsis. *British journal of anaesthesia* 90(2), 221-232 (2003).
6. Rinaldi S, Landucci F, De Gaudio A: Antioxidant therapy in critically septic patients. *Current drug targets* 10(9), 872-880 (2009).
7. Springer TA: Adhesion receptors of the immune system. *Nature* 346(6283), 425-434 (1990).
8. Dinarello CA: Proinflammatory cytokines. *CHEST Journal* 118(2), 503-508 (2000).
9. Wolff B, Burns AR, Middleton J, Rot A: Endothelial cell "memory" of inflammatory stimulation: human venular endothelial cells store interleukin 8 in Weibel-Palade bodies. *The Journal of experimental medicine* 188(9), 1757-1762 (1998).
10. Schreck R, Albermann K, Baeuerle PA: Nuclear factor kB: an oxidative stress-responsive transcription factor of eukaryotic cells (a review). *Free Radical Research* 17(4), 221-237 (1992).
11. Finkel T, Holbrook NJ: Oxidants, oxidative stress and the biology of ageing. *Nature* 408(6809), 239-247 (2000).
12. Kaneto H, Matsuoka T-A, Nakatani Y *et al.*: Oxidative stress, ER stress, and the JNK pathway in type 2 diabetes. *Journal of molecular medicine* 83(6), 429-439 (2005).
13. Muraoka K-I, Shimizu K, Sun X *et al.*: Hypoxia, But Not Reoxygenation, Induces Interleukin-6 Gene Expression Through NF-kappa B activation. *Transplantation* 63(3), 466-470 (1997).
14. Bevilacqua MP, Pober JS, Wheeler ME, Cotran RS, Gimbrone Jr MA: Interleukin 1 acts on cultured human vascular endothelium to increase the adhesion of polymorphonuclear leukocytes, monocytes, and related leukocyte cell lines. *Journal of Clinical Investigation* 76(5), 2003 (1985).
15. Xie Q, Kashiwabara Y, Nathan C: Role of transcription factor NF-kappa B/Rel in induction of nitric oxide synthase. *Journal of Biological Chemistry* 269(7), 4705-4708 (1994).
16. Schwarz KB: Oxidative stress during viral infection: a review. *Free Radical Biology and Medicine* 21(5), 641-649 (1996).
17. Anderson JM, Rodriguez A, Chang DT: Foreign body reaction to biomaterials. *Seminars in Immunology* 20(2), 86-100 (2008).
18. Vaziri ND, Wang XQ, Oveisi F, Rad B: Induction of oxidative stress by glutathione depletion causes severe hypertension in normal rats. *Hypertension* 36(1), 142-146 (2000).
19. Rangel-Frausto MS, Pittet D, Costigan M, Hwang T, Davis CS, Wenzel RP: The natural history of the systemic inflammatory response syndrome (SIRS). *JAMA: the journal of the American Medical Association* 273(2), 117-123 (1995).

20. Winterbourn CC, Kettle AJ: Radical–radical reactions of superoxide: a potential route to toxicity. *Biochemical and biophysical research communications* 305(3), 729-736 (2003).
21. Davies MJ: Identification of a globin free radical in equine myoglobin treated with peroxides. *Biochimica et Biophysica Acta (BBA)-Protein Structure and Molecular Enzymology* 1077(1), 86-90 (1991).
22. Wattamwar PP, Mo Y, Wan R, Palli R, Zhang Q, Dziubla TD: Antioxidant activity of degradable polymer poly (trolox ester) to suppress oxidative stress injury in the cells. *Advanced Functional Materials* 20(1), 147-154 (2010).
23. Granado-Serrano AB, Martín MA, Bravo L, Goya L, Ramos S: Quercetin modulates NF-κ B and AP-1/JNK pathways to induce cell death in human hepatoma cells. *Nutrition and cancer* 62(3), 390-401 (2010).
24. Cho S-Y, Park S-J, Kwon M-J *et al.*: Quercetin suppresses proinflammatory cytokines production through MAP kinases and NF-κB pathway in lipopolysaccharide-stimulated macrophage. *Molecular and cellular biochemistry* 243(1-2), 153-160 (2003).
25. Dunlap WC, Yamamoto Y: Small-molecule antioxidants in marine organisms: Antioxidant activity of mycosporine-glycine. *Comparative Biochemistry and Physiology Part B: Biochemistry and Molecular Biology* 112(1), 105-114 (1995).
26. Seo JY, Kim H, Seo JT, Kim KH: Oxidative Stress Induced Cytokine Production in Isolated Rat Pancreatic Acinar Cells: Effects of Small-Molecule Antioxidants. *Pharmacology* 64(2), 63-70 (2002).
27. Frei B: Molecular and biological mechanisms of antioxidant action. *The FASEB Journal* 13(9), 963-964 (1999).
28. Shek PN, Suntres ZE, Brooks JI: Liposomes in Pulmonary Applications: Physicochemical Considerations, Pulmonary Distribution and Antioxidant Delivery. *Journal of Drug Targeting* 2(5), 431-442 (1994).
29. Kosaraju SL, D'ath L, Lawrence A: Preparation and characterisation of chitosan microspheres for antioxidant delivery. *Carbohydrate Polymers* 64(2), 163-167 (2006).
30. Chen X-L, Dodd G, Thomas S *et al.*: Activation of Nrf2/ARE pathway protects endothelial cells from oxidant injury and inhibits inflammatory gene expression. *American Journal of Physiology-Heart and Circulatory Physiology* 290(5), H1862-H1870 (2006).
31. Meyer M, Schreck R, Baeuerle PA: H2O2 and antioxidants have opposite effects on activation of NF-kappa B and AP-1 in intact cells: AP-1 as secondary antioxidant-responsive factor. *The EMBO journal* 12(5), 2005 (1993).
32. Simon AR, Rai U, Fanburg BL, Cochran BH: Activation of the JAK-STAT pathway by reactive oxygen species. *American Journal of Physiology-Cell Physiology* 275(6), C1640-C1652 (1998).
33. Hollman PC, Van Trijp JM, Buysman MN, Mengelers MJ, De Vries JH, Katan MB: Relative bioavailability of the antioxidant flavonoid quercetin from various foods in man. *FEBS letters* 418(1), 152-156 (1997).
34. Manach C, Morand C, Crespy V *et al.*: Quercetin is recovered in human plasma as conjugated derivatives which retain antioxidant properties. *FEBS letters* 426(3), 331-336 (1998).
35. Kobuchi H, Roy S, Sen CK, Nguyen HG, Packer L: Quercetin inhibits inducible ICAM-1 expression in human endothelial cells through the JNK pathway. *American Journal of Physiology-Cell Physiology* 277(3), C403-C411 (1999).
36. Choi J-S, Choi Y-J, Park S-H, Kang J-S, Kang Y-H: Flavones mitigate tumor necrosis factor-α-induced adhesion molecule upregulation in cultured human endothelial cells: role of nuclear factor-κB. *The Journal of nutrition* 134(5), 1013-1019 (2004).

37. Shen K-H, Hung S-H, Yin L-T *et al.*: Acacetin, a flavonoid, inhibits the invasion and migration of human prostate cancer DU145 cells via inactivation of the p38 MAPK signaling pathway. *Molecular and cellular biochemistry* 333(1-2), 279-291 (2010).
38. Garbisa S, Sartor L, Biggin S, Salvato B, Benelli R: Tumor gelatinases and invasion inhibited by the green tea flavanol epigallocatechin-3-gallate. *Cancer* 91(4), 822-832 (2001).
39. Lindenmeyer F, Li H, Menashi S, Soria C, Lu H: Apigenin acts on the tumor cell invasion process and regulates protease production. *Nutrition and cancer* 39(1), 139-147 (2001).
40. Conner EM, Grisham MB: Inflammation, free radicals, and antioxidants. *Nutrition* 12(4), 274-277 (1996).
41. O'leary KA, Pascual-Tereasa SD, Needs PW, Bao Y-P, O'brien NM, Williamson G: Effect of flavonoids and vitamin E on cyclooxygenase-2 (COX-2) transcription. *Mutation Research/Fundamental and Molecular Mechanisms of Mutagenesis* 551(1), 245-254 (2004).
42. Gerritsen ME, Carley WW, Ranges GE *et al.*: Flavonoids inhibit cytokine-induced endothelial cell adhesion protein gene expression. *The American journal of pathology* 147(2), 278 (1995).
43. Yoshizumi M, Tsuchiya K, Suzaki Y *et al.*: Quercetin glucuronide prevents VSMC hypertrophy by angiotensin II via the inhibition of JNK and AP-1 signaling pathway. *Biochemical and biophysical research communications* 293(5), 1458-1465 (2002).
44. Ha SK, Lee P, Park JA *et al.*: Apigenin inhibits the production of NO and PGE< sub> 2</sub> in microglia and inhibits neuronal cell death in a middle cerebral artery occlusion-induced focal ischemia mice model. *Neurochemistry international* 52(4), 878-886 (2008).
45. Wattamwar PP, Hardas SS, Butterfield DA, Anderson KW, Dziubla TD: Tuning of the pro-oxidant and antioxidant activity of trolox through the controlled release from biodegradable poly (trolox ester) polymers. *Journal of Biomedical Materials Research Part A* 99(2), 184-191 (2011).
46. David F W: Definitions in Biomaterials. Elsevier, Amsterdam. (1987).
47. Gole J, Burda C, Fedorov A, White M: Enhanced reactivity and phase transformation at the nanoscale: Efficient formation of active silica and doped and metal seeded TiO2-xNx photocatalysts. *Reviews on Advanced Materials Science* 5(4), 265-269 (2003).
48. Oberdorster G, Finkelstein JN, Johnston C *et al.*: Acute pulmonary effects of ultrafine particles in rats and mice. *Res Rep Health Eff Inst* (96), 5-74; disc 75-86 (2000).
49. David F W: On the mechanisms of biocompatibility. *Biomaterials* 29(20), 2941-2953 (2008).
50. Nordberg J, Arner ES: Reactive oxygen species, antioxidants, and the mammalian thioredoxin system. *Free radical biology and medicine* 31(11), 1287-1312 (2001).
51. Thannickal VJ, Fanburg BL: Reactive oxygen species in cell signaling. *American Journal of Physiology-Lung Cellular and Molecular Physiology* 279(6), L1005-L1028 (2000).
52. Hensley K, Robinson KA, Gabbita SP, Salsman S, Floyd RA: Reactive oxygen species, cell signaling, and cell injury. *Free Radical Biology and Medicine* 28(10), 1456-1462 (2000).
53. Stadtman ER, Levine RL: Protein oxidation. *Annals of the New York Academy of Sciences* 899(1), 191-208 (2000).
54. Berlett BS, Stadtman ER: Protein oxidation in aging, disease, and oxidative stress. *Journal of Biological Chemistry* 272(33), 20313-20316 (1997).
55. Torres MA, Jones JD, Dangl JL: Reactive oxygen species signaling in response to pathogens. *Plant physiology* 141(2), 373-378 (2006).

56. Ogasawara MA, Zhang H: Redox regulation and its emerging roles in stem cells and stem-like cancer cells. *Antioxidants & redox signaling* 11(5), 1107-1122 (2009).
57. Sharma RK, Zhou Q, Netland PA: Effect of oxidative preconditioning on neural progenitor cells. *Brain research* 1243, 19-26 (2008).
58. Ott M, Gogvadze V, Orrenius S, Zhivotovsky B: Mitochondria, oxidative stress and cell death. *Apoptosis* 12(5), 913-922 (2007).
59. Mittler R: Oxidative stress, antioxidants and stress tolerance. *Trends in plant science* 7(9), 405-410 (2002).
60. Valko M, Rhodes C, Moncol J, Izakovic M, Mazur M: Free radicals, metals and antioxidants in oxidative stress-induced cancer. *Chemico-biological interactions* 160(1), 1-40 (2006).
61. D'aiuto F, Nibali L, Parkar M, Patel K, Suvan J, Donos N: Oxidative stress, systemic inflammation, and severe periodontitis. *Journal of dental research* 89(11), 1241-1246 (2010).
62. Koechlin C, Couillard A, Cristol J *et al.*: Does systemic inflammation trigger local exercise-induced oxidative stress in COPD? *European Respiratory Journal* 23(4), 538-544 (2004).
63. Niu X, Smith CW, Kubes P: Intracellular oxidative stress induced by nitric oxide synthesis inhibition increases endothelial cell adhesion to neutrophils. *Circulation research* 74(6), 1133-1140 (1994).
64. Miller FJ, Gutterman DD, Rios CD, Heistad DD, Davidson BL: Superoxide production in vascular smooth muscle contributes to oxidative stress and impaired relaxation in atherosclerosis. *Circulation Research* 82(12), 1298-1305 (1998).
65. Thornalley PJ, Vašák M: Possible role for metallothionein in protection against radiation-induced oxidative stress. Kinetics and mechanism of its reaction with superoxide and hydroxyl radicals. *Biochimica et Biophysica Acta (BBA)-Protein Structure and Molecular Enzymology* 827(1), 36-44 (1985).
66. Turrens JF: Superoxide production by the mitochondrial respiratory chain. *Bioscience reports* 17(1), 3-8 (1997).
67. Parks D, Granger D: Xanthine oxidase: biochemistry, distribution and physiology. *Acta physiologica Scandinavica. Supplementum* 548, 87 (1986).
68. Mccord JM: Oxygen-derived free radicals in postischemic tissue injury. *The New England Journal of Medicine* 312(3), 159-163 (1985).
69. Torres MA, Jones JD, Dangl JL: Pathogen-induced, NADPH oxidase–derived reactive oxygen intermediates suppress spread of cell death in Arabidopsis thaliana. *Nature genetics* 37(10), 1130-1134 (2005).
70. Neill S, Desikan R, Hancock J: Hydrogen peroxide signalling. *Current opinion in plant biology* 5(5), 388-395 (2002).
71. Sampson JB, Ye Y, Rosen H, Beckman JS: Myeloperoxidase and horseradish peroxidase catalyze tyrosine nitration in proteins from nitrite and hydrogen peroxide. *Archives of biochemistry and biophysics* 356(2), 207-213 (1998).
72. Imlay JA, Chin SM, Linn S: Toxic DNA damage by hydrogen peroxide through the Fenton reaction in vivo and in vitro. *Science* 240(4852), 640-642 (1988).
73. Cadet J, Delatour T, Douki T *et al.*: Hydroxyl radicals and DNA base damage. *Mutation Research/Fundamental and Molecular Mechanisms of Mutagenesis* 424(1), 9-21 (1999).
74. Willson RL: Hydroxyl radicals and biological damage in vitro: what relevance in vivo. *Oxygen Free Radicals and Tissue Damage*, 19-42 (1979).
75. Wardman P, Candeias LP: Fenton chemistry: an introduction. *Radiation research* 145(5), 523-531 (1996).

76. Gutteridge J: Lipid peroxidation and antioxidants as biomarkers of tissue damage. *Clinical chemistry* 41(12), 1819-1828 (1995).
77. Gutteridge J: Iron promoters of the Fenton reaction and lipid peroxidation can be released from haemoglobin by peroxides. *FEBS letters* 201(2), 291-295 (1986).
78. Maritim A, Sanders R, Watkins RJ: Diabetes, oxidative stress, and antioxidants: a review. *Journal of biochemical and molecular toxicology* 17(1), 24-38 (2003).
79. Liochev SI: Reactive oxygen species and the free radical theory of aging. *Free Radical Biology and Medicine* 60, 1-4 (2013).
80. Karpinska A, Gromadzka G: Oxidative stress and natural antioxidant mechanisms: the role in neurodegeneration. From molecular mechanisms to therapeutic strategies. *Postep. Hig. Med. Dosw.* 67, 43-53 (2013).
81. Droge W: Free radicals in the physiological control of cell function. *Physiological Reviews* 82(1), 47-95 (2002).
82. Sikka SC: Relative impact of oxidative stress on male reproductive function. *Current Medicinal Chemistry* 8(7), 851-862 (2001).
83. Fridovich I: Superoxide Radical and Superoxide Dismutases. *Annual Review of Biochemistry* 64, 97-112 (1995).
84. Halliwell B: Free radicals, antioxidants, and human disease: curiosity, cause, or consequence? *The Lancet* 344(8924), 721-724 (1994).
85. Adler G: Radiation chemistry of organic compounds. A. J. Swallow. pcrgamon press, New York, 1960. XIII + 380 pp. $15.00. *Journal of Polymer Science* 55(161), S5-S5 (1961).
86. Garrison WM: Reaction mechanisms in the radiolysis of peptides, polypeptides, and proteins. *Chemical Reviews* 87(2), 381-398 (1987).
87. Schuessler H, Schilling K: Oxygen Effect in the Radiolysis of Proteins. *International Journal of Radiation Biology* 45(3), 267-281 (1984).
88. Cooke MS, Evans MD, Dizdaroglu M, Lunec J: Oxidative DNA damage: mechanisms, mutation, and disease. *The FASEB Journal* 17(10), 1195-1214 (2003).
89. Grasso P: Essentials of pathology for toxicologists. CRC Press, (2002).
90. Anderson JM: Biological Responses To Materials. *Annual Review of Materials Research* 31(1), 81 (2001).
91. Dolores W, Christian R, Harald N, Hildegunde P, Georg W: Cellular and molecular composition of fibrous capsules formed around silicone breast implants with special focus on local immune reactions. *Journal of Autoimmunity* 23(1), 81-91 (2004).
92. Owens Iii DE, Peppas NA: Opsonization, biodistribution, and pharmacokinetics of polymeric nanoparticles. *International Journal of Pharmaceutics* 307(1), 93-102 (2006).
93. Cooper S, Peppas N: Biomaterials: Interfacial Phenomena and Applications. AMERICAN CHEMICAL SOCIETY, 199, (1982).
94. Tegoulia VA, Cooper SL: Leukocyte adhesion on model surfaces under flow: Effects of surface chemistry, protein adsorption, and shear rate. *Journal of Biomedical Materials Research* 50(3), 291-301 (2000).
95. Roach P, Farrar D, Perry CC: Interpretation of Protein Adsorption: Surface-Induced Conformational Changes. *Journal of the American Chemical Society* 127(22), 8168-8173 (2005).
96. Xu L-C, Siedlecki CA: Effects of surface wettability and contact time on protein adhesion to biomaterial surfaces. *Biomaterials* 28(22), 3273-3283 (2007).
97. Leonard EF, Vroman L: Is the Vroman effect of importance in the interaction of blood with artificial materials? *Journal of Biomaterials Science, Polymer Edition* 3(1), 95-107 (1992).

98. Jenney CR, Anderson JM: Adsorbed serum proteins responsible for surface dependent human macrophage behavior. *J Biomed Mater Res* 49(4), 435-447 (2000).
99. Chang CC, Lieberman SM, Moghe PV: Leukocyte spreading behavior on vascular biomaterial surfaces: consequences of chemoattractant stimulation. *Biomaterials* 20(3), 273-281 (1999).
100. Nathan C: Neutrophils and immunity: challenges and opportunities. *Nat Rev Immunol* 6(3), 173-182 (2006).
101. Aukrust P, Berge RK, Ueland T *et al.*: Interaction between chemokines and oxidative stress: possible pathogenic role in acute coronary syndromes. *Journal of the American College of Cardiology* 37(2), 485-491 (2001).
102. Klyubin IV, Kirpichnikova KM, Gamaley IA: Hydrogen peroxide-induced chemotaxis of mouse peritoneal neutrophils. *Eur J Cell Biol* 70(4), 347-351 (1996).
103. Hattori H, Subramanian KK, Sakai J *et al.*: Small-molecule screen identifies reactive oxygen species as key regulators of neutrophil chemotaxis. *Proceedings of the National Academy of Sciences of the United States of America* 107(8), 3546-3551 (2010).
104. Forman HJ, Torres M: Reactive oxygen species and cell signaling: Respiratory burst in macrophage signaling. American Thoracic Society, New York, NY, ETATS-UNIS. (2002).
105. Seres T, Knickelbein RG, Warshaw JB, Johnston RB: The phagocytosis-associated respiratory burst in human monocytes is associated with increased uptake of glutathione. *J Immunol* 165(6), 3333-3340 (2000).
106. Jenney CR, Defife KM, Colton E, Anderson JM: Human monocyte/macrophage adhesion, macrophage motility, and IL-4-induced foreign body giant cell formation on silane-modified surfaces in vitro. *Journal of Biomedical Materials Research* 41(2), 171-184 (1998).
107. Mcnally AK, Anderson JM: Interleukin-4 induces foreign body giant cells from human monocytes/macrophages : differential lymphokine regulation of macrophage fusion leads to morphological variants of multinucleated giant cells. American Society for Investigative Pathology, Bethesda, MD, ETATS-UNIS. 147, (1995).
108. Mcnally AK, Anderson JM: β1 and β2 Integrins Mediate Adhesion during Macrophage Fusion and Multinucleated Foreign Body Giant Cell Formation. *The American journal of pathology* 160(2), 621-630 (2002).
109. Paynter RW, Askill IN, Glick SH, Guidoin R: The hydrolytic stability of mitrathane (a polyurethane urea)—an x-ray photoelectron spectroscopy study. *Journal of Biomedical Materials Research* 22(8), 687-698 (1988).
110. Mathur AB, Collier TO, Kao WJ *et al.*: In vivo biocompatibility and biostability of modified polyurethanes. *Journal of Biomedical Materials Research* 36(2), 246-257 (1997).
111. Stokes K, Mcvenes R, Anderson JM: Polyurethane Elastomer Biostability. *Journal of Biomaterials Applications* 9(4), 321-354 (1995).
112. Stokes K, Cobian K: Polyether polyurethanes for implantable pacemaker leads. *Biomaterials* 3(4), 225-231 (1982).
113. Kinov P, Leithner A, Radl R *et al.*: Role of free radicals in aseptic loosening of hip arthroplasty. *Journal of Orthopaedic Research* 24(1), 55-62 (2006).
114. Konttinen YT, Zhao D, Beklen A *et al.*: The Microenvironment around Total Hip Replacement Prostheses. *Clinical Orthopaedics and Related Research* 430, 28-38 10.1097/1001.blo.0000150451.0000150452.da (2005).
115. Sampathkumar K, Jeyam M, Evans CE, Andrew JG: Role of cyclical pressure and particles in the release of M-CSF, chemokines, and PGE2 and their role in loosening of implants. *J Bone Joint Surg Br* 85-B(2), 288-291 (2003).

116. Fu K, Pack DW, Klibanov AM, Langer R: Visual Evidence of Acidic Environment Within Degrading Poly(lactic-co-glycolic acid) (PLGA) Microspheres. *Pharmaceutical Research* 17(1), 100-106 (2000).
117. Springer TA: Traffic signals on endothelium for lymphocyte recirculation and leukocyte emigration. Marcel Dekker, Inc., NY, (1997).
118. Springer C, Benita S, Sherman Y, Gursoy N, Gilhar D, Avital A: Poly-lactic-glycolic Acid Microspheres: A Biodegradable Marker for the Diagnosis of Aspiration in Hamsters. *Pediatric Research* 58(3), 537-541 (2005).
119. William R M: Oxidative Stress Hypothesis in Alzheimer's Disease. *Free Radical Biology and Medicine* 23(1), 134-147 (1997).
120. Jenner P: Oxidative stress in Parkinson's disease. *Annals of Neurology* 53(S3), S26-S38 (2003).
121. Greco E, Iacobelli M, Rienzi L, Ubaldi F, Ferrero S, Tesarik J: Reduction of the Incidence of Sperm DNA Fragmentation by Oral Antioxidant Treatment. *J Androl* 26(3), 349-353 (2005).
122. Beckman JA, Goldfine AB, Gordon MB, Garrett LA, Keaney JF, Creager MA: Oral antioxidant therapy improves endothelial function in Type 1 but not Type 2 diabetes mellitus. *American Journal of Physiology - Heart and Circulatory Physiology* 285(6), H2392-H2398 (2003).
123. Cangemi F: TOZAL Study: An open case control study of an oral antioxidant and omega-3 supplement for dry AMD. *BMC Ophthalmology* 7(1), 3 (2007).
124. Huang D, Ou B, Prior RL: The chemistry behind antioxidant capacity assays. *J Agric Food Chem* 53(6), 1841-1856 (2005).
125. Anderson DG, Lynn DM, Langer R: Semi-automated synthesis and screening of a large library of degradable cationic polymers for gene delivery. *Angew Chem Int Edit* 42(27), 3153-3158 (2003).
126. Anderson DG, Tweedie CA, Hossain N *et al.*: A combinatorial library of photocrosslinkable and degradable materials. *Adv Mater* 18(19), 2614-+ (2006).
127. Puoci F, Iemma F, Curcio M *et al.*: Synthesis of Methacrylic−Ferulic Acid Copolymer with Antioxidant Properties by Single-Step Free Radical Polymerization. *Journal of Agricultural and Food Chemistry* 56(22), 10646-10650 (2008).
128. Kurisawa M, Chung JE, Uyama H, Kobayashi S: Enzymatic Synthesis and Antioxidant Properties of Poly(rutin). *Biomacromolecules* 4(5), 1394-1399 (2003).
129. Pan J-Q, Liu NC, Lau WWY: Preparation and properties of new antioxidants with higher MW. *Polymer Degradation and Stability* 62(1), 165-170 (1998).
130. Chumsae C, Gaza-Bulseco G, Sun J, Liu H: Comparison of methionine oxidation in thermal stability and chemically stressed samples of a fully human monoclonal antibody. *Journal of Chromatography B* 850(1-2), 285-294 (2007).
131. Pikal MJ, Dellerman KM, Roy ML, Riggin RM: The Effects of Formulation Variables on the Stability of Freeze-Dried Human Growth Hormone. *Pharmaceutical Research* 8(4), 427-436 (1991).
132. Levine RL, Moskovitz J, Stadtman ER: Oxidation of Methionine in Proteins: Roles in Antioxidant Defense and Cellular Regulation. *IUBMB Life* 50(4-5), 301-307 (2000).
133. Knepp VM, Whatley JL, Muchnik A, Calderwood TS: Identification of Antioxidants for Prevention of Peroxide-Mediated Oxidation of Recombinant Human Ciliary Neurotrophic Factor and Recombinant Human Nerve Growth Factor. *PDA Journal of Pharmaceutical Science and Technology* 50(3), 163-171 (1996).

134. Lam XM, Yang JY, Cleland JL: Antioxidants for prevention of methionine oxidation in recombinant monoclonal antibody HER2. *Journal of Pharmaceutical Sciences* 86(11), 1250-1255 (1997).
135. Fleming C, Maldjian A, Costa DD *et al.*: A carbohydrate-antioxidant hybrid polymer reduces oxidative damage in spermatozoa and enhances fertility. *Nature chemical biology.* 1(5), 270-274 (2005).
136. Ta. S: Adhesion receptors of the immune system. *Nature* 346, 425-434 (1990).
137. Ramani AK, Marcotte EM: Exploiting the Co-evolution of Interacting Proteins to Discover Interaction Specificity. *Journal of Molecular Biology* 327(1), 273-284 (2003).
138. Pearlstein DP, Ali MH, Mungai PT, Hynes KL, Gewertz BL, Schumacker PT: Role of Mitochondrial Oxidant Generation in Endothelial Cell Responses to Hypoxia. *Arteriosclerosis, Thrombosis, and Vascular Biology* 22(4), 566-573 (2002).
139. Hakomori S-I: Tumor Malignancy Defined by Aberrant Glycosylation and Sphingo(glyco)lipid Metabolism. *Cancer Research* 56(23), 5309-5318 (1996).
140. Fukuda M: Possible Roles of Tumor-associated Carbohydrate Antigens. *Cancer Research* 56(10), 2237-2244 (1996).
141. Haddad O, Chotard-Ghodsnia R, Verdier C, Duperray A: Tumor cell/endothelial cell tight contact upregulates endothelial adhesion molecule expression mediated by NFκB: Differential role of the shear stress. *Experimental Cell Research* 316(4), 615-626 (2010).
142. Arabzadeh A, Beauchemin N: *Cell Adhesion Molecules in Colon Cancer Metastasis*

Metastasis of Colorectal Cancer. In: Beauchemin N,Huot J (Ed.^(Eds). Springer Netherlands, 173-203 (2010).
143. Li L, Braiteh FS, Kurzrock R: Liposome-encapsulated curcumin. *Cancer* 104(6), 1322-1331 (2005).
144. Purkayastha S, Berliner A, Fernando SS *et al.*: Curcumin blocks brain tumor formation. *Brain Research* 1266(0), 130-138 (2009).
145. Wang Y-J, Pan M-H, Cheng A-L *et al.*: Stability of curcumin in buffer solutions and characterization of its degradation products. *Journal of Pharmaceutical and Biomedical Analysis* 15(12), 1867-1876 (1997).
146. Tang HD, Murphy CJ, Zhang B *et al.*: Curcumin polymers as anticancer conjugates. *Biomaterials* 31(27), 7139-7149 (2010).
147. Fiore VF, Lofton MC, Roser-Page S *et al.*: Polyketal microparticles for therapeutic delivery to the lung. *Biomaterials* 31(5), 810-817 (2010).
148. Woodfield TBF, Malda J, De Wijn J, Peters F, Riesle J, Van Blitterswijk CA: Design of porous scaffolds for cartilage tissue engineering using a three-dimensional fiber-deposition technique. *Biomaterials* 25(18), 4149-4161 (2004).
149. J. MF, M. KS, J. HW *et al.*: Gamma Inert Sterilization: A Solution to Polyethylene Oxidation? Journal of Bone and Joint Surgery Incorporated, Boston, MA, ETATS-UNIS. 91A, (2009).
150. Oral E, Christensen SD, Malhi AS, Wannomae KK, Muratoglu OK: Wear Resistance and Mechanical Properties of Highly Cross-linked, Ultrahigh–Molecular Weight Polyethylene Doped With Vitamin E. *The Journal of Arthroplasty* 21(4), 580-591 (2006).
151. Costa L, Carpentieri I, Bracco P: Post electron-beam irradiation oxidation of orthopaedic Ultra-High Molecular Weight Polyethylene (UHMWPE) stabilized with vitamin E. *Polymer Degradation and Stability* 94(9), 1542-1547 (2009).

152. Savarino L, Benetti D, Baldini N *et al.*: A preliminary in vitro and in vivo study of the effects of new anthraquinones on neutrophils and bone remodeling. *Journal of Biomedical Materials Research Part A* 75A(2), 324-332 (2005).
153. Riley C, Young G, Chalmers R: Prevalence of Ocular Surface Symptoms, Signs, and Uncomfortable Hours of Wear in Contact Lens Wearers: The Effect of Refitting with Daily-Wear Silicone Hydrogel Lenses (Senofilcon A). *Eye & Contact Lens* 32(6), 281-286 210.1097/1001.icl.0000224522.0000204723.0000224527a (2006).
154. Curcio M, Cirillo G, Parisi OI *et al.*: Poly(2-hydroxyethyl methacrylate)-quercetin Conjugate as Biomaterial in Ophthalmology: An "ab initio" Study. *Journal of Functional Biomaterials* 2(1), 1-17 (2011).
155. Lefeuvre M, Amjaad W, Goldberg M, Stanislawski L: TEGDMA induces mitochondrial damage and oxidative stress in human gingival fibroblasts. *Biomaterials* 26(25), 5130-5137 (2005).
156. Li N, Xia T, Nel AE: The role of oxidative stress in ambient particulate matter-induced lung diseases and its implications in the toxicity of engineered nanoparticles. *Free Radical Biology and Medicine* 44(9), 1689-1699 (2008).
157. Richter AW, Åkerblom E: Antibodies against Polyethylene Glycol Produced in Animals by Immunization with Monomethoxy Polyethylene Glycol Modified Proteins. *International Archives of Allergy and Immunology* 70(2), 124-131 (1983).
158. Gerzina TM, Hume WR: Diffusion of monomers from bonding resin-resin composite combinations through dentine in vitro. *Journal of Dentistry* 24(1-2), 125-128 (1996).
159. Stanislawski L, Lefeuvre M, Bourd K, Soheili-Majd E, Goldberg M, Périanin A: TEGDMA-induced toxicity in human fibroblasts is associated with early and drastic glutathione depletion with subsequent production of oxygen reactive species. *Journal of Biomedical Materials Research Part A* 66A(3), 476-482 (2003).
160. Engelmann, J., Leyhausen *et al.*: Effect of TEGDMA on the intracellular glutathione concentration of human gingival fibroblasts. John Wiley & Sons, New York, NY, ETATS-UNIS. 63, (2002).
161. Schweikl H, Hartmann A, Hiller KA *et al.*: Inhibition of TEGDMA and HEMA-induced genotoxicity and cell cycle arrest by N-acetylcysteine. *Dental Materials* 23(6), 688-695 (2007).
162. Udipi K, Ornberg RL, Thurmond KB, Settle SL, Forster D, Riley D: Modification of inflammatory response to implanted biomedical materials in vivo by surface bound superoxide dismutase mimics. *Journal of Biomedical Materials Research* 51(4), 549-560 (2000).
163. Gopinath D, Ahmed MR, Gomathi K, Chitra K, Sehgal PK, Jayakumar R: Dermal wound healing processes with curcumin incorporated collagen films. *Biomaterials* 25(10), 1911-1917 (2004).
164. Gomathi K, Gopinath D, Rafiuddin Ahmed M, Jayakumar R: Quercetin incorporated collagen matrices for dermal wound healing processes in rat. *Biomaterials* 24(16), 2767-2772 (2003).
165. Merrell JG, Mclaughlin SW, Tie L, Laurencin CT, Chen AF, Nair LS: Curcumin-loaded poly(epsilon-caprolactone) nanofibres: Diabetic wound dressing with anti-oxidant and anti-inflammatory properties. *Clin Exp Pharmacol P* 36(12), 1149-1156 (2009).
166. Frimpong RA, Hilt JZ: Magnetic nanoparticles in biomedicine: synthesis, functionalization and applications. *Nanomedicine* 5(9), 1401-1414 (2010).

167. Pouliquen D, Perroud H, Calza F, Jallet P, Le Jeune JJ: Investigation of the magnetic properties of iron oxide nanoparticles used as contrast agent for MRI. *Magnetic Resonance in Medicine* 24(1), 75-84 (1992).
168. Lu M, Suh K, Lee H, Cohen M, Rieves D, Pazdur R: FDA review of ferumoxytol (Feraheme) for the treatment of iron deficiency anemia in adults with chronic kidney disease. *Am J Hematol* 85, 315-319 (2010).
169. Hilger I, Hiergeist R, Hergt R, Winnefeld K, Schubert H, Kaiser WA: Thermal Ablation of Tumors Using Magnetic Nanoparticles: An In Vivo Feasibility Study. *Investigative Radiology* 37(10), 580-586 (2002).
170. Gupta AK, Gupta M: Synthesis and surface engineering of iron oxide nanoparticles for biomedical applications. *Biomaterials* 26(18), 3995-4021 (2005).
171. Chertok B, Moffat BA, David AE *et al.*: Iron oxide nanoparticles as a drug delivery vehicle for MRI monitored magnetic targeting of brain tumors. *Biomaterials* 29(4), 487-496 (2008).
172. Zhu MT, Wang Y, Feng WY *et al.*: Oxidative stress and apoptosis induced by iron oxide nanoparticles in cultured human umbilical endothelial cells. *Journal of nanoscience and nanotechnology* 10(12), 8584-8590 (2010).
173. Buyukhatipoglu K, Clyne AM: Superparamagnetic iron oxide nanoparticles change endothelial cell morphology and mechanics via reactive oxygen species formation. *Journal of Biomedical Materials Research Part A* 96(1), 186-195 (2011).
174. Stroh A, Zimmer C, Gutzeit C *et al.*: Iron oxide particles for molecular magnetic resonance imaging cause transient oxidative stress in rat macrophages. *Free Radical Biology and Medicine* 36(8), 976-984 (2004).
175. Wu X, Tan Y, Mao H, Zhang M: Toxic effects of iron oxide nanoparticles on human umbilical vein endothelial cells. *International journal of nanomedicine* 5, 385 (2010).
176. Thorek DLJ, Chen AK, Czupryna J, Tsourkas A: Superparamagnetic iron oxide nanoparticle probes for molecular imaging. *Annals of biomedical engineering* 34(1), 23-38 (2006).
177. Zhang C, Jugold M, Woenne EC *et al.*: Specific targeting of tumor angiogenesis by RGD-conjugated ultrasmall superparamagnetic iron oxide particles using a clinical 1.5-T magnetic resonance scanner. *Cancer research* 67(4), 1555-1562 (2007).
178. Spencer JPE: Metabolism of Tea Flavonoids in the Gastrointestinal Tract. *The Journal of Nutrition* 133(10), 3255S-3261S (2003).
179. Newman PJ: The biology of PECAM-1. *The Journal of Clinical Investigation* 99(1), 3-8 (1997).
180. Albelda SM, Muller WA, Buck CA, Newman PJ: Molecular and cellular properties of PECAM-1 (endoCAM/CD31): a novel vascular cell-cell adhesion molecule. *The Journal of Cell Biology* 114(5), 1059-1068 (1991).
181. Bogen S, Pak J, Garifallou M, Deng X, Muller WA: Monoclonal antibody to murine PECAM-1 (CD31) blocks acute inflammation in vivo. *The Journal of Experimental Medicine* 179(3), 1059-1064 (1994).
182. Dziubla TD, Shuvaev VV, Hong NK *et al.*: Endothelial targeting of semi-permeable polymer nanocarriers for enzyme therapies. *Biomaterials* 29(2), 215-227 (2008).
183. Muro S, Dziubla T, Qiu W *et al.*: Endothelial Targeting of High-Affinity Multivalent Polymer Nanocarriers Directed to Intercellular Adhesion Molecule 1. *Journal of Pharmacology and Experimental Therapeutics* 317(3), 1161-1169 (2006).
184. Dziubla TD, Karim A, Muzykantov VR: Polymer nanocarriers protecting active enzyme cargo against proteolysis. *Journal of Controlled Release* 102(2), 427-439 (2005).

185. Muro S, Garnacho C, Champion JA *et al.*: Control of Endothelial Targeting and Intracellular Delivery of Therapeutic Enzymes by Modulating the Size and Shape of ICAM-1-targeted Carriers. *Mol Ther* 16(8), 1450-1458 (2008).
186. Anderson ME, Siahaan TJ: Mechanism of Binding and Internalization of ICAM-1-Derived Cyclic Peptides by LFA-1 on the Surface of T Cells: A Potential Method for Targeted Drug Delivery. *Pharmaceutical Research* 20(10), 1523-1532 (2003).
187. Christofidou-Solomidou M, Scherpereel A, Wiewrodt R *et al.*: PECAM-directed delivery of catalase to endothelium protects against pulmonary vascular oxidative stress. *American Journal of Physiology - Lung Cellular and Molecular Physiology* 285(2), L283-L292 (2003).
188. Wattamwar PP, Biswal D, Cochran DB *et al.*: Synthesis and characterization of poly(antioxidant β-amino esters) for controlled release of polyphenolic antioxidants. *Acta Biomaterialia* 8(7), 2529-2537 (2012).
189. Frimpong RA, Dou J, Pechan M, Hilt JZ: Enhancing remote controlled heating characteristics in hydrophilic magnetite nanoparticles via facile co-precipitation. *Journal of Magnetism and Magnetic Materials* 322(3), 326-331 (2010).
190. Muro S, Wiewrodt R, Thomas A *et al.*: A novel endocytic pathway induced by clustering endothelial ICAM-1 or PECAM-1. *Journal of cell science* 116(8), 1599-1609 (2003).
191. Garnacho C, Albelda SM, Muzykantov VR, Muro S: Differential intra-endothelial delivery of polymer nanocarriers targeted to distinct PECAM-1 epitopes. *Journal of Controlled Release* 130(3), 226-233 (2008).
192. Qiao R, Yang C, Gao M: Superparamagnetic iron oxide nanoparticles: from preparations to in vivo MRI applications. *Journal of Materials Chemistry* 19(35), 6274-6293 (2009).
193. Taupitz M, Wagner S, Schnorr J *et al.*: Phase I clinical evaluation of citrate-coated monocrystalline very small superparamagnetic iron oxide particles as a new contrast medium for magnetic resonance imaging. *Investigative Radiology* 39(7), 394-405 (2004).
194. Griffiths SM, Singh N, Jenkins GJS *et al.*: Dextran coated ultrafine superparamagnetic iron oxide nanoparticles: compatibility with common fluorometric and colorimetric dyes. *Analytical chemistry* 83(10), 3778 (2011).
195. Ding BS, Dziubla T, Shuvaev VV, Muro S, Muzykantov VR: Advanced drug delivery systems that target the vascular endothelium. *Molecular interventions* 6(2), 98 (2006).
196. Xia T, Kovochich M, Liong M *et al.*: Comparison of the mechanism of toxicity of zinc oxide and cerium oxide nanoparticles based on dissolution and oxidative stress properties. *Acs Nano* 2(10), 2121-2134 (2008).
197. Madamanchi NR, Vendrov A, Runge MS: Oxidative stress and vascular disease. *Arteriosclerosis, thrombosis, and vascular biology* 25(1), 29-38 (2005).
198. Bannerman DD, Goldblum SE: Mechanisms of bacterial lipopolysaccharide-induced endothelial apoptosis. *Am J Physiol Lung Cell Mol Physiol* 284(6), L899-L914 (2003).
199. Jansen T, Hortmann M, Oelze M *et al.*: Conversion of biliverdin to bilirubin by biliverdin reductase contributes to endothelial cell protection by heme oxygenase-1—evidence for direct and indirect antioxidant actions of bilirubin. *J Mol Cell Cardiol* 49(2), 186-195 (2010).
200. Sun B, Zou X, Chen Y, Zhang P, Shi G: Preconditioning of carbon monoxide releasing molecule-derived CO attenuates LPS-induced activation of HUVEC. *Int J Biol Sci* 4(5), 270 (2008).
201. Hanini A, Schmitt A, Kacem K, Chau F, Ammar S, Gavard J: Evaluation of iron oxide nanoparticle biocompatibility. *International journal of nanomedicine* 6, 787 (2011).

202. Firestein GS: Evolving concepts of rheumatoid arthritis. *Nature* 423(6937), 356-361 (2003).
203. Yamanishi Y, Boyle DL, Rosengren S, Green DR, Zvaifler NJ, Firestein GS: Regional analysis of p53 mutations in rheumatoid arthritis synovium. *Proceedings of the National Academy of Sciences* 99(15), 10025-10030 (2002).
204. Jaswal S, Mehta HC, Sood AK, Kaur J: Antioxidant status in rheumatoid arthritis and role of antioxidant therapy. *Clinica Chimica Acta* 338(1), 123-129 (2003).
205. Frei B, Stocker R, Ames BN: Antioxidant defenses and lipid peroxidation in human blood plasma. *Proceedings of the National Academy of Sciences* 85(24), 9748-9752 (1988).
206. Wolf G: How an Increased Intake of Alpha-Tocopherol Can Suppress the Bioavailability of Gamma-Tocopherol. *Nutrition reviews* 64(6), 295-299 (2006).
207. Kuo F, Subramanian B, Kotyla T, Wilson TA, Yoganathan S, Nicolosi RJ: Nanoemulsions of an anti-oxidant synergy formulation containing gamma tocopherol have enhanced bioavailability and anti-inflammatory properties. *International journal of pharmaceutics* 363(1), 206-213 (2008).
208. Jelic S, Padeletti M, Kawut SM *et al.*: Inflammation, oxidative stress, and repair capacity of the vascular endothelium in obstructive sleep apnea. *Circulation* 117(17), 2270-2278 (2008).
209. Chenevard R, Hürlimann D, Béchir M *et al.*: Selective COX-2 inhibition improves endothelial function in coronary artery disease. *Circulation* 107(3), 405-409 (2003).
210. Dandona P, Aljada A, Bandyopadhyay A: Inflammation: the link between insulin resistance, obesity and diabetes. *Trends in immunology* 25(1), 4-7 (2004).
211. Brown DM, Wilson MR, Macnee W, Stone V, Donaldson K: Size-dependent proinflammatory effects of ultrafine polystyrene particles: a role for surface area and oxidative stress in the enhanced activity of ultrafines. *Toxicology and applied pharmacology* 175(3), 191-199 (2001).
212. Singh U, Devaraj S, Jialal I: Vitamin E, oxidative stress, and inflammation. *Annu. Rev. Nutr.* 25, 151-174 (2005).
213. Mantovani A, Allavena P, Sica A, Balkwill F: Cancer-related inflammation. *Nature* 454(7203), 436-444 (2008).
214. Martey CA, Pollock SJ, Turner CK *et al.*: Cigarette smoke induces cyclooxygenase-2 and microsomal prostaglandin E2 synthase in human lung fibroblasts: implications for lung inflammation and cancer. *American Journal of Physiology-Lung Cellular and Molecular Physiology* 287(5), L981-L991 (2004).
215. Mossman BT, Kamp DW, Weitzman SA: Mechanisms of carcinogenesis and clinical features of asbestos-associated cancers. *Cancer investigation* 14(5), 466-480 (1996).
216. Berwick M, Armstrong BK, Ben-Porat L *et al.*: Sun exposure and mortality from melanoma. *Journal of the National Cancer Institute* 97(3), 195-199 (2005).
217. Clayton AJ, Danson S, Jolly S *et al.*: Incidence of cerebral metastases in patients treated with trastuzumab for metastatic breast cancer. *British journal of cancer* 91(4), 639-643 (2004).
218. Disibio G, French SW: Metastatic Patterns of Cancers: Results From a Large Autopsy Study. *Archives of Pathology & Laboratory Medicine* 132(6), 931-939 (2008).
219. Vera-Llonch M, Weycker D, Glass A *et al.*: Healthcare costs in women with metastatic breast cancer receiving chemotherapy as their principal treatment modality. *BMC Cancer* 11(1), 250 (2011).
220. Lin NU, Thomssen C, Cardoso F *et al.*: International guidelines for management of metastatic breast cancer (MBC) from the European School of Oncology (ESO)-MBC Task

Force: Surveillance, staging, and evaluation of patients with early-stage and metastatic breast cancer. *Breast* 22(3), 203-210 (2013).
221. Yukhananov A, Prasad S: FDA rejects Amgen's application for Xgeva. (2012).
222. Balkwill F: Tumor necrosis factor or tumor promoting factor? *Cytokine & growth factor reviews* 13(2), 135-141 (2002).
223. Woodworth CD, Mcmullin E, Iglesias M, Plowman GD: Interleukin 1 alpha and tumor necrosis factor alpha stimulate autocrine amphiregulin expression and proliferation of human papillomavirus-immortalized and carcinoma-derived cervical epithelial cells. *Proceedings of the National Academy of Sciences* 92(7), 2840-2844 (1995).
224. Damas P, Canivet J-L, De Groote D *et al.*: Sepsis and serum cytokine concentrations. *Critical Care Medicine* 25(3), 405-412 (1997).
225. Albelda SM, Buck CA: Integrins and other cell adhesion molecules. *The FASEB Journal* 4(11), 2868-2880 (1990).
226. Aoudjit F, Potworowski EF, Springer TA, St-Pierre Y: Protection from Lymphoma Cell Metastasis in ICAM-1 Mutant Mice: A Posthoming Event. *The Journal of Immunology* 161(5), 2333-2338 (1998).
227. Albelda SM: Endothelial and epithelial cell adhesion molecules. *Am J Respir Cell Mol Biol* 4(3), 195-203 (1991).
228. Whinney C: Perioperative medication management: General principles and practical applications. *Cleveland Clinic Journal of Medicine* 76(Suppl 4), S126-S132 (2009).
229. Møiniche S, Rømsing J, Dahl JB, Tramèr MR: Nonsteroidal Antiinflammatory Drugs and the Risk of Operative Site Bleeding After Tonsillectomy: A Quantitative Systematic Review. *Anesthesia & Analgesia* 96(1), 68-77 (2003).
230. Lanza FL, Chan FK, Quigley EM: Guidelines for prevention of NSAID-related ulcer complications. *The American journal of gastroenterology* 104(3), 728-738 (2009).
231. Hillner BE, Ingle JN, Chlebowski RT *et al.*: American Society of Clinical Oncology 2003 Update on the Role of Bisphosphonates and Bone Health Issues in Women With Breast Cancer. *Journal of Clinical Oncology* 21(21), 4042-4057 (2003).
232. Herr I, Pfitzenmaier J: Glucocorticoid use in prostate cancer and other solid tumours: implications for effectiveness of cytotoxic treatment and metastases. *The Lancet Oncology* 7(5), 425-430 (2006).
233. Löwenberg M, Tuynman J, Bilderbeek J *et al.*: Rapid immunosuppressive effects of glucocorticoids mediated through Lck and Fyn. *Blood* 106(5), 1703-1710 (2005).
234. Auphan N, Didonato JA, Rosette C, Helmberg A, Karin M: Immunosuppression by glucocorticoids: inhibition of NF-κB activity through induction of IκB synthesis. *Science* 270(5234), 286-290 (1995).
235. Ashwell JD, Lu FW, Vacchio MS: Glucocorticoids in T cell development and function*. *Annual review of immunology* 18(1), 309-345 (2000).
236. Cohen JJ, Duke RC: Glucocorticoid activation of a calcium-dependent endonuclease in thymocyte nuclei leads to cell death. *The Journal of Immunology* 132(1), 38-42 (1984).
237. Bach J-F: The mode of action of immunosuppressive agents. *Frontiers of biology* 41, 1 (1975).
238. Yin F, Giuliano AE, Law RE, Van Herle AJ: Apigenin inhibits growth and induces G2/M arrest by modulating cyclin-CDK regulators and ERK MAP kinase activation in breast carcinoma cells. *Anticancer research* 21(1A), 413-420 (2000).
239. Liang Y-C, Huang Y-T, Tsai S-H, Lin-Shiau S-Y, Chen C-F, Lin J-K: Suppression of inducible cyclooxygenase and inducible nitric oxide synthase by apigenin and related flavonoids in mouse macrophages. *Carcinogenesis* 20(10), 1945-1952 (1999).

240. Gupta S, Afaq F, Mukhtar H: Involvement of nuclear factor-kappa B, Bax and Bcl-2 in induction of cell cycle arrest and apoptosis by apigenin in human prostate carcinoma cells. *Oncogene* 21(23), 3727-3738 (2002).
241. Di Carlo G, Mascolo N, Izzo AA, Capasso F: Flavonoids: Old and new aspects of a class of natural therapeutic drugs. *Life Sciences* 65(4), 337-353 (1999).
242. Koes R, Verweij W, Quattrocchio F: Flavonoids: a colorful model for the regulation and evolution of biochemical pathways. *Trends in plant science* 10(5), 236-242 (2005).
243. Kim J-D, Liu L, Guo W, Meydani M: Chemical structure of flavonols in relation to modulation of angiogenesis and immune-endothelial cell adhesion. *The Journal of nutritional biochemistry* 17(3), 165-176 (2006).
244. Ross JA, Kasum CM: Dietary flavonoids: bioavailability, metabolic effects, and safety. *Annual review of nutrition* 22, 19-34 (2002).
245. Lotito SB, Frei B: Consumption of flavonoid-rich foods and increased plasma antioxidant capacity in humans: Cause, consequence, or epiphenomenon? *Free Radical Biology and Medicine* 41(12), 1727-1746 (2006).
246. Hollman PC, Van Trijp JM, Mengelers MJ, De Vries JH, Katan MB: Bioavailability of the dietary antioxidant flavonol quercetin in man. *Cancer letters* 114(1), 139-140 (1997).
247. Anand P, Nair HB, Sung B *et al.*: Design of curcumin-loaded PLGA nanoparticles formulation with enhanced cellular uptake, and increased bioactivity< i> in vitro</i> and superior bioavailability< i> in vivo</i>. *Biochemical pharmacology* 79(3), 330-338 (2010).
248. Hu J, Johnston KP, Williams Iii RO: Nanoparticle engineering processes for enhancing the dissolution rates of poorly water soluble drugs. *Drug development and industrial pharmacy* 30(3), 233-245 (2004).
249. Moghimi SM, Hunter AC, Murray JC: Long-circulating and target-specific nanoparticles: theory to practice. *Pharmacological reviews* 53(2), 283-318 (2001).
250. Kumari A, Yadav SK, Yadav SC: Biodegradable polymeric nanoparticles based drug delivery systems. *Colloids and Surfaces B: Biointerfaces* 75(1), 1-18 (2010).
251. Santos AR: Anti-inflammatory compounds of plant origin. Part II. Modulation of pro-inflammatory cytokines, chemokines and adhesion molecules. *Planta Med* 70, 93-103 (2004).
252. Moss M, Zimmer S, Anderson K: Role of metastatic potential in the adhesion of human breast cancer cells to endothelial monolayers. *Anticancer research* 20(3A), 1425 (2000).
253. Lee SJ, Son KH, Chang HW *et al.*: Antiinflammatory activity of naturally occurring flavone and flavonol glycosides. *Archives of Pharmacal Research* 16(1), 25-28 (1993).
254. Cotelle N, Bernier J-L, Catteau J-P, Pommery J, Wallet J-C, Gaydou EM: Antioxidant properties of hydroxy-flavones. *Free Radical Biology and Medicine* 20(1), 35-43 (1996).
255. Jang S, Kim H, Hwang K *et al.*: Hepatoprotective effect of baicalin, a major flavone from Scutellaria radix, on acetaminophen-induced liver injury in mice. *Immunopharmacology and immunotoxicology* 25(4), 585-594 (2003).
256. Ahlemeyer B, Krieglstein J: Pharmacological studies supporting the therapeutic use of Ginkgo biloba extract for Alzheimer's disease. *Pharmacopsychiatry* 36(1), 8-14 (2003).
257. Hans M, Lowman A: Biodegradable nanoparticles for drug delivery and targeting. *Current Opinion in Solid State and Materials Science* 6(4), 319-327 (2002).
258. Song X, Zhao Y, Hou S *et al.*: Dual agents loaded PLGA nanoparticles: Systematic study of particle size and drug entrapment efficiency. *European Journal of Pharmaceutics and Biopharmaceutics* 69(2), 445-453 (2008).

259. Silva AC, Oliveira TR, Mamani JB *et al.*: Application of hyperthermia induced by superparamagnetic iron oxide nanoparticles in glioma treatment. *International Journal of Nanomedicine* 6, 591-603 (2011).
260. Bhaskar S, Tian F, Stoeger T *et al.*: Multifunctional Nanocarriers for diagnostics, drug delivery and targeted treatment across blood-brain barrier: perspectives on tracking and neuroimaging. *Part Fibre Toxicol* 7, 3 (2010).
261. Weinstein JS, Varallyay CG, Dosa E *et al.*: Superparamagnetic iron oxide nanoparticles: diagnostic magnetic resonance imaging and potential therapeutic applications in neurooncology and central nervous system inflammatory pathologies, a review. *J Cerebr Blood F Met* 30(1), 15-35 (2010).
262. Wankhede M, Bouras A, Kaluzova M, Hadjipanayis CG: Magnetic nanoparticles: an emerging technology for malignant brain tumor imaging and therapy. *Expert Rev Clin Pharmacol* 5(2), 173-186 (2012).
263. Hu JM, Qian YF, Wang XF, Liu T, Liu SY: Drug-Loaded and superparamagnetic iron oxide nanoparticle surface-embedded amphiphilic block copolymer micelles for integrated chemotherapeutic drug delivery and MR imaging. *Langmuir* 28(4), 2073-2082 (2012).
264. Dilnawaz F, Singh A, Mewar S, Sharma U, Jagannathan NR, Sahoo SK: The transport of non-surfactant based paclitaxel loaded magnetic nanoparticles across the blood brain barrier in a rat model. *Biomaterials* 33(10), 2936-2951 (2012).
265. Cole AJ, David AE, Wang J, Galbán CJ, Yang VC: Magnetic brain tumor targeting and biodistribution of long-circulating PEG-modified, cross-linked starch-coated iron oxide nanoparticles. *Biomaterials* 32(26), 6291-6301 (2011).
266. Veiseh O, Sun C, Fang C *et al.*: Specific targeting of brain tumors with an optical/magnetic resonance imaging nanoprobe across the blood-brain barrier. *Cancer Research* 69(15), 6200-6207 (2009).
267. Bernacki J, Dobrowolska A, Nierwinska K, Malecki A: Physiology and pharmacological role of the blood-brain barrier. *Pharmacological Reports* 60(5), 600-622 (2008).
268. Kenzaoui BH, Bernasconi CC, Hofmann H, Juillerat-Jeanneret L: Evaluation of uptake and transport of ultrasmall superparamagnetic iron oxide nanoparticles by human brain-derived endothelial cells. *Nanomedicine* 7(1), 39-53 (2012).
269. Scherpereel A, Rome JJ, Wiewrodt R *et al.*: Platelet-endothelial cell adhesion molecule-1-directed immunotargeting to cardiopulmonary vasculature. *Journal of Pharmacology and Experimental Therapeutics* 300(3), 777-786 (2002).
270. Wong D, Dorovini-Zis K: Platelet/endothelial cell adhesion molecule-1 (PECAM-1) expression by human brain microvessel endothelial cells in primary culture. *Brain Res* 731(1-2), 217-220 (1996).
271. Kalinowska A, Losy J: PECAM-1, a key player in neuroinflammation. *Eur J Neurol* 13(12), 1284-1290 (2006).
272. Meenach SA, Hilt JZ, Anderson KW: Poly(ethylene glycol)-based magnetic hydrogel nanocomposites for hyperthermia cancer therapy. *Acta Biomater* 6(3), 1039-1046 (2010).
273. Dan M, Scott DF, Hardy PA *et al.*: Block copolymer cross-linked nanoassemblies improve particle stability and biocompatibility of superparamagnetic iron oxide nanoparticles. *Pharm Res* 30(2), 552-561 (2013).
274. Salacinski PR, Mclean C, Sykes JE, Clement-Jones VV, Lowry PJ: Iodination of proteins, glycoproteins, and peptides using a solid-phase oxidizing agent, 1, 3, 4, 6-tetrachloro-3α, 6α-diphenyl glycoluril (Iodogen). *Analytical biochemistry* 117(1), 136-146 (1981).

275. Poller B, Gutmann H, Krahenbuhl S *et al.*: The human brain endothelial cell line hCMEC/D3 as a human blood-brain barrier model for drug transport studies. *Journal of Neurochemistry* 107(5), 1358-1368 (2008).
276. Carl SM, Lindley DJ, Couraud PO *et al.*: ABC and SLC transporter expression and pot substrate characterization across the human CMEC/D3 blood-brain barrier cell Line. *Molecular Pharmaceutics* 7(4), 1057-1068 (2010).
277. Weksler BB, Subileau EA, Perriere N *et al.*: Blood-brain barrier-specific properties of a human adult brain endothelial cell line. *FASEB J* 19(13), 1872-1874 (2005).
278. Papademetriou J, Garnacho C, Serrano D, Bhowmick T, Schuchman EH, Muro S: Comparative binding, endocytosis, and biodistribution of antibodies and antibody-coated carriers for targeted delivery of lysosomal enzymes to ICAM-1 versus transferrin receptor. *J Inherit Metab Dis* 36(3), 467-477 (2013).
279. Triguero D, Buciak J, Pardridge WM: Capillary depletion method for quantification of blood-brain barrier transport of circulating peptides and plasma proteins. *Journal of Neurochemistry* 54(6), 1882-1888 (1990).
280. Crossgrove JS, Allen DD, Bukaveckas BL, Rhineheimer SS, Yokel RA: Manganese distribution across the blood-brain barrier. I. Evidence for carrier-mediated influx of managanese citrate as well as manganese and manganese transferrin. *NeuroToxicology* 24(1), 3-13. (2003).
281. Smith QR: Brain perfusion systems for studies of drug uptake and metabolism in the central nervous system. *Pharmaceutical Biotechnology* 8, 285-307 (1996).
282. Nozinic D, Milic A, Mikac L, Ralic J, Padovan J, Antolovic R: Assessment of macrolide transport using PAMPA, Caco-2 and MDCKII-hMDR1 assays. *Croat Chem Acta* 83(3), 323-331 (2010).
283. Chacko AM, Nayak M, Greineder CF, Delisser HM, Muzykantov VR: Collaborative enhancement of antibody binding to distinct PECAM-1 epitopes modulates endothelial targeting. *PLoS One* 7(4), e34958 (2012).
284. Yu YJ, Zhang Y, Kenrick M *et al.*: Boosting brain uptake of a therapeutic antibody by reducing its affinity for a transcytosis target. *Sci Transl Med* 3(84), 84ra44 (2011).
285. Peng X-H, Qian X, Mao H, Wang AY: Targeted magnetic iron oxide nanoparticles for tumor imaging and therapy. *International journal of nanomedicine* 3(3), 311 (2008).
286. Jiang W, Xie H, Ghoorah D *et al.*: Conjugation of functionalized SPIONs with transferrin for targeting and imaging brain glial tumors in rat model. *PLoS One* 7(5), e37376 (2012).
287. Corot C, Robert P, Idée J-M, Port M: Recent advances in iron oxide nanocrystal technology for medical imaging. *Advanced drug delivery reviews* 58(14), 1471-1504 (2006).
288. Doherty GJ, Mcmahon HT: Mechanisms of endocytosis. *Annual Review of Biochemistry* 78, 857-902 (2009).
289. Hillaireau H, Couvreur P: Nanocarriers' entry into the cell: relevance to drug delivery. *Cellular and Molecular Life Sciences* 66(17), 2873-2896 (2009).
290. Conner SD, Schmid SL: Regulated portals of entry into the cell. *Nature* 422(6927), 37-44 (2003).
291. Chang J, Jallouli Y, Kroubi M *et al.*: Characterization of endocytosis of transferrin-coated PLGA nanoparticles by the blood-brain barrier. *International Journal of Pharmaceutics* 379(2), 285-292 (2009).
292. Minshall RD, Tiruppathi C, Vogel SM *et al.*: Endothelial cell-surface gp60 activates vesicle formation and trafficking via G(i)-coupled Src kinase signaling pathway. *J Cell Biol* 150(5), 1057-1070 (2000).

293. Hansen SH, Sandvig K, Van Deurs B: Clathrin and HA2 adaptors: effects of potassium depletion, hypertonic medium, and cytosol acidification. *J Cell Biol* 121(1), 61-72 (1993).
294. Garnacho C, Shuvaev V, Thomas A *et al.*: RhoA activation and actin reorganization involved in endothelial CAM-mediated endocytosis of anti-PECAM carriers: critical role for tyrosine 686 in the cytoplasmic tail of PECAM-1. *Blood* 111(6), 3024-3033 (2008).
295. Wu DF, Kang YS, Bickel U, Pardridge WM: Blood-brain barrier permeability to morphine-6-glucuronide is markedly reduced compared with morphine. *Drug Metab Dispos* 25(6), 768-771 (1997).
296. Jones AR, Shusta EV: Blood-brain barrier transport of therapeutics via receptor-mediation. *Pharmaceutical Research* 24(9), 1759-1771 (2007).
297. Zhang P, Hu L, Yin Q, Zhang Z, Feng L, Li Y: Transferrin-conjugated polyphosphoester hybrid micelle loading paclitaxel for brain-targeting delivery: synthesis, preparation and in vivo evaluation. *J Control Release* 159(3), 429-434 (2012).
298. Shin SU, Friden P, Moran M *et al.*: Transferrin-antibody fusion proteins are effective in brain targeting. *Proc Natl Acad Sci U S A* 92(7), 2820-2824 (1995).
299. Crowe A, Morgan EH: Iron and transferrin uptake by brain and cerebrospinal fluid in the rat. *Brain Res* 592(1-2), 8-16 (1992).
300. Morgan EH, Moos T: Mechanism and developmental changes in iron transport across the blood-brain barrier. *Dev Neurosci* 24(2-3), 106-113 (2002).
301. Shuvaev VV, Tliba S, Nakada M, Albelda SM, Muzykantov VR: Platelet-endothelial cell adhesion molecule-1-directed endothelial targeting of superoxide dismutase alleviates oxidative stress caused by either extracellular or intracellular Superoxide. *Journal of Pharmacology and Experimental Therapeutics* 323(2), 450-457 (2007).
302. Danilov SM, Gavrilyuk VD, Franke FE *et al.*: Lung uptake of antibodies to endothelial antigens: key determinants of vascular immunotargeting. *American Journal of Physiology - Lung Cellular and Molecular Physiology* 280(6), L1335-L1347 (2001).
303. Kawabe T, Phi JH, Yamamoto M, Kim DG, Barfod BE, Urakawa Y: Treatment of brain metastasis from lung cancer. *Prog Neurol Surg* 25, 148-155 (2012).
304. Kuang BH, Wen XZ, Ding Y *et al.*: The prognostic value of platelet endothelial cell adhesion molecule-1 in non-small-cell lung cancer patients. *Med Oncol* 30(2), 536 (2013).

VITA

David Cochran received his B.S. and M.S. in Chemical and Biological Engineering from Drexel University and is now a Ph.D. candidate under Dr. Thomas Dziubla in Chemical and Materials Engineering at the University of Kentucky, Lexington KY. David is also a participant in the Integrative Graduate Education and Research Traineeship (IGERT) program. His research focused on the development of actively targeted antioxidant polymers for the treatment of inflammation mediated events such as metal particulate inhalation, ischemia/reperfusion injury, and cancer metastasis.

Honors and Awards

- IGERT National Poster and Video Presenter – February 2013
- IGERT Fellowship – July 2011
- Overall Presentation Award – Biomaterials Day – November 2011
- Biological Materials Poster Award – Graduate Student Poster Competition – September 2011
- Biological Materials and Processes Poster Award – Graduate Student Poster Competition – September 2010
- University Design Competition – Winner in Chemical Engineering for Biodiesel Reactor Design – June 2008
- EPA Grant - Number: SU833524 $70,000 – May 2008

Publications

- P. Wattamwar, D. Biswal, **David Cochran**, R. Eitel, K. Anderson, J. Hilt, T. Dziubla. Synthesis and characterization of poly(antioxidant β-amino esters) for controlled release of polyphenolic antioxidants, Acta Biomaterialia
- J. Ambati, A. Lopez, **David Cochran**, P. Wattamwar, K. Bean, T. Dziubla, S. Rankin. Engineered silica nanocarriers as a high-payload delivery vehicle for antioxidant enzymes, Acta Biomaterialia
- **David Cochran**, T. Dziubla. Antioxidant Polymers for Tuning Biomaterial Biocompatibility: From Drug Delivery to Tissue Engineering. In G. Cirillo, *Antioxidant Polymers Synthesis, Properties, and Applications*. Salem, MA: Scrivener.
- **David Cochran**, P. Wattamwar, R. Wydra, J. Hilt, K. Anderson, T. Dziubla. Suppressing iron oxide nanoparticle toxicity by vascular targeted antioxidant nanoparticles, *Biomaterials*

- **David Cochran**, M. Dan, R. Wydra, R. Yokel, T. Dziubla. Binding, transcytosis, and biodistribution of anti-PECAM-1 iron oxide nanoparticles for brain-targeted delivery, (*submitted PLOS ONE)*
- **David Cochran,** L. Gray, K. Anderson, T. Dziubla. Encapsulated apigenin-based polymers for the prevention of tumor cell adhesion and metastasis, (*in review)*

Patents

- T. Dziubla, J. Hilt, D. Biswal, **David Cochran**, P. Wattamwar 2011. Compounds and methods for reducing oxidative stress. U. S. Patent Application 13/290752, filed November 2011. Patent Pending

Presentations

Oral

- **David Cochran**, L. Crofford, R. Bader, and T. Dziubla, Society for Biomaterials Annual Conference, (2013)
- **David Cochran**, K. Anderson, R. Eitel and T. Dziubla, National IGERT competition, (2013)
- **David Cochran**, K. Anderson, R. Eitel and T. Dziubla, American Institute of Chemical Engineers Annual Conference, (2011)
- **David Cochran**, P. Wattamwar and T. Dziubla, Society For Biomaterials Annual Conference, (2011)
- J.Ambati, A.M. Lopez, **David Cochran**, P. Wattamwar, K. Bean, T. Dziubla, and S. Rankin. American Institute of Chemical Engineers Annual Conference, (2010)
- **David Cochran**, P. Wattamwar and T. Dziubla, American Institute of Chemical Engineers Annual Conference, (2010)
- **David Cochran**, C. Cavan, T. Wilson, R. Cairncross. EPA P3 2008, (2008)

Poster

- **David Cochran**, K. Anderson, and T. Dziubla, Society for Biomaterials Annual Conference, (2012)
- **David Cochran**, P. Wattamwar, and T. Dziubla, Bluegrass Biophysics Symposium, (2011)
- **David Cochran**, P. Wattamwar and T. Dziubla, UK Graduate Student Poster Session, (2011)
- **David Cochran**, P. Wattamwar and T. Dziubla, Biomaterials Day, (2010)